VECTOR-MODEL-BASED CASE RETRIEVAL APPROACH FOR IMPROVING AND EXPEDITING OPTIMIZATION IN INTENSITY MODULATED RADIOTHERAPY

LIU SAU FAN, EVA

Ph.D

The Hong Kong Polytechnic University

2017

The Hong Kong Polytechnic University
Department of Health Technology and Informatics

Vector-Model-Based Case Retrieval Approach for Improving and Expediting Optimization in Intensity Modulated Radiotherapy

Liu Sau Fan, Eva

A thesis submitted in partial fulfilment of the requirements for the degree of Doctor of Philosophy

January 2017

CERTIFICATE OF ORIGINALITY

I hereby declare that this thesis is my own work and that, to the best of my knowledge and belief, it reproduces no material previously published or written nor material which has been accepted for the award of any other degree or diploma, except where due acknowledgement has been made in the text.

_____ (Signed)

LIU SAU FAN, EVA (Name of student)

ABSTRACT

A similarity reference database is a database of previous radiotherapy treatment cases. Currently there is no such database for intensity modulated radiotherapy (IMRT) or volumetric arc radiotherapy (VMAT). Every IMRT/VMAT plan is based on an individual oncologist's preferences of prescription dose and an individual planner's experience. Without a similarity reference database, it is impossible to manually identify, retrieve and assess all similar IMRT/VMAT cases from thousands of patient records. This forces a planner to use the trial-and-error method to search for optimization parameters and overcome the dose difference between final accurate dose calculation and fast optimization dose calculation which normally takes several days. Because of the long planning time, this means that adaptive IMRT/VMAT planning is unfeasible without a reduction in planning time. With a similarity reference database, a vector model could retrieve previously successful radiotherapy cases that share various anatomical/physiological features with the current case. Using the optimization parameters from those references as a template for the current case, the IMRT/VMAT optimization time can be reduced and the plan quality can be guaranteed.

In this study, two similarity reference databases were first created from 100 previous static field IMRT cases and 100 previous VMAT cases. A vector model was then created using a combination of features extracted from the cases' CT images and structure contours in the DICOM-RT files. After the vector model was completed, the similarity between a present case and each reference case was measured by the direction cosine between their feature vectors. Planning parameters were retrieved from the selected most similar reference case and applied to the

present case to bypass many gradual adjustments of optimization parameters. Prostate cases were replanned with both the conventional manual optimization and the vector-model-based optimization based on the oncologists' clinical dose prescriptions. A total of 360 plans (30 cases of IMRT, 30 cases of 1-arc VMAT, and 30 cases of 2-arc VMAT plans including first optimization and final optimization with/without the vector-model-based optimization) were compared using the two-sided t-test and paired Wilcoxon signed rank test with a significance level of 0.05 with a false discovery rate of less than 0.05.

For IMRT, 1-arc VMAT and 2-arc VMAT prostate plans, there was a significant reduction in the planning time with the vector-model-based optimization by 2 hours ($p = 3.4\text{x}10^{-6}$), 5.44 hours ($p = 4.6\text{x}10^{-7}$) and 2.77 hours ($p = 1.7\text{x}10^{-6}$), respectively. Similarly, the number of iterations was significantly reduced with the vector-model-based optimization. From the first optimization plans comparison, CTV D_{99} of IMRT and 1-arc VMAT with the vector-model-based optimization was 0.7 Gy higher than that of the conventional manual optimization. The volume receiving 35 Gy in the femoral head for 2-arc VMAT plans was reduced by 10% with the vector-model-based optimization compared to the conventional manual optimization approach. Otherwise, the quality of plans from both approaches was comparable.

From the results, the vector model approach of former cases retrieval was shown to expedite the optimization of IMRT/VMAT while maintaining the plan quality.

PRESENTATIONS AND PUBLICATIONS

Oral Presentations

1. Sau Fan Liu, Vincent Wing Cheung Wu, Benjamin Harris, Matthew Foote, Margot Lehman, Lawrence Wing Chi Chan. Vector-model-based optimization in volumetric modulated arc stereotactic radiotherapy for brain tumours. Pinnacle User Group Meeting 2015, Sydney.
2. Sau Fan Liu, Vincent Wing Cheung Wu, Benjamin Harris, Margot Lehman, David Pryor, Lawrence Wing Chi Chan. Vector-model-based case retrieval approach in IMRT/VMAT prostate plan optimization. Engineering and Physical Sciences in Medicine 2016, Sydney.

Paper Publications

1. Sau Fan Liu, Vincent Wing Cheung Wu, Benjamin Harris, Matthew Foote, Margot Lehman, Lawrence Wing Chi Chan. Vector-model-based optimization in volumetric modulated arc stereotactic radiotherapy for brain tumours. Medical Dosimetry. 42(2): 79-84; 2017.
2. Sau Fan Liu, Vincent Wing Cheung Wu, Benjamin Harris, Margot Lehman, David Pryor, Lawrence Wing Chi Chan. Vector-model-supported approach in prostate plan optimization. Medical Dosimetry. 42(2): 85-89; 2017.

ACKNOWLEDGMENTS

I would like to express my deep gratitude to my supervisor Dr. Chan Wing Chi Lawrence for the continuous support of my PhD study. Without his encouragement and supervision, I would never complete my PhD. I am also grateful to Dr. Wu Wing Cheung Vincent for his contributions to the direction and richness of this research. In addition, I thank Dr. Fung Ka Lok Karl for his advice.

I also thank all my colleagues of radiation oncology Department at the Princess Alexandra Hospital for their help and encouragement. I am very grateful as well as thankful to my colleague Catherine Jones who kindly helped me to troubleshoot the MATLAB scripts and gave me many precious comments on my study. I would like to thank my colleague Paul Charles for his valuable advice. I would also like to thank Dr. Margot Lehman, Dr. David Pryor and Dr. Matthew Foote for their support.

Last but not least, I would like to thank my family: my parents and to my husband and children for supporting me throughout my PhD study and my life in general.

TABLE OF CONTENTS

FIGURE LEGENDS

TABLE LEGENDS

ABBREVIATIONS

AAA	analytic anisotropic algorithm
AACR	Australasian Association of Cancer Registries
AAPM	American Association of Physicists in Medicine
ACR	American College of Radiology
ADT	androgen deprivation therapy
AIHW	Australian Institute of Health and Welfare
AJCC	American Joint Committee on Cancer
AUA	American Urological Association
BAO	beam angle optimization
BEV	beam's-eye-view
BHFDR	Benjamini–Hochberg false discovery rate
CCCS	collapsed cone convolution superposition
CI	conformity index
CT	computed tomography
CTV	clinical target volume
DICOM	digital imaging and communications in medicine
DICOM-RT	digital imaging and communications in medicine in radiotherapy

DMPO	direct machine parameters optimization
DRE	digital rectal examination
DRR	digitally reconstructed radiograph
DVH	dose-volume histogram
DVO	dose volume optimizer
Dmax	maximum dose receiving
Dx	dose covering x % of the volume
EAU	European Association of Urology
FDR	false discovery rate
FOV	field of view
gEUD	generalized equivalent uniform dose
GS	Gleason score
Gy	gray
GTV	gross tumour volume
HI	homogeneity index
HU	Hounsfield Unit
IARC	International Agency for Research on Cancer
ICRU	International Commission on Radiation Units and Measurements

IM	internal margin
IMRT	intensity modulated radiotherapy
IOD	information objection definition
ITV	internal target volume
M	metastasis staging
MLCs	multileaf collimators
MRI	magnetic resonance imaging
MUs	Monitor Units
N	nodes staging
NCCN	National Comprehensive Cancer Network
NEMA	National Electrical Manufacturers Association
NTCP	normal tissue complication probability
OARs	organs at risk
PET	positron emission tomography
PIV	planned isodose volume
PSA	prostate-specific antigen
PTV	planning target volume
REV	room's-eye-view
ROI	region of interest

RT	radiotherapy
S&S IMRT	step-and-shoot IMRT
SM	setup margin
SOP	service-object pair
T	tumour staging
TCP	tumour control probability
TNM	tumour node metastasis
TPS	treatment planning system
TRUS	transrectal ultrasound
TURP	transurethral resection
TV	tumour volume
TV in PIV	tumour volume covered in planned isodose volume
UICC	Union for International Cancer Control
UID	unique identifier
VMAT	volumetric arc radiotherapy
Vx	volume receiving x Gy of dose

Chapter 1 Introduction

1.1 Intensity Modulated Radiotherapy (IMRT)

Radiotherapy is a cancer treatment option that uses radiation to damage the tumour cells making them unable to sustain life process or eventually suppressing their ability to divide and grow (Cancer Council Australia, 2016b). If the radiation dose is delivered at a rate such that it cannot be balanced by the repair mechanism of cancerous cells, their number and size will decrease, leading to the shrinkage and elimination of the tumour. Radiation can be delivered from outside the patient using a linear accelerator (external beam radiotherapy) or deposited from radioactive sources within the patient (brachytherapy) (National Cancer Institute, 2012b). In both cases, the main goal is to deliver the prescribed dose to the entire tumour volume while the surrounding healthy tissue receives as little dose as possible.

Intensity modulated radiotherapy (IMRT) is an external beam radiotherapy treatment modality that can achieve steep dose gradients between the tumour and nearby healthy tissue by using computer controlled multileaf collimators (MLCs) to divide a beam into smaller beamlets of varying radiation intensities (Bortfeld, 2006). IMRT, where the MLCs move while the gantry is stationary, is the treatment for tumours located in the brain, head and neck, lung, liver and prostate.

Volumetric modulated radiotherapy (VMAT) is a more recent development in intensity modulated radiotherapy that combines MLC motion with gantry speed and dose rate modulation (Kopp et al., 2011). Today, VMAT is the preferred treatment at the Princess Alexandra Hospital in Australia because of the shorter treatment time and

better plan quality for prostate cancer. Normally, IMRT treatment takes around 10-20 minutes whereas VMAT treatment takes approximately 3-5 minutes. The shorter VMAT treatment time increases patient comfort, decreases the influence of organ motion on the treatment results and increases the number of patients treated per day on a linear accelerator machine. Additionally, an IMRT plan involves just 7-9 beams of static gantry angle, whereas a VMAT plan allows 360 degrees gantry rotation around the patient which spreads dose in healthy tissues over a larger volume and therefore delivers a much lower dose per unit volume to non-target tissue. Hence, a VMAT plan can offer superior plan quality over a static beam IMRT plan (Quan et al., 2012; Pancewicz-Janczuk, Topczewska-Bruns, & Filipowski, 2013; Dewhurst, Lucas, & Hardy, 2015).

1.2 Issues of IMRT/VMAT Optimization

1.2.1 Difference between Optimized Dose and Final Dose

In order to create an IMRT or a VMAT plan, the planner must first obtain a computed tomography (CT) data set of the patient. Next, the planning target volume (PTV) and organs at risk (OARs) need to be contoured. This can be done in the contouring mode of the treatment planning system (TPS). From there, initial beams of appropriate angles are created in the planning mode. Then, an optimization module iteratively alters the intensity modulation to best meet the objectives entered by the planner. These objectives are generally limits on the minimum dose received by the target volume and maximum dose received by OARs.

In the Eclipse TPS (Varian Medical Systems, Palo Alto, CA) and Pinnacle TPS (Philips Radiation Oncology Systems, Fitchburg, WI), a fast dose algorithm during optimization is performed to save the optimization time (Varian Medical Systems, 2010; Philips Medical Systems, 2008).

Once the optimization module has reached its end point (e.g. after number of iterations), a final dose calculation using Analytic Anisotropic Algorithm (AAA) in Eclipse or Collapsed Cone Convolution Superposition (CCCS) in Pinnacle calculates the final dose distribution with all dosimetric MLC leaf sequencing parameters and heterogeneity corrections (Philips Medical Systems, 2008; Varian Medical Systems, 2010). Dose differences are always observed between the optimization dose and the final dose due to different dose algorithms. This is because the initial optimization calculates dose with the fast dose algorithm which does not account for heterogeneity (Varian Medical Systems, 2010; Philips Medical Systems, 2008). Also the optimization in Eclipse does not account for the physical and dosimetric characteristics of the MLC (Varian Medical Systems, 2010). Hence, final dose calculation with the superior accurate dose algorithm is required for accurate dose calculation (Varian Medical Systems, 2010; Philips Medical Systems, 2008; Ezzell et al., 2003).

1.2.2 Local Minima

IMRT/VMAT treatments often incorporate a higher number of fields than the conventional conformal radiotherapy plan. This has the advantage of depositing dose from various directions, enabling escalated dose to targets and reduced dose to critical organs (Webb, 2005). According to the American Association of Physicists in Medicine (AAPM) Report No. 82 (Ezzell et al., 2003), deterministic methods and

stochastic methods are two principles of planning optimization. Deterministic methods (e.g. gradient descent) search for an optimal solution using the gradient of the objective function. Gradient descent method is a quick way to find a minimum, but it may get trapped in a local minimum (Ezzell et al., 2003). On the other hand, stochastic methods (e.g. simulated annealing) seek an optimal solution by randomly changing beamlet intensities to avoid a local minimum (Ezzell, et al., 2003). These stochastic methods are much more time-consuming than deterministic methods (Chu, Zinchenko, Henderson, & Sharpe, 2005; Xing, Li, Donaldson, Le, & Boyer, 1999). Speed of the optimization using the gradient descent method is the real advantage in comparison to stochastic methods (Ezzell et al., 2003).

The optimization in Eclipse TPS and in Pinnacle TPS both use the deterministic gradient descent method which quickly converges to a minima (Philips Medical Systems, 2008; Varian Medical Systems, 2010). Although the gradient descent method may not return the optimal solution if the optimization finds a local minima, this local minima may often provide a solution which is clinically acceptable.

1.2.3 Lengthy Optimization Time

Most commercial planning systems use deterministic method based algorithms to provide fast optimization. However, the planner spends a long time manually adjusting the dose constraint parameters to meet the requirements for a clinically acceptable plan because of the difference between the fast optimization estimation and final dose calculation (Bortfeld, 2006; Zhang et al., 2010). Thus conventional inverse planning involves a trial-and-error dose-volume optimization method, and the quality heavily depends on the experience of the planner (Webb, 2003). However,

there is no guarantee that the final plan is truly optimized even if a large amount of time has been spent on optimization. This is because there can be many local minima solutions of the optimization equation (Wu & Mohan, 2002). A more optimal plan may be achievable with different optimization parameters.

1.2.4 Adaptive IMRT/VMAT Planning

The location and size of the tumour and OARs may change during the treatment course due to tumour shrinkage, weight change and the presence of the rectal gas. There is an increasing need for adaptive IMRT/VMAT planning to allow treatment to continue after detected changes in the volume, shape and location of critical structures in the patient. In some plans the use of minimal margins around the PTV without accounting for anatomical changes may result in poor tumour coverage and therefore increased probability of recurrence. When the anatomy has changed the planner needs to create a new treatment plan as soon as possible for the remaining treatment fractions. Due to this limited time frame and current long optimization times, the plan quality of adaptive IMRT/VMAT may be compromised.

1.2.5 Optimization Algorithms in Research

To optimize an IMRT/VMAT plan faster, some authors have researched different optimization algorithms (Breedveld, Storchi, Keijzer, Heemink, & Heijmen, 2007; Lu, 2007). However, they are not easy to verify and implement on a commercial TPS because the commercial TPS is a complete standalone software package and does not allow any external optimization algorithms to be implemented in its system.

1.2.6 Template Solution without Any Similarity Comparison

TPS provides structures, plans and objectives templates as starting points for IMRT/VMAT planning, but it is up to the planner to choose the most appropriate template. Template choice is subjective, and the planner may not know if a template is suitable for the current case, and whether it has been successful meeting oncologist's dose constraint criteria in similar previous cases.

1.2.7 Lack of References

An optimal plan in modern IMRT treatment planning is generated through the processing of a large amount of patient-related data in pursuit of finding optimal values to a number of treatment parameters. There is no available reference database that allows comparison with previous similar cases for which those parameters values were already found. Every IMRT/VMAT plan is based on an individual oncologist's preferences of prescription dose and an individual planner's experience. While previous similar plans could be used as starting points for those treatment parameters, it is not feasible to manually identify, retrieve and assess all similar IMRT/VMAT cases from thousands of patient records for every patient because the workload would prohibitively increase the planning time.

1.3 Study Purpose

The purpose of this study is to improve the IMRT/VMAT optimization results and reduce IMRT/VMAT planning optimization time by providing a planning parameters template through the vector-model-based reference to previous successful radiotherapy cases. The goal of this PhD research was to develop a vector-model-based, retrieval of similar radiotherapy cases, with respect to the structural and physiological features extracted from the diagnostic images and structure contour files. Measures of plan quality, such as the normal tissue dose, the target coverage, conformity, and homogeneity of the plan generated by the vector model were compared with the conventional manual planning approach. The proposed approach is a robust planning technique able to quickly generate IMRT/VMAT plans, and the planning parameters provided by the vector model require fewer adjustments than the existing approach to fulfill the dose constraint criteria. The feature extraction, similarity calculation and statistical analysis were all performed in MATLAB (The MathWorks, Inc., version 7.10.0.499, 2010).

1.4 Research Question

Does the vector-model-based retrieval approach of reference cases outperform the conventional manual approach in reducing the IMRT/VMAT planning time and maintaining the plan quality?

1.4.1 Research Hypothesis

IMRT/VMAT plan with the vector-model-based approach can reduce IMRT/VMAT planning time and guarantees that the plan quality is comparable with the plan developed using the conventional manual approach.

1.4.2 Objectives of the Study

1. To develop MATLAB scripts for features extraction from Digital Imaging and Communications in Medicine (DICOM) files
2. To implement a vector model for the IMRT/VMAT previous cases database
3. To apply the vector-model-based approach for reference case searching among cases with similar tumour size, tumour volume, OAR volume and overlap volume between the tumour and the OAR.
4. To compare the IMRT/VMAT plans between the vector-model-based optimization and the conventional manual optimization approach regarding the planning time, the number of monitor units (MUs), the target coverage, the conformity, the homogeneity index, and the normal tissues dose.

The IMRT/VMAT cases were collected retrospectively. As this vector model approach is a new concept to radiotherapy, it is not currently being used to generate plans for treatment. The new approach will not be used clinically until it has been tested, and the ethics approval is offered by Hong Kong Polytechnic University and the oncology department at the Princess Alexandra Hospital. Clinical treatment outcomes cannot be compared because patients have different sensitivity to radiation, different chemotherapy response and different initial health status. To have an objective and realistic conclusion, the aim of this study was to compare the planning time and the dose-volume histogram (DVH) results from the existing conventional IMRT/VMAT approach with the vector-model-based approach.

1.4.3 Data Collection

This was a retrospective study in which the previous IMRT/VMAT plans data were retrieved and were used to compare the effectiveness of optimization with the vector model and the existing conventional manual optimization. Since this was a retrospective study, informed consent was not required. Unique study numbers were used to identify particular cases and patient identity was not known throughout the study. The human research ethics approvals were obtained from the Hong Kong Polytechnic University and the clinical radiotherapy department at the Princess Alexandra Hospital.

To record the planning time for each optimization method, a total of ninety previous IMRT/VMAT plans were replanned using the conventional manual optimization approach and the vector-model-based optimization approach as a template for the planning parameters. Next, the OARs dose, the target dose, the

conformity and the homogeneity of the vector-model-based optimization approach and the conventional manual optimization for the same case were compared. This study has focused on prostate IMRT/VMAT cases due to the high number treated in the clinical radiotherapy department at the Princess Alexandra Hospital. To have enough cases for statistical comparison, only prescriptions of 78 Gray (Gy) in 39 fractions were included. 66 Gy in 33 fractions were excluded due to limited number of cases.

All static beams step-and-shoot IMRT (S&S IMRT) cases were replanned using Eclipse TPS version 10.0 (Varian Medical Systems, Palo Alto, CA) and all VMAT cases were replanned using Pinnacle TPS version 9.4 and 9.8 (Philips Radiation Oncology Systems, Fitchburg, WI). One hundred prostate step-and-shoot IMRT (S&S IMRT) cases and one hundred prostate VMAT cases were chosen as references. Thirty new prostate S&S IMRT cases, thirty new prostate 1-arc VMAT and thirty new 2-arc VMAT were planned with and without the vector model and statistically analysed. A total of 360 plans (30 cases of IMRT, 30 cases of 1-arc VMAT, and 30 cases of 2-arc VMAT plans including first optimization and final optimization with/without the vector-model-based optimization) were compared using the two-sided t-test or paired Wilcoxon signed rank test with a significance level of 0.05 with false discovery rate (FDR) of less than 0.05.

1.5 Outline of the Thesis

This thesis is split into six chapters and is organized as follows. Chapter 1 introduces this thesis including existing planning issues, purpose and a brief methodology of this study. Since this study concentrates on the prostate cancer IMRT/VMAT plans, chapter 2 provides background on the prostate, prostate cancer statistics, prostate cancer treatments, radiotherapy planning, planning optimization and DICOM information for this research. In order to provide a better perspective on this study, chapter 3 describes the details of the study methodology. It provides detailed information about the vector model solution for IMRT/VMAT such as feature extraction, the vector model implementation, similarity calculation, planning parameters and statistical analysis. Chapter 4 presents the results of this study such as features extraction, the vector model implementation, and plans comparison. Chapter 5 discusses the research findings and limitations. Finally, chapter 6 concludes this study.

Chapter 2 Background

2.1 Prostate Gland

The prostate displayed in Figure 2.1 is a small gland that is part of the male reproductive system (Cancer Council Australia, 2010). It produces the main component of seminal fluid, which protects sperm (Cancer Council Australia, 2016a; National Cancer Institute, 2012b). The prostate relies on the male hormone testosterone to grow and develop (Cancer Council Australia, 2016a). The prostate is about the size of a walnut and is located between the rectum and the bladder.

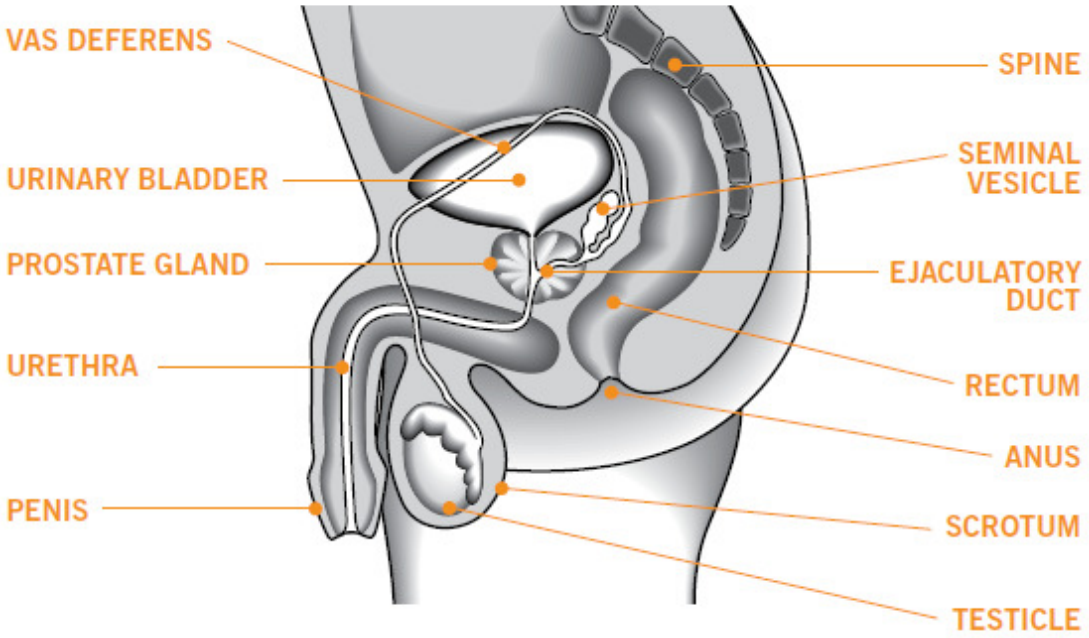

Figure 2.1. Prostate anatomy. Adapted from "Localised prostate cancer: a guide for men and their families (p. 9)," by Cancer Council Australia, 2010. Retrieved from http://www.cancer.org.au/content/pdf/HealthProfessionals/ClinicalGuidelines/Localised_Prostate_Cancer_book_Web_2010.pdf. Copyright 2010 by Cancer Council Australia.

2.2 Prostate Cancer

Tumor causes cells to behave abnormally and grow into a lump, which can be benign or malignant. Prostate cancer is a malignant growth in the prostate gland. It can be categorized as localized prostate cancer, locally advanced prostate cancer or metastatic prostate cancer.

2.2.1 Statistics of Prostate Cancer

The International Agency for Research on Cancer (IARC, 2012) reported that prostate cancer was the second most common cancer in men worldwide in 2012. The incidence of prostate cancer is highest in Australia/New Zealand. The combination of digital rectal examination, prostate-specific antigen (PSA) serum testing, and subsequent biopsy has become widespread in Australia/New Zealand (IARC, 2012). The Australian Institute of Health and Welfare (AIHW) and the Australasian Association of Cancer Registries (AACR) (2012) predicted that there are about 20,000 new prostate cancers diagnosed in Australia every year (see Figure 2.2), accounting for approximately 30% of all new cancers in men. The AIHW (2012) estimated that Australian men have a one in five chance of being diagnosed with prostate cancer before the age 85 because the chance of prostate cancer increases with age (Figure 2.3), with more than 80% of prostate cancer patients being aged over 60 in 2012. The AIHW (2012) suggested that prostate cancer is the second leading cause of cancer death in Australian men.

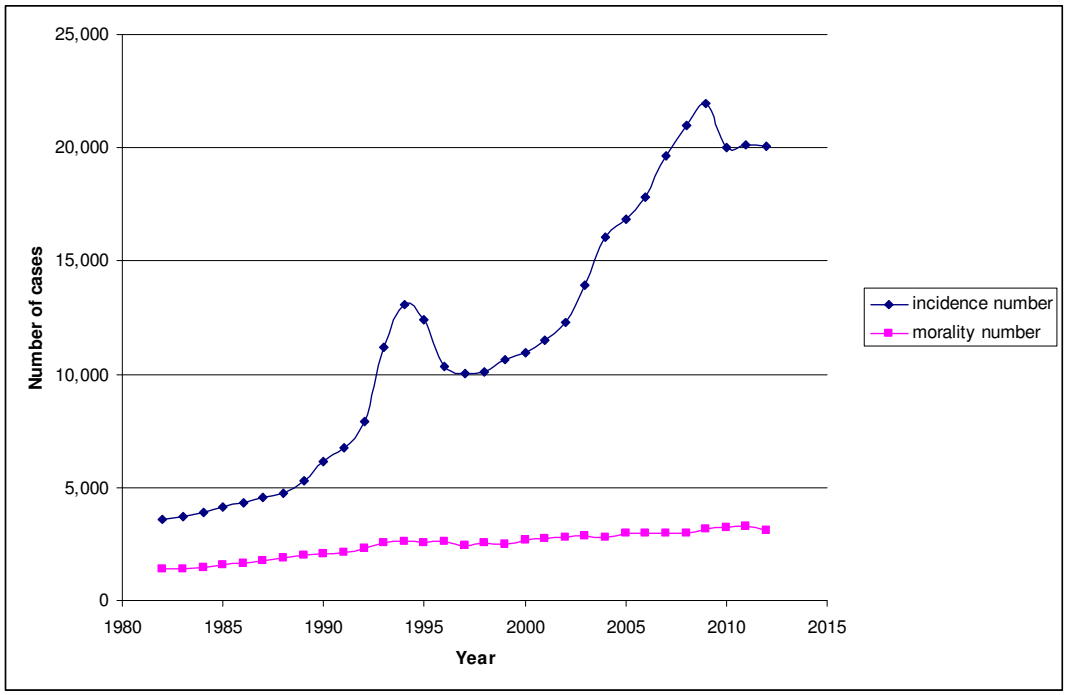

Figure 2.2. Trends of prostate cancer incidence and mortality in Australian men 1982-2012.

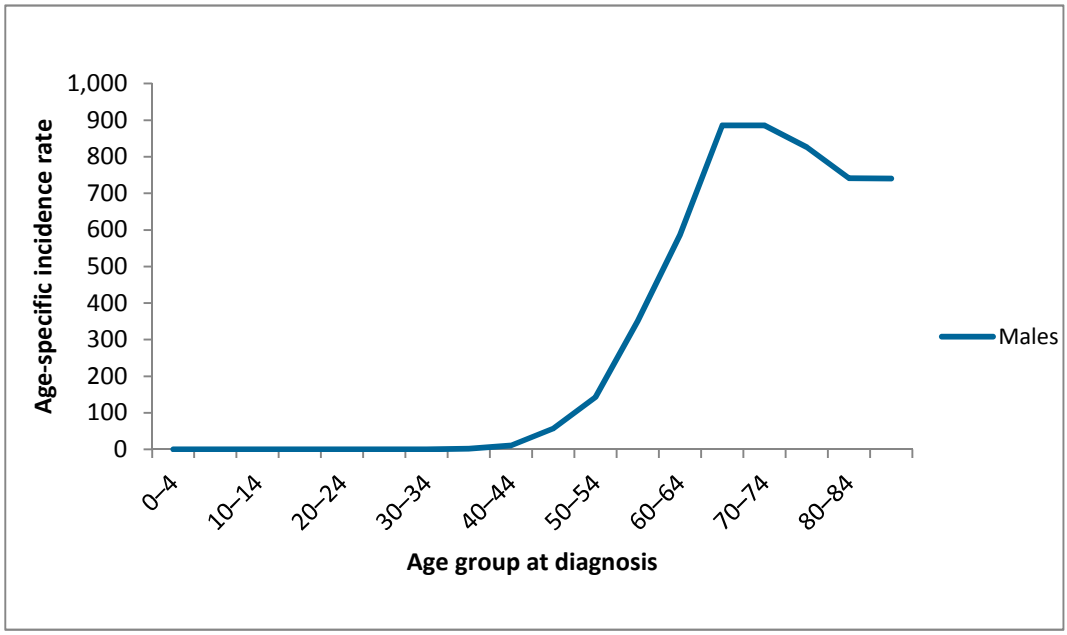

Figure 2.3. Age-specific incidence rates in Australia for 2012.

2.2.2 Diagnosis of Prostate Cancer

2.2.2.1 Prostate-specific Antigen (PSA)

Prostate-specific antigen (PSA) is a protein in blood that is produced by the prostate gland (National Cancer Institute, 2012a; Cancer Council Australia, 2009). The general guideline for suspicion of prostate cancer is a PSA threshold of 4.0 ng/ml (National Cancer Institute, 2012a; Chou et al., 2011). A high PSA reading warrants further investigation because it may indicate prostate cancer, or a benign condition such as benign prostatic enlargement (Cancer Council Australia, 2010). Croswell, Kramer, and Crawford (2011) commented that the PSA test has limitations of specificity (false positive detection) and sensitivity (false negative detection). Thus, screening based on PSA levels alone is not recommended (Cancer Council Australia, 2010).

2.2.2.2 Digital Rectal Examination

The digital rectal examination (DRE) checks for abnormality in size, shape or texture of the prostate gland (National Cancer Institute, 2012b; Council Australia, 2010). The doctor examines the prostate through the rectal wall with a gloved and lubricated finger (see Figure 2.4). The ability of DRE to determine the clinical stage is limited because the doctor's finger cannot reach the whole prostate, and cannot detect a very small tumour (Cancer Council Australia, 2016a). Therefore, DRE is often performed at the same time as a PSA test for prostate cancer diagnosis (Cancer Council Australia, 2010).

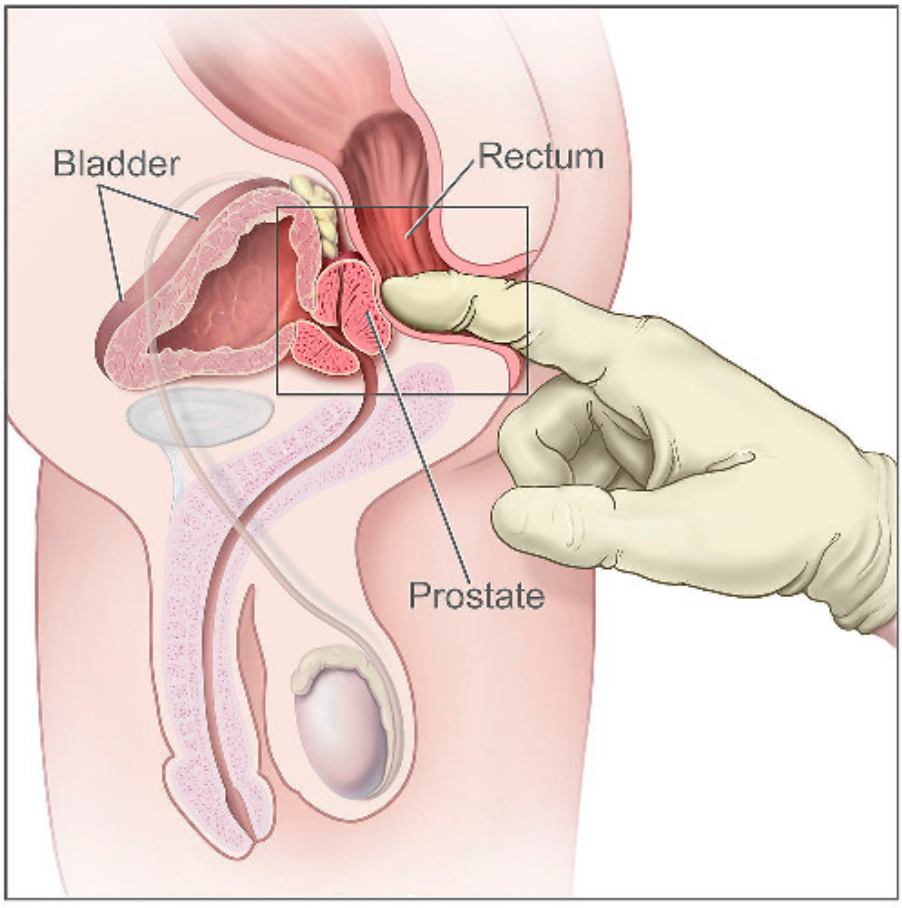

Figure 2.4. DRE examination. Adapted from "Digital Rectal Exam (Male)," by A. Hoofring, 2007. Retrieved from https://visualsonline.cancer.gov/details.cfm?imageid=4351. Copyright 2007 by National Cancer Institute. Reprinted with permission.

2.2.2.3 Prostate Biopsy

The biopsy takes small pieces of prostate tissue which are sent to a pathologist to differentiate benign and malignant conditions. The most common biopsy technique is transrectal ultrasound (TRUS) guided biopsy. Magnetic resonance imaging (MRI) provides better image quality than ultrasound image so the latest MRI-guided targeted biopsy can localize the prostate lesion better than TRUS guided biopsy (see Figure 2.5). Therefore, this technique can reduce the frequency of false-negative findings from the ultrasound-guided biopsy, hence reducing the number of repeat biopsies (Liu, Tian, Zhang, & Fei, 2016).

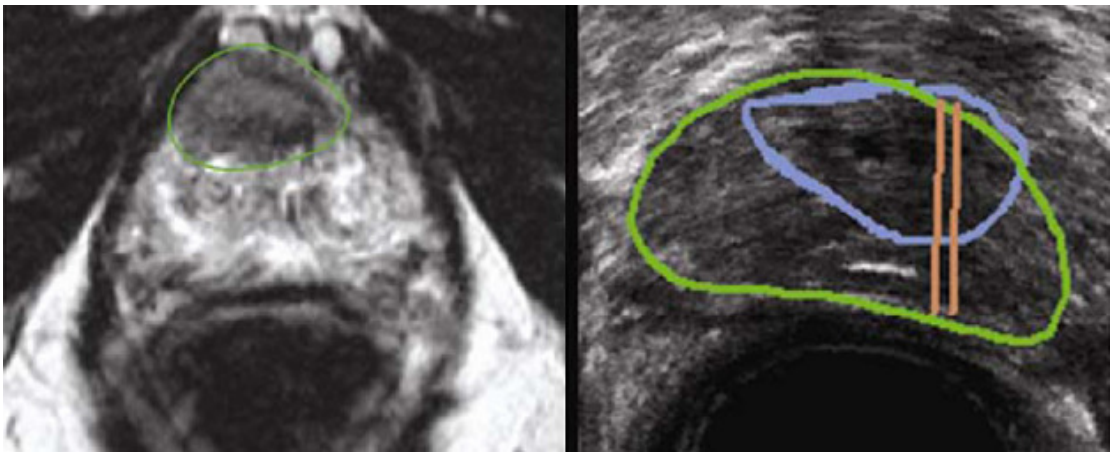

Figure 2.5. MRI (left) and ultrasound (right) images target the same prostate lesion. Adapted from "Computer-aided Detection of Prostate Cancer with MRI: Technology and Applications (p.1039)," by L. Liu, Z. Tian, Z. Zhang, and B. Fei, 2016, *Academic Radiology, 23(8)*, 1024-1046. doi: 10.1016/j.acra.2016.03.010. Copyright 2016 by the Association of University Radiologists. Adapted with permission.

2.2.3 Classification of Prostate Cancer

The cancer grade and the cancer stage both affect the treatment decision (Cancer Council Australia, 2016a). The stage of prostate cancer shows how far the cancer has spread from the prostate. The clinical staging can be found by digital rectal examination, PSA blood test, ultrasound, bone scan, CT, MRI or positron emission tomography (PET) scan. The pathological staging is the examination of the prostate tissue (Cancer Council Australia, 2016a).

The Tumour-Node-Metastasis (TNM) classification is used to classify the stage of the cancer. The definition of TNM (American Joint Committee on Cancer [AJCC], 2009; Union for International Cancer Control [UICC], 2010) is partially summarized in Table 2.1.

Table 2.1. Part of TNM staging system for prostate cancer.

Primary tumour (T)	
T1	Tumour is so small that is not palpable or visible by imaging
T1a	Tumour histologic finding ≤ 5% of resected tissue
T1b	Tumour histologic finding > 5% of resected tissue
T1c	Tumour identified by biopsy
T2	Tumour can be felt, but is confined within prostate
T2a	Tumour involves ≤ half of one lobe
T2b	Tumour involves > half of one lobe but not both lobes
T2c	Tumour involves both lobes
T3	Tumour extends outside the prostate
T3a	Extracapsular extension

T3b	Tumour invades seminal vesicle(s)
T4	Tumour invades adjacent structures other than seminal vesicles
Lymph nodes involvement (N)	
N0	No regional lymph node involvement
N1	Tumour is found in regional lymph node(s)
Distant metastasis (M)	
M0	No distant metastasis
M1	Distant metastasis

2.2.4 Gleason Grading system

The grade of the prostate cancer shows how fast the cancer grows and the Gleason score is a pathological scale to grade prostate cancer (Cancer Council Australia, 2009). The pathologist differentiates the two most common tissue patterns and gives them a score from 1 (well differentiated) to 5 (poorly differentiated) (Cancer Council Australia, 2016a). The first number is the most common pattern and the second number is the next most common pattern. Two numbers added together to give the Gleason score (GS) out of 10 (Thompson el al., 2007). Table 2.2 summarizes the Gleason score and the corresponding grade. Low-grade prostate cancer is more likely to grow slowly and is less likely to spread (Cancer Council Australia, 2010).

Table 2.2. Gleason grading system.

Gleason score	Grade
GS ≤6	Low grade, well differentiated tumour
GS 7	Intermediate grade, moderately differentiated
GS 8-10	High grade, poorly differentiated or undifferentiated

2.2.5 Risk Stratification Systems

The prostate cancer risk stratification system combines the clinical staging, pre-treatment PSA, and Gleason score to categorize treatment outcome in terms of low risk, intermediate risk, and high risk (Cancer Council Australia, 2010). There are many organizational risk stratification systems have been developed by various cancer organizations such as American Urological Association (AUA), European Association of Urology (EAU), and National Comprehensive Cancer Network (NCCN) (Rodrigues, et al., 2012). All prostate cancer patients are stratified into low risk, intermediate risk, and high risk at the Princess Alexandra Hospital as per NCCN clinical practice guidelines (Mohler et al., 2010) demonstrated in Table 2.3.

Table 2.3. Prostate cancer risk stratification systems.

Risk level	Clinical stage	Gleason score	PSA level (ng/ml)
Low risk	T1-T2a	≤6	<10
Intermediate risk	T2b-c	7	10-20
High risk	T3	8-10	>20

2.3 Treatment of Prostate Cancer

Some prostate cancer grows so slowly that the patient does not require treatment (Cancer Council Australia, 2010). However, some prostate cancer requires treatment including radical prostatectomy, radiotherapy, chemotherapy or hormonal treatments.

2.3.1 Radical Prostatectomy

Radical prostatectomy is surgical treatment of prostate cancer that removes the prostate, the seminal vesicles, part of urethra and small part of the vas deferens (which pass through the prostate) shown in Figure 2.6 (Cancer Council Australia, 2010). Cancer Council Australia (2010) suggested that radical prostatectomy is a good option for a localised prostate cancer patient who is fit for surgery and expected to live longer than 10 years. The most common side effects of radical prostatectomy are urinary incontinence, erectile dysfunction and infertility (Cancer Council Australia, 2010).

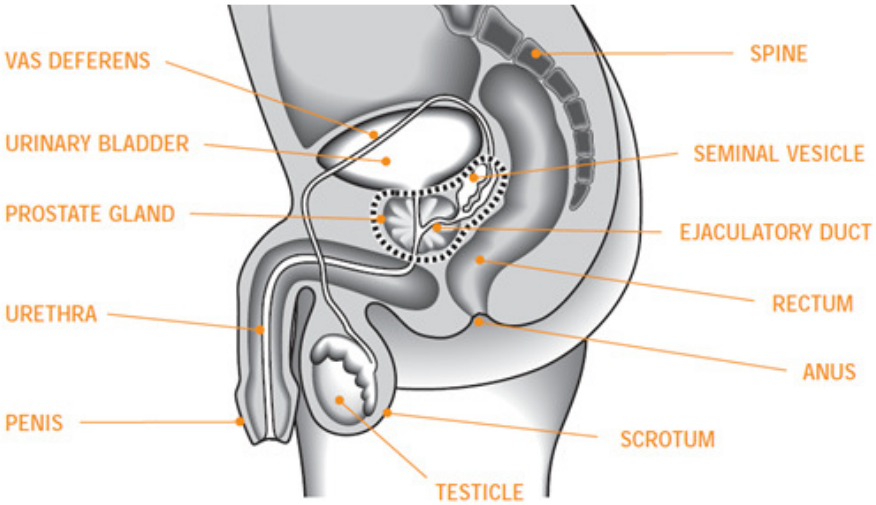

Figure 2.6. Radical prostatectomy removes the organs surrounded by the dotted line. Adapted from "Localised prostate cancer: a guide for men and their families (p. 39)," by Cancer Council Australia, 2010. Retrieved from http://www.cancer.org.au/content/pdf/HealthProfessionals/ClinicalGuidelines/Localised_Prostate_Cancer_book_Web_2010.pdf . Copyright 2010 by Cancer Council Australia.

2.3.2 Hormone Therapy

The male hormone testosterone is required for prostate cancer cells to grow (Cancer Council Australia, 2009). Androgen deprivation therapy (ADT) or hormone therapy is used to reduce the growth of the cancer by controlling the hormone testosterone level. The side effects of ADT include tiredness, hot flushes, breast growth, erection problems, depression and loss of bone strength (Cancer Council Australia, 2009).

2.3.3 Chemotherapy

In chemotherapy drugs are injected into the bloodstream to kill advanced prostate cancer cells. Chemotherapy damages cancer cells as well as healthy normal cells, and the common side effects of chemotherapy include fatigue, mouth sores, diarrhoea, nausea and hair loss (Cancer Council Australia, 2009).

2.3.4 Radiotherapy of Prostate Cancer

Radiotherapy can treat any stage of prostate cancer. Early-stage prostate cancer can be treated with radiotherapy to avoid the surgical complications. For advanced stage prostate cancer, radiotherapy can destroy the tumour bed after surgery or relieve pain. Radiotherapy uses high energy beams to kill cancer cells. External beam radiotherapy and brachytherapy are two types of radiotherapy. The common side effects of radiotherapy are tiredness, bowel and bladder problems (Cancer Council Australia, 2016a). Radiotherapy offers excellent clinical outcomes with acceptable toxicity (Shiraishi, Yamamoto, Haga, Sakumi, & Nakagawa, 2014; Spratt et al., 2012).

2.3.4.1 Brachytherapy

During brachytherapy a radioactive source is placed inside the tumour. Brachytherapy can be given at either a low dose rate or at a high dose rate. In low dose rate brachytherapy, permanent radioactive seeds are permanently inserted into the prostate. In high dose rate brachytherapy, a single radioactive source irradiates the prostate by moving through temporary needle implants for few minutes in Figure 2.7. Disadvantages of brachytherapy include patient's discomfort, implantation problems such as prostate swelling or seeds dislodged, and increase in resources.

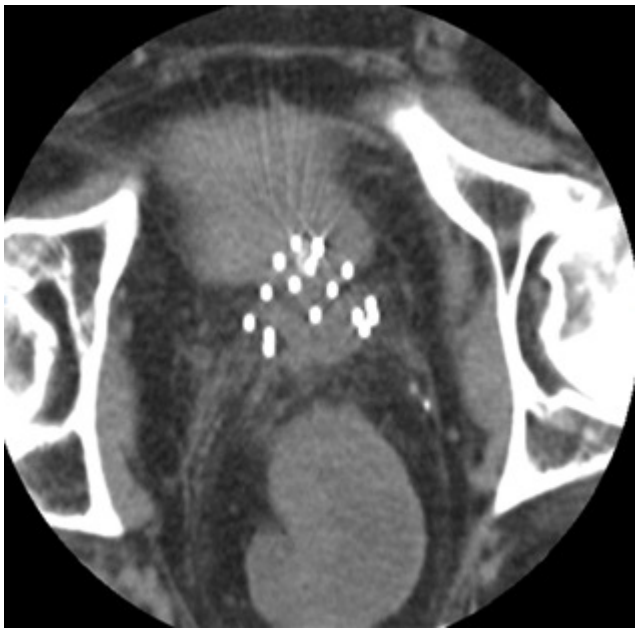

Figure 2.7. Prostate high dose rate brachytherapy.

2.3.4.2 External Beam Radiotherapy

External beam radiotherapy uses the radiation beam generated from a machine external to the body. External beam radiotherapy is planned to ensure a high dose of radiation is delivered accurately to the tumour target while minimizing the harm to the normal surrounding tissues. Treatment planning system is used to create an IMRT

plan or a VMAT plan for prostate cancer. According to NCCN clinical practice guidelines (Mohler et al., 2010), a prescribed dose of 75.6 to 79 Gy is appropriate dose for low-risk prostate cancers, and 75 to 80 Gy for intermediate and high-risk prostate cancers. Each IMRT delivery usually takes about 15 minutes and treatments are usually 5 days per week for eight to nine weeks. VMAT delivery in Figure 2.8 takes even shorter time that is within 10 minutes for each VMAT delivery.

Figure 2.8. Example of gantry rotation during VMAT delivery. Adapted from "Elekta Synergy," by R. Canzeri, 2010. Retrieved from http://blog.elekta.com/blog/2010/10/fortis-hospitals-launches-comprehensive-cancer-care-under-one-roof/elekta-synergy-oncology-linac_jpg-med/. Copyright 2010 by Elekta.

2.4 Radiotherapy Planning

Radiotherapy planning first requires a CT image acquisition, and then the oncologist draws regions of interest (ROIs) on the CT images. Next, the planner arranges the beams and optimizes the dose constraints for the IMRT/VMAT plan.

2.4.1 CT Images

A CT scan is mandatory to locate the tumour target and normal tissues, and to derive the electron density information necessary for a quantitative dose calculation. The standard CT scanning protocol for prostate at the Princess Alexandra Hospital is 2 mm slice thickness and 550 mm field of view (FOV).

The boundary of prostate gland is difficult to see from the CT images (Figure 2.9). MRI and PET images can assist with tumour localization and assessment of tumour extent. MRI can help to differentiate the prostate boundary seen in Figure 2.10. Although the use of MRI and PET-CT is increasing, most of IMRT/VMAT cases are still planned without any MRI or PET-CT images. Due to the cost of MRI or PET-CT scans, the accessibility of MRI or PET-CT facility is still limited.

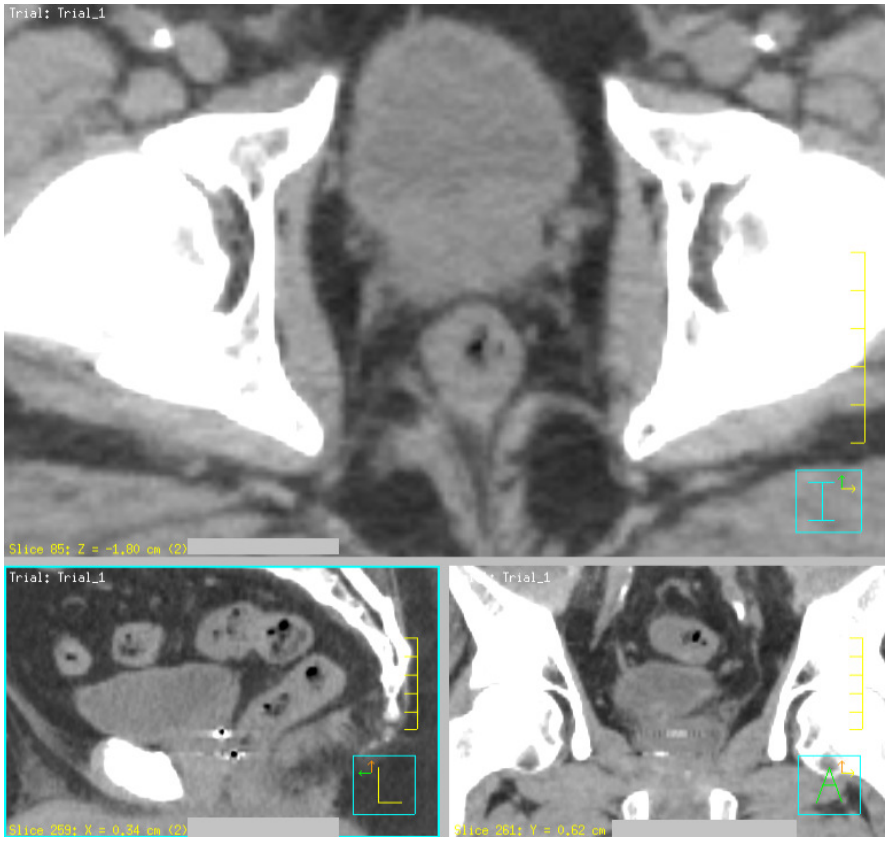

Figure 2.9. Prostate is difficult to differentiate from bladder in the CT images.

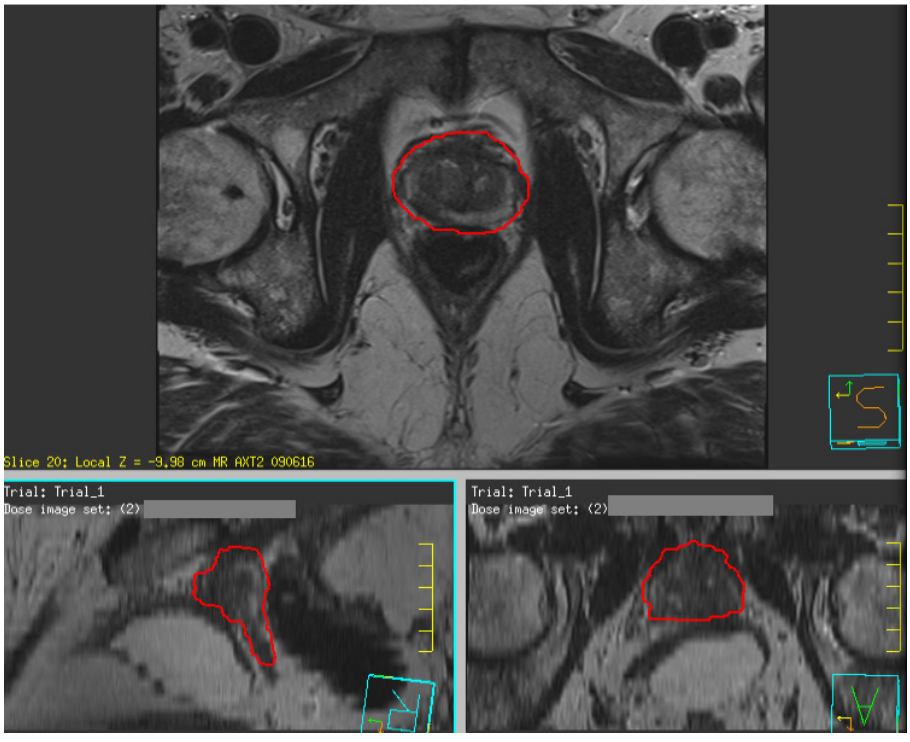

Figure 2.10. Prostate is easier to differentiate from bladder in the MRI images.

2.4.2 Prostate Target Delineation

The oncologist draws the tumour target as a region of interest (ROI) for the IMRT/VMAT planning. According to the International Commission on Radiation Units & Measurements (ICRU) Report 50 (1993), Gross Tumour Volume (GTV) contains the mass of tumour that is visible on CT images. The tumour mass is usually surrounded by subclinical microscopic malignant disease that is too small to be visible on any imaging. To account for this, the GTV is expanded by a margin in order to make sure that the entire tumour is included in the irradiated volume. This expanded volume is the Clinical Target Volume (CTV). To account for daily setup variations and uncertainties in patient and beam positioning, as well as tumour motion caused by breathing or variation in filling of adjacent organs, the CTV is further widened to create the Planning Target Volume (PTV).

ICRU Report 62 (1999) introduced the Internal Target Volume (ITV) that consists of the CTV surrounded by an Internal Margin (IM) taking in account variation in size, shape and position of the organ motion. The PTV includes the ITV and a setup margin to account for the uncertainty in patient setup error. GTV, CTV and PTV are illustrated in Figure 2.11.

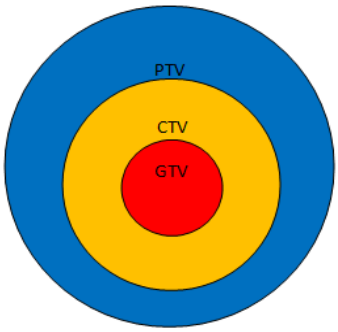

Figure 2.11. GTV, CTV and PTV of the tumour target.

Tumour in the prostate is difficult to differentiate from the soft tissue on the CT images, so it is not possible to delineate the GTV on the CT images. Hence, CTV and PTV are the main target ROIs for prostate cancer. CTV delineation is determined by the risk stratification of prostate cancer patient and example of CTV delineation is shown in Table 2.4.

. The PTV margin is dependent on the setup protocol and measurement of random and systematic errors in prostate position. Example of prostate target delineation is in Figure 2.12.

Table 2.4. CTV delineation related to the risk stratification system.

Risk level of prostate cancer	CTV contouring
Low risk	Prostate only.
Intermediate risk	Prostate ± proximal 1-2 cm of seminal vesicles.
High risk	• Prostate and proximal 2 cm of seminal vesicles, visible extra-capsular extension disease. • For T3b, prostate and whole seminal vesicles. • For T3a or a high-risk of extra-capsular extension, a 2- to 5-mm margin around the prostate and known extra-capsular extension of disease.

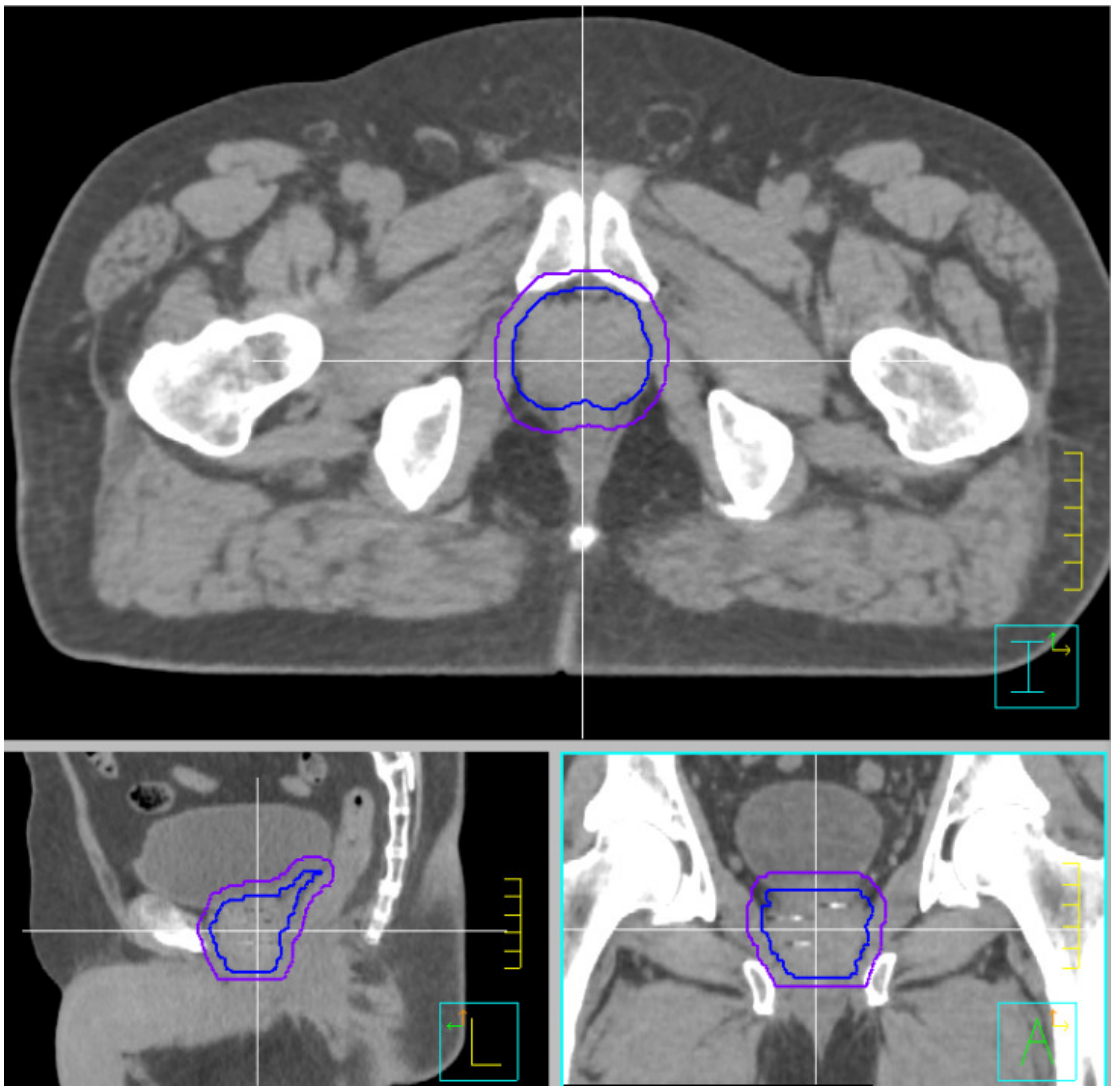

Figure 2.12. CTV is in blue color and PTV is in purple color. CTV covers prostate and seminal vesicles because this patient has high risk prostate cancer.

2.4.3 Beams Setup

2.4.3.1 IMRT Beams Setup

Before proceeding to optimization, the number and gantry/collimator angles of beams to be used need to be chosen in IMRT shown in Figure 2.13. Eclipse TPS offers the option of Beam Angle Optimization (BAO) which is capable of calculating optimal beam numbers and angles for the user (Varian Medical Systems, 2010). Despite this, many experienced planners prefer to do it manually, and it is not in clinical use in this department. The planner uses the beam's-eye-view (BEV) in Figure 2.14 to adjust the gantry angle and collimator angle to minimize the irradiation of rectum, bladder and femoral heads while maximizing the target irradiation. Usually five to seven IMRT beams are required for prostate cancer treatment.

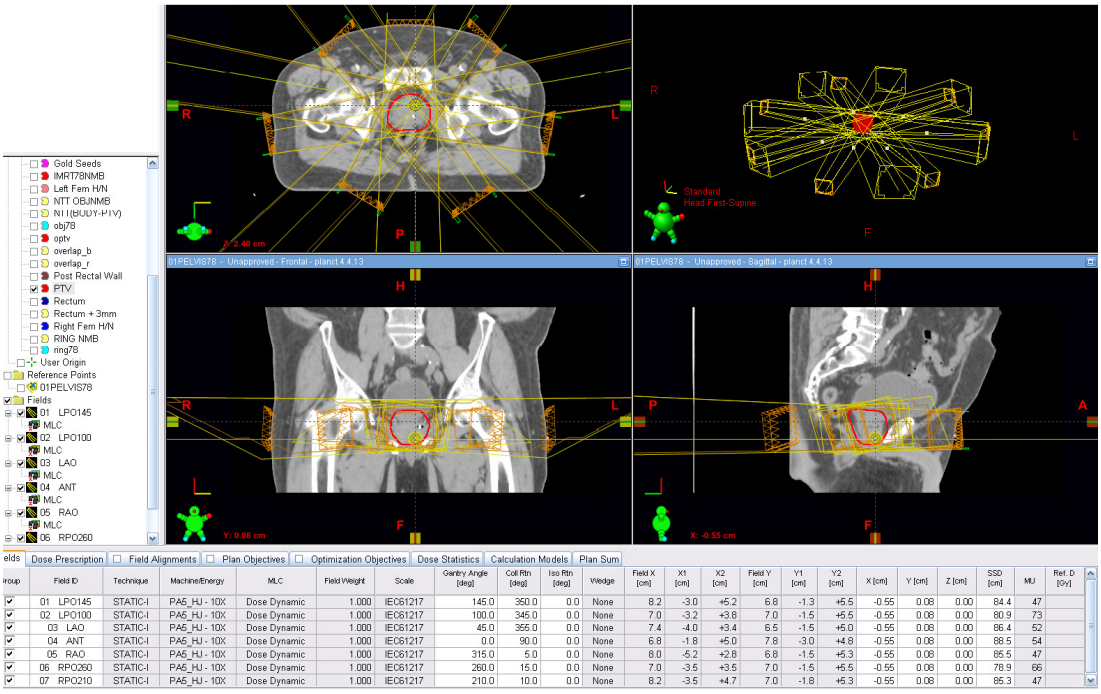

Field ID	Technique	Machine/Energy	MLC	Field Weight	Scale	Gantry Angle [deg]	Coll Rtn [deg]	Iso Rtn [deg]	Wedge	Field X [cm]	X1 [cm]	X2 [cm]	Field Y [cm]	Y1 [cm]	Y2 [cm]	X [cm]	Y [cm]	Z [cm]	SSD [cm]	MU	Ref. D [Gy]
01 LPO145	STATIC-I	PA5_HJ - 10X	Dose Dynamic	1.000	IEC61217	145.0	350.0	0.0	None	8.2	-3.0	+5.2	6.8	-1.3	+5.5	-0.55	0.08	0.00	84.4	47	
02 LPO100	STATIC-I	PA5_HJ - 10X	Dose Dynamic	1.000	IEC61217	100.0	345.0	0.0	None	7.0	-3.2	+3.8	7.0	-1.5	+5.5	-0.55	0.08	0.00	80.9	73	
03 LAO	STATIC-I	PA5_HJ - 10X	Dose Dynamic	1.000	IEC61217	45.0	355.0	0.0	None	7.4	-4.0	+3.4	6.5	-1.5	+5.0	-0.55	0.08	0.00	86.4	52	
04 ANT	STATIC-I	PA5_HJ - 10X	Dose Dynamic	1.000	IEC61217	0.0	90.0	0.0	None	6.8	-1.8	+5.0	7.8	-3.0	+4.8	-0.55	0.08	0.00	88.5	54	
05 RAO	STATIC-I	PA5_HJ - 10X	Dose Dynamic	1.000	IEC61217	315.0	5.0	0.0	None	8.0	-5.2	+2.8	6.8	-1.5	+5.3	-0.55	0.08	0.00	85.5	47	
06 RPO260	STATIC-I	PA5_HJ - 10X	Dose Dynamic	1.000	IEC61217	260.0	15.0	0.0	None	7.0	-3.5	+3.5	7.0	-1.5	+5.5	-0.55	0.08	0.00	78.9	66	
07 RPO210	STATIC-I	PA5_HJ - 10X	Dose Dynamic	1.000	IEC61217	210.0	10.0	0.0	None	8.2	-3.5	+4.7	7.0	-1.8	+5.3	-0.55	0.08	0.00	85.3	47	

Figure 2.13. IMRT beam arrangement.

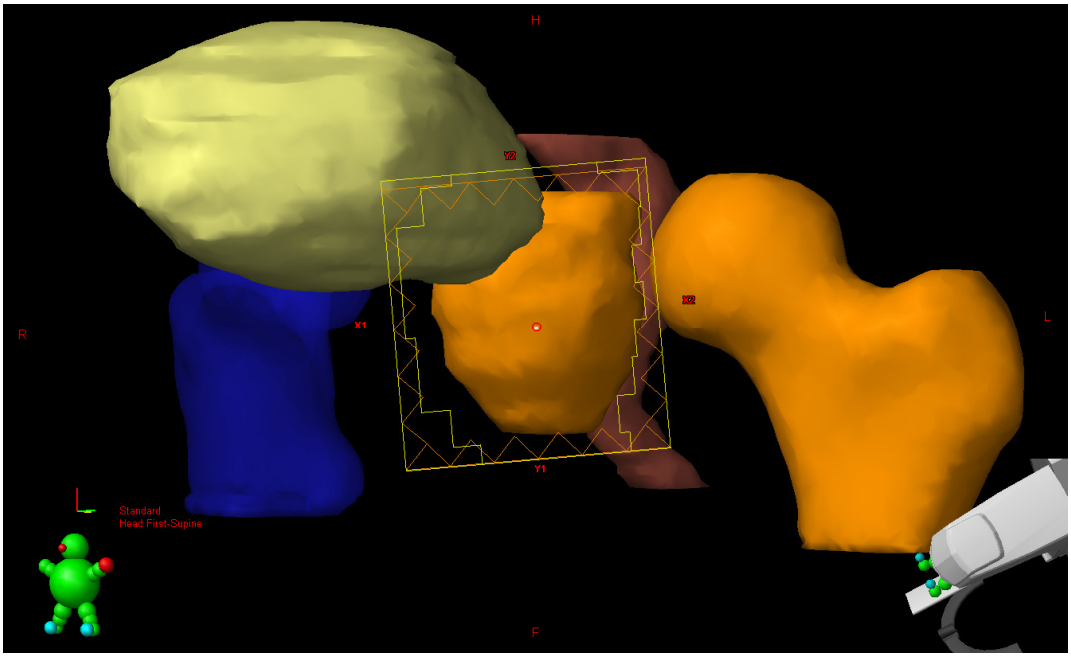

Figure 2.14. BEV for one IMRT beam.

2.4.3.2 VMAT Arcs Setup

VMAT allows MLC modulation during full rotation of gantry angles. Figure 2.15 shows the VMAT arc arrangment and the correspoindg room's-eye-view (REV) for a full arc VMAT in Figure 2.16. To keep a reasonable irradiation time, the maximum number of arcs for prostate cancer is two. VMAT optimization in Pinnacle requires the planner to chose the gantry spacing for the dose calculation (see Figure 2.17). To have a quick and accurate dose calculation, 4 degree of gantry spacing is the default value at at the Princess Alexandra Hospital.

Figure 2.15. VMAT arc arrangement.

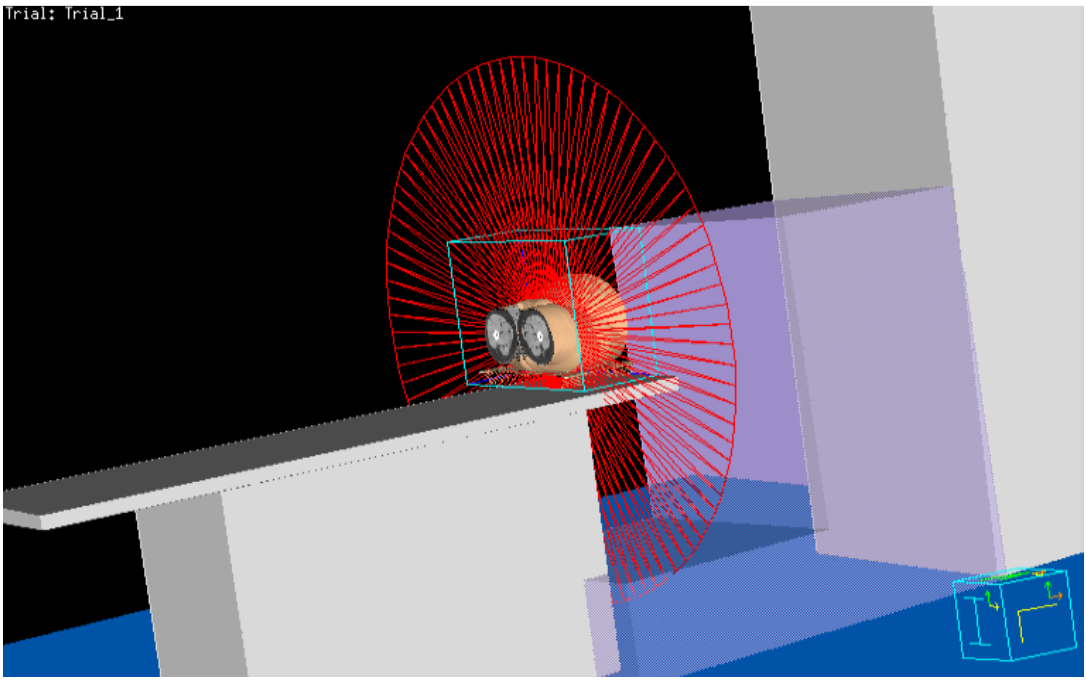

Figure 2.16. REV for VMAT in Pinnacle.

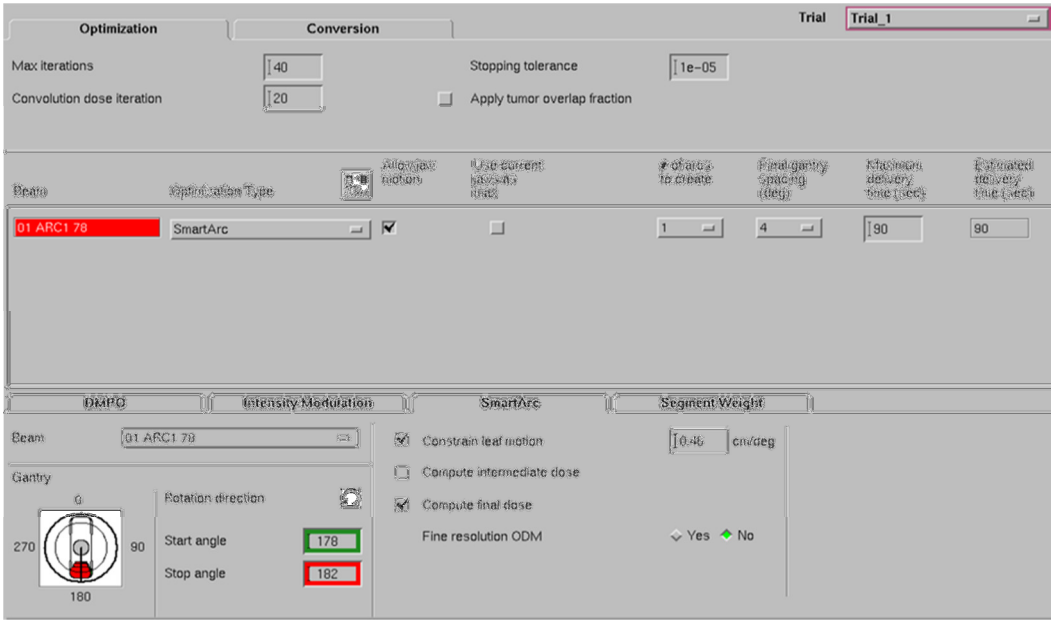

Figure 2.17. VMAT gantry spacing angle.

To avoid couch collision during gantry rotation, the couch is always zero for prostate cancer. Therefore, the only parameter left for the planner to adjust is the collimator angle for VMAT planning. However, more stingent requirement is needed for the collimator angle in VMAT. The planner uses the BEV (Figure 2.18) to review the target shape and determine a collimator angle that uses the least number of MLC leaf-pairs. This will typically be an angle 5° away from an orthogonal collimator angle. Orthogonal collimator angles should still be avoided to prevent the summing of inter-leaf leakage over the whole arc.

During planning of VMAT treatments, the BEV is also used to check for small MLC apertures outside the target. Leaves that will not be used for arc segment creation are parked during delivery and never move into the unshielded area. This is necessary to maintain the dynamic and continuous delivery of VMAT. If the sequencer was to park the leaves that generate the field shape, delivery time would increase because the machine would need to beam off, move the leaves, then beam on

again to continue delivery. If this occurred several times during a full rotation, then the VMAT plan would degrade in delivery time and motion.

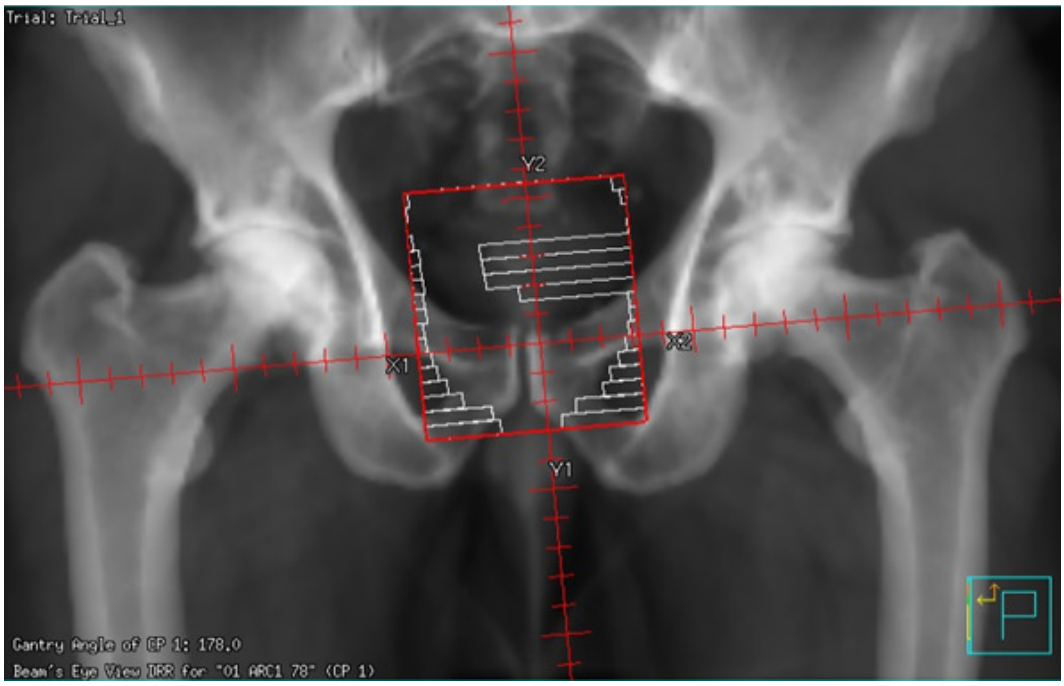

Figure 2.18. BEV for one control point of VMAT.

2.4.4 Planning Optimization

For each iteration of an optimization, the dose is calculated and evaluated by an objective function. This objective function is a measure of the difference between the proposed solution and the requirements set as dose constraints. Equation 1 proposed by Eclipse TPS (Varian Medical Systems, 2010):

$$F_{obj}(j) = \sum_{i=1}^{N_i} (d_i - p)^2 \qquad \textbf{Equation 1}$$

where $F_{obj}(j)$ is j-th objective function at the end of iteration, N_i is total number of points in the structure, d_i is dose at the i-th point in the structure, and p is dose objective.

The optimal solution is reached when the value of the objective function reaches its minimum. Minimising the objective function is equivalent to setting its derivative to zero. Ideally the objective function should reach zero and all constraints would be satisfied. In reality this happens very rarely and when it does, the time to achieve the constraints is very long. Very often contradicting constraints are used (e.g. high dose to the target, low dose to the adjacent healthy tissue) and in this situation the goal is to find the minima of the objective function rather than zero.

For these contradictions soft objectives have been introduced. A soft objective is an objective that may be violated with a penalty. It allows implementation of an objective defined as non-equality. This type of objective has been implemented for all objectives used in the TPS. A penalty is only applied if a dose point is above (or below) the objective. Equation 2 used in Eclipse TPS (Varian Medical Systems, 2010)

allows the implementation of clinical judgement in the form of priorities assigned to each objective.

$$\boldsymbol{F_{obj}(j) = \varepsilon_j \cdot w_j \cdot \sum_{i=1}^{N_i}(d_i - p)^2} \qquad \textbf{Equation 2}$$

where w_j is priority of the j-th objective, N_i is total number of points in the structure, d_i is dose at i-th point in the structure, p is dose objective, and ε_j is flag set to 1 if violated, otherwise set to 0.

The penalty function combines all ROIs objectives, MLC smoothing and minimum fluence of each field into a single function defined as Equation 3 (Varian Medical Systems, 2010):

$$\boldsymbol{F_{obj} = \sum_{allPTVs} F_{PTV} + \sum_{allOARs} F_{OAR} + \sum_{Fields} F_{SmoothXY} + \sum_{Fields} F_{MinFluence}} \qquad \textbf{Equation 3}$$

where F_{PTV} is the objective of each PTV, F_{OAR} is the objective of each OAR normal tissue, $F_{SmoothXY}$ is the objective of fluence smoothing in both X and Y-directions per field basis, and $F_{MinFluence}$ is the objective of minimization of the fluence outside the target per field basis.

At the end of each iteration there is only a single penalty value that defines the quality of the solution. Structures are split in the formula just to highlight that there are target structures, critical structures, smoothness objectives and minimization of the fluence outside the target objectives involved in the optimization process.

The Dose Volume Optimizer (DVO) algorithm in Eclipse TPS (Varian Medical Systems, 2010) for IMRT and the Singular Value Decomposition (SVD)

algorithm in Pinnacle TPS (Philips Medical Systems, 2008) for VMAT are fast dose calculation algorithms used during optimization that are different from the algorithms used for the final dose calculation. Eclipse TPS use analytical anisotropic algorithm (AAA) and Pinnacle TPS uses Collapse Cone Convolution superposition (CCCS) algorithm for the photon final dose calculation. As mentioned before, the fast optimization dose algorithm will not always be representative of the dose as calculated by the final dose calculation. Due to the dose difference between the fast dose calculation during optimization and the final dose calculation (Ezzell et al., 2003), each IMRT/VMAT plan requires many optimizations and the final dose calculations to achieve the goal target.

2.4.5 Dose-Volume Histogram

A dose-volume histogram (DVH) is a plot of either a cumulative or a differential dose-volume frequency distribution. A differential DVH helps to provide variable dose distribution with a structure. On the other hand, a cumulative DVH provides the volume of structure receiving greater than or equal to certain dose. The normalized volume is on the vertical axis and the dose is on the horizontal axis in a cumulative DVH (see Figure 2.19). A cumulative DVH is generally used to evaluate the plan quality without spatial information and assess the optimization progress.

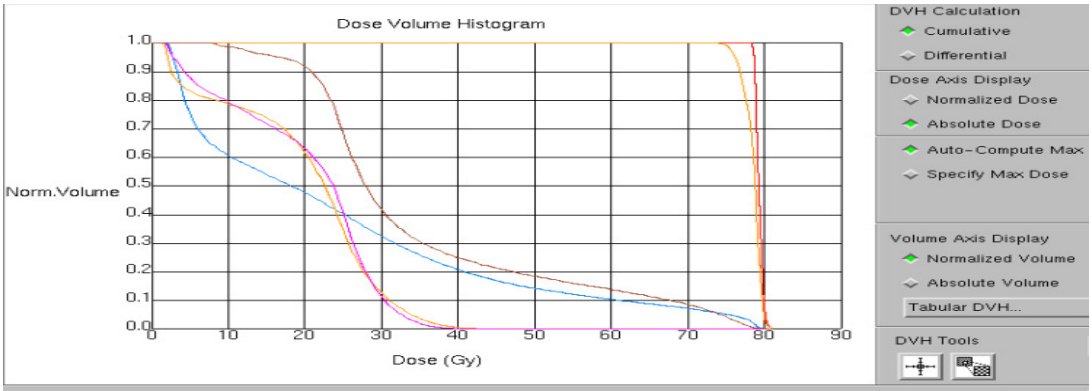

ROI Statistics

Line Type	ROI	Trial or Record	Min.	Max.	Mean	Std. Dev.	% Outside Grid	% > Max
	CTV1	Trial_1	77.86	81.11	79.33	0.42	0.00 %	0.00 %
	PTV1	Trial_1	72.12	81.11	78.51	1.16	0.00 %	0.00 %
	Bladder	Trial_1	1.88	80.11	24.10	22.04	0.00 %	0.00 %
	Femur_L	Trial_1	1.41	42.32	19.86	10.02	0.00 %	0.00 %
	Femur_R	Trial_1	1.69	39.41	20.25	9.50	0.00 %	0.00 %
	Rectum	Trial_1	7.20	79.67	34.67	17.17	0.00 %	0.00 %

Figure 2.19. Example of Cumulative DVH.

2.4.6 Dose Constraints

IMRT/VMAT is an inverse treatment planning technique. In other words, its optimization module uses iterative adjustments to achieve the planner's objectives. This is achieved by setting mathematical objectives, called dose constraints, to assigned structures that were defined during the contouring mode.

2.4.6.1 Physical Dose Constraints

The physical dose constraints can include the maximum, the minimum dose, and the variable DVHs within the structure (Figure 2.20).

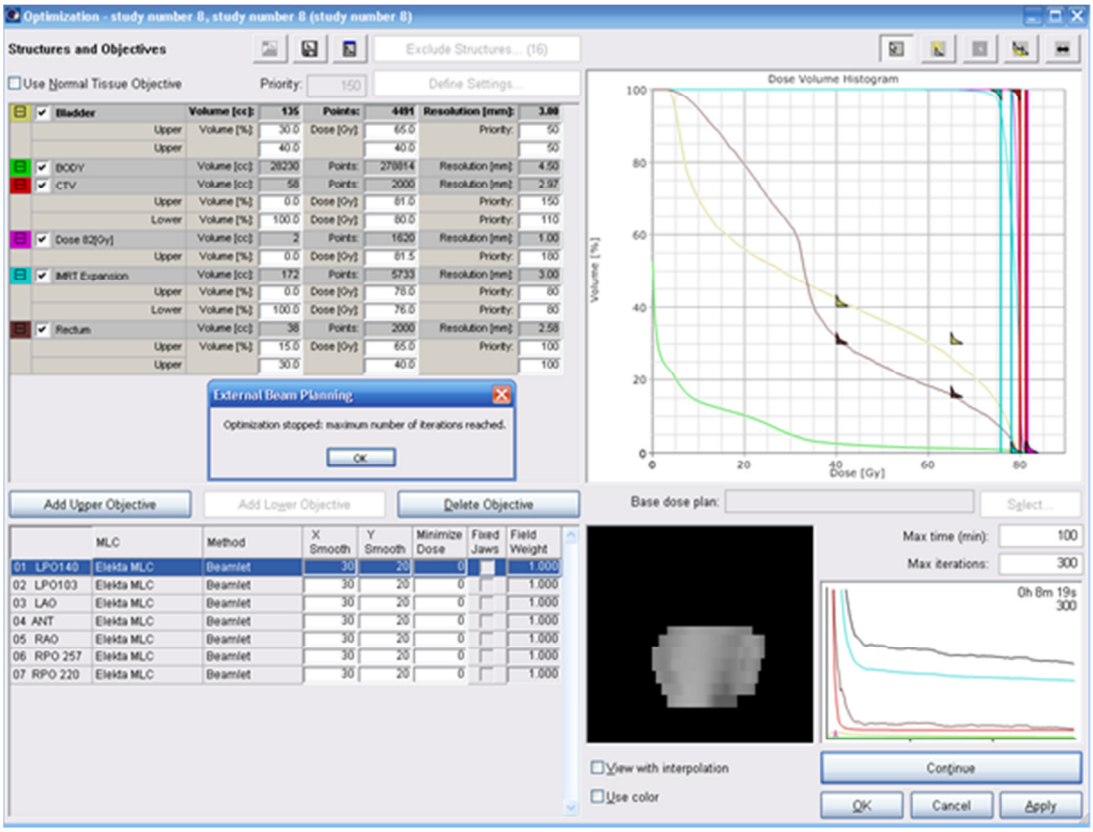

Figure 2.20. Dose constraints prescribed in the Eclipse TPS.

2.4.6.2 Biological Dose Constraints

Treatment planning systems allow the use of physical dose constraints and biological dose constraints together for plan optimization shown in Figure 2.21. The generalized equivalent uniform dose (*gEUD*) proposed by Niemierko can be used for tumour target and OARs (Niemierko, 1997):

$$\boldsymbol{gEUD} = (\sum_i \boldsymbol{v_i D_i^a})^{1/a} \qquad \textbf{Equation 4}$$

where v_i is the fractional volume receiving a dose D_i and a is a tissue-specific parameter for the volume effect.

According to the Pinnacle TPS planning manual (Philips Medical Systems, 2010), *gEUD* is the mean dose of the structure when a is equal to 1. When a is less than 1, the *gEUD* constraint is more sensitive to cold spots whereas the *gEUD* constraint is more sensitive to hot spots when a is greater than 1 (Philips Medical Systems, 2010). Biological dose constraints such as the target *EUD*, the maximum *EUD* and the minimum *EUD* are also available in Pinnacle (see Figure 2.21).

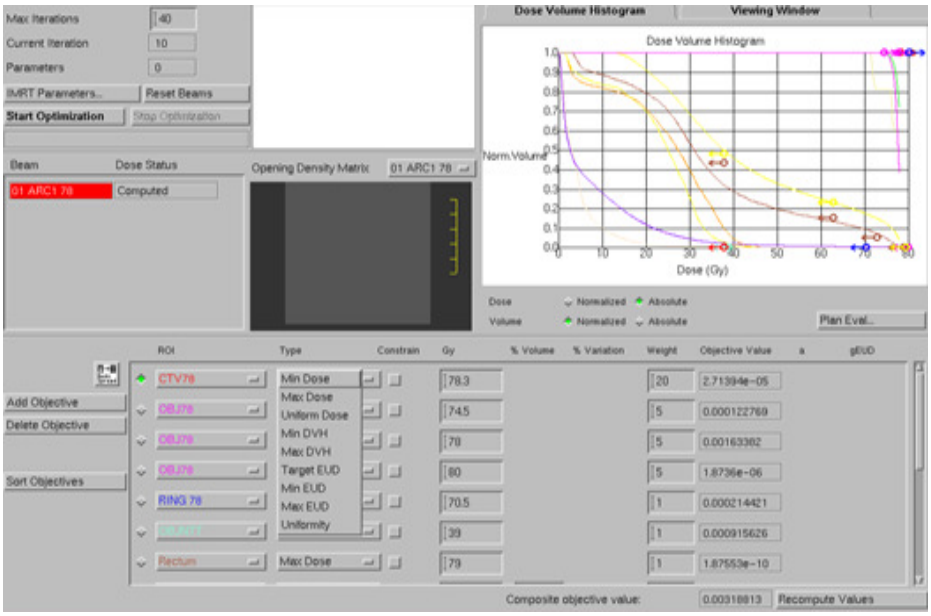

Figure 2.21. Dose constraints prescribed in the Pinnacle TPS.

The AAPM Report No. 166 (2012) showed that the biological dose constraint has different weightings along the DVH curve in Figure 2.22. On the other hand, the physical dose constraint has a heavy weighting at a single point of DVH in Figure 2.23.

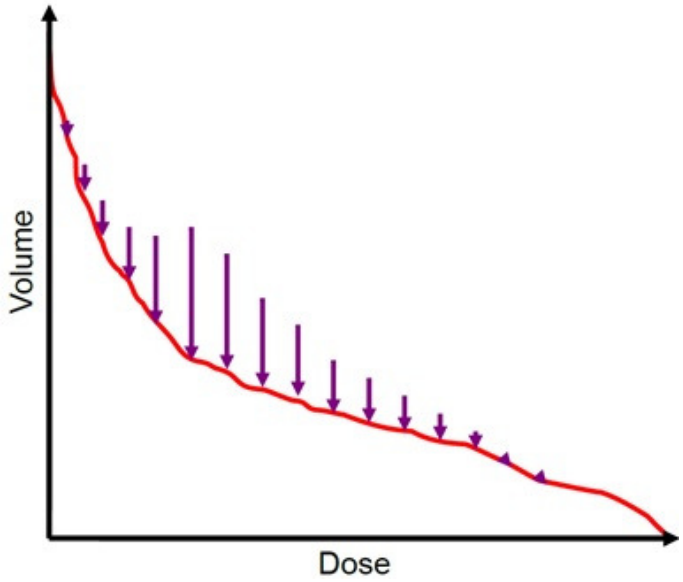

Figure 2.22 Weights of the biological dose constraint for the parallel-type OAR. Adapted from "AAPM Report No. 166 - The Use and QA of Biologically Related Models for Treatment Planning," by AAPM, 2012. Retrieved from http://www.aapm.org/pubs/reports/RPT_166.pdf. Copyright 2012 by AAPM.

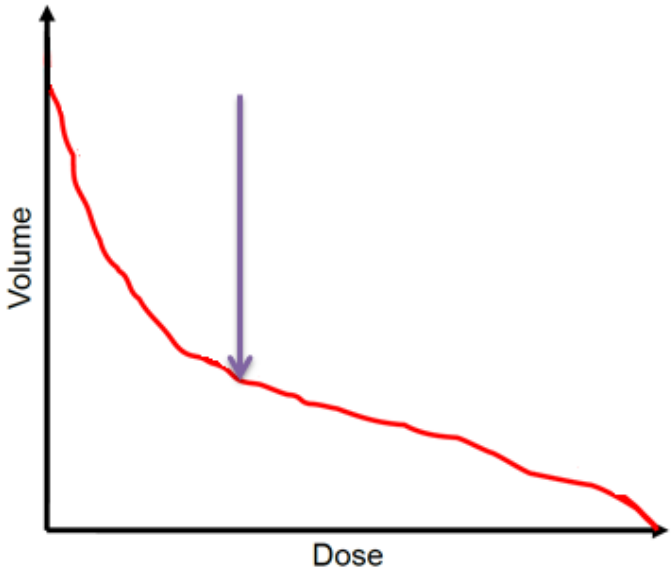

Figure 2.23 Weight of the physical dose constraint.

2.4.6.3 Combination of Physical and Biological Dose Constraints

Planners of radiation therapy treatments at the Princess Alexandra Hospital use a combination of physical and biological constraints. An example of VMAT constraints is illustrated in Figure 2.24. The weight of each dose constraint can be within the range from 1 to 100 in Pinnacle TPS. Most of the OARs constraints use both the physical dose constraints and the biological dose constraints with lower weight relative to the target. The tumour target constraints use the physical dose constraints to achieve the requested minimum dose, the maximum dose and the uniform dose within the tumour target.

The objective value in Pinnacle TPS (see Figure 2.24) is a measure of how successfully the optimization achieved the requested dose level. An objective value of zero means that the dose constraint was achieved, while high objective value indicates that the optimization was less successful.

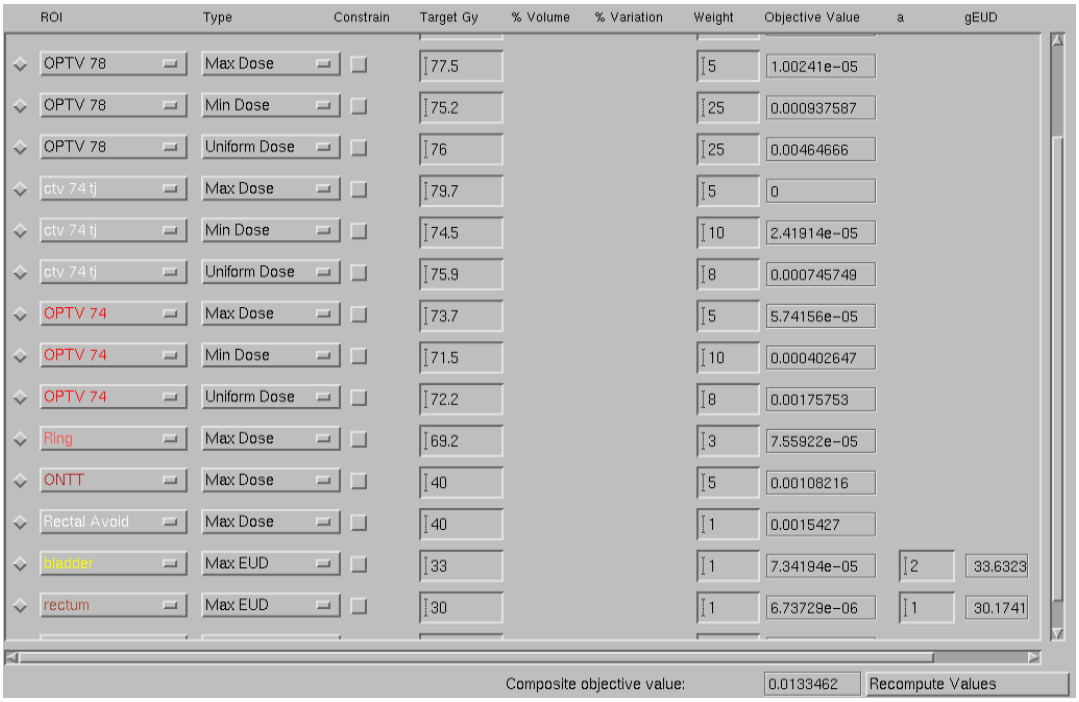

Figure 2.24 Example of VMAT constraints and their objective value in Pinnacle.

2.5 Digital Imaging and Communications in Medicine

Since Digital Imaging and Communications in Medicine (DICOM) files and MATLAB programming were involved in this research, some background of DICOM and MATLAB are described in this section. DICOM is a standard file format in medical imaging from the American College of Radiology (ACR) and National Electrical Manufacturers Association (NEMA). DICOM-RT is the supplement of 11 in DICOM for radiotherapy (RT) objects (National Electrical Manufacturers Association (NEMA), 1997). The information object definition (IOD) determines the RT series modality. Example of RT objects is displayed in Table 2.5.

Table 2.5. Example of RT objects.

IOD	RT Series Module	Example
RT image	RTIMAGE	Digitally reconstructed radiograph (DRR), simulator image
RT dose	RTDOSE	2D or 3D dose matrix, isodose lines, DVH
RT structure set	RTSTRUCT	Contour of OARs or target volumes
RT plan	RTPLAN	External beam information such as angles of gantry angle, collimator angle and couch angle. Brachytherapy channel number, channel length and channel total time

RT beams treatment record	RTRECORD	RT session record of external beam and brachytherapy. Summary of RT treatments

A Service-Object Pair (SOP) class in the storage service identifies the IODs to be stored. Table 2.6 shows examples of SOP Classes. DICOM attribute or data element includes a tag for element identification, a value representation (data type and format of the attribute's value) and a value length for the attribute's value. For this research, the ROIs contour and HU of the rectum were extracted and transformed into the vector. Therefore, the CT images DICOM files and the RT structure set DICOM-RT file were needed in this research.

Table 2.6. SOP Classes and individual UID.

SOP Class Name	SOP Class UID
CT Image Storage	1.2.840.10008.5.1.4.1.1.2
RT Structure Set Storage	1.2.840.10008.5.1.4.1.1.481.3

dicomread('filename') and dicominfo('filename') were the MATLAB commands to read DICOM CT images and DICOM-RT structure set file, respectively. Example of RT structure set information, ROI name and ROI contour data are demonstrated in Figure 2.25, Figure 2.26, and Figure 2.27, respectively.

Figure 2.25. Example of attributes of a structure set that contains all the ROIs information shown in MATLAB. MediaStorageSOPClassUID shows the modality and the '1.2.840.10008.5.1.4.1.1.481.3' refers to RTstructure set.

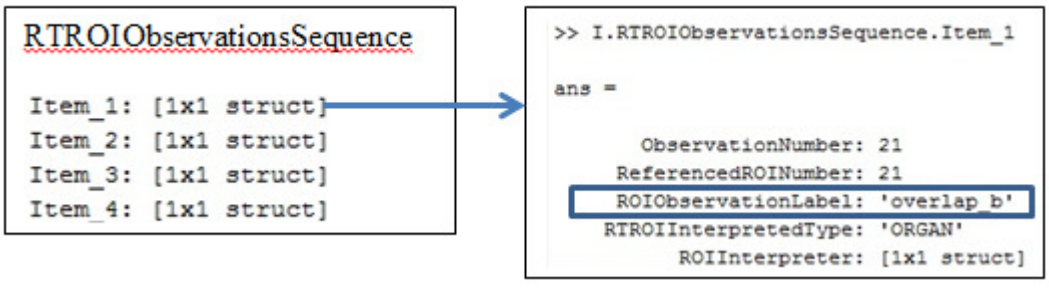

Figure 2.26. RTROIObservationSequence shows four ROIs structures and the first structure ROI name can be found from ROIObservationLabel

ROIContourSequence in Figure 2.27 contains five ROIs structures' contouring information including unique reference ROI number, ROI colour and ROI contour data. The first ROI structure has contour data for 5 slices in the ContourSequence that contains the contour coordinates in ContourData and specific CT slice information in the ContourImageSequence. ReferenceSOPClassUID corresponds to CT images and ReferenceSOPInstanceUID refers to specific CT slice in the ContourImageSequence.

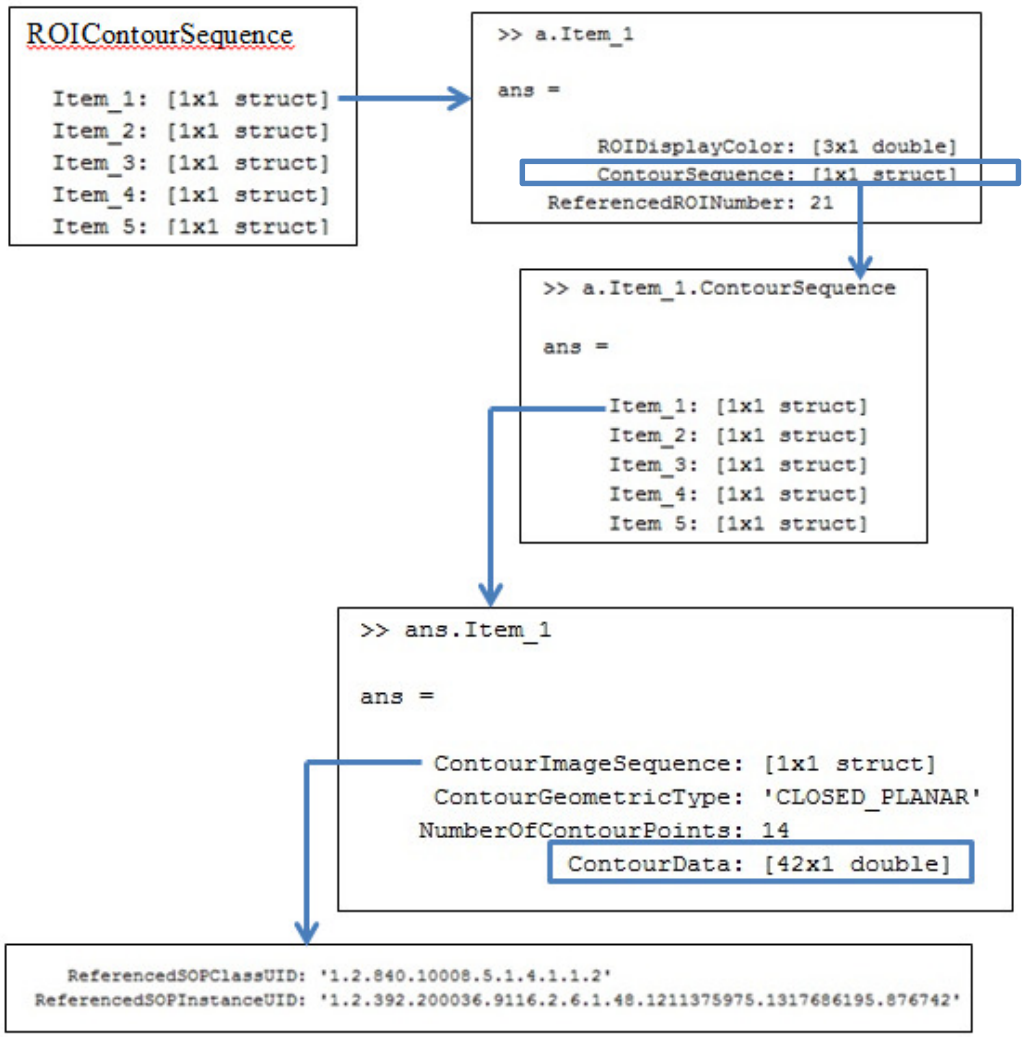

Figure 2.27. ROIContourSequence contains five ROI structures' contouring.

Chapter 3 Methodology

3.1 Vector Model

Features are characteristics of a contour. For example, for CT image structures, features can include the height of the PTV, the volume of the PTV and the shape of the PTV. A vector model is an extraction of all the features from a specific object (Salton & Buckley, 1991; Chan, Chan, Cheng, & Mak, 2010; Chan, Liu, Shyu, & Benzie, 2011). The similarity between two cases can be then found from the direction cosine between two vectors (the normalized dot product of the two vectors) and is shown in Equation 5 (Salton, 1991). Vector models can be applied on medical images to find their similarity according to different weights of features (Allampalli-Nagaraj & Bichindaritz, 2009). Euclidean distance in Equation 6 is another method to quantify similarity (Frey & Dueck, 2007). Two similarity matching equations have been developed for image retrieval based on feature extraction:

$$\textbf{Direction cosine for similarity} = \frac{\sum_{i=1}^{t} w_i X_i Y_i}{\sqrt{\sum_{i=1}^{t} (X_i)^2 \sum_{i=1}^{t} (Y_i)^2}} \qquad \textbf{Equation 5}$$

$$\textbf{Euclidean distance for similarity} = \sqrt{\sum_{i=1}^{t} (X_i - Y_i)^2} \qquad \textbf{Equation 6}$$

where X and Y are the feature vectors of two sample cases, w is the weight of each feature, i is the features number and t is total feature number.

Between two vectors, either an angle (in Equation 5) or a difference can be computed (in Equation 6). These values (angle or difference) are zero when two

vectors are identical. This means that Equation 5 gives the cosine of the angle and the similarity score is equal to 1 when there is a perfect match between the vectors.

The Euclidean distance, defined by Equation 6, is commonly used to evaluate the similarity between two quantities, such as image and signal patterns. However, this conventional approach adopts a kernel of patterns to be compared, which involves a heavy computational load. The vector model gives any absent feature a zero value and replaces the kernel with a direction cosine calculation, defined by Equation 5, making the work of the CPU much simpler. For example, Equation 5 saves more calculation time in the case of an absent feature (e.g. comparing a case with the rectal gas to one without). However, since different combinations of features can result in the same similarity value, a human intervention is still required to filter the cases to determine the best match.

3.2 Vector Model Solution for IMRT/VMAT

A few authors have applied the direction cosine to medical images (Saldana et al., 2010; Shapiro et al., 2008; Megalooikonomou, Barnathan, Kontos, Bakic, & Maidment, 2009; Moreno, Caicedo, & Gonzalez, 2010). However, there are no studies directly applying the concept to radiotherapy. There are many publications related to features extraction in the localization or classification of malignant tumours, and some studies found that the feature extraction was variant to scaling, rotation and translation (Tourassi, Harrawood, Singh, Lo, & Floyd, 2007; Lee, Chen, & Chiang, 2007; Gletsos et al., 2003; Wang et al., 2010; Sachdeva, Kumar, Gupta, Khandelwal, & Ahuja, 2013; Zhou, Liao, Li, & Shen, 2011; Huang, Chen, & Shen, 2006; Felipe et al., 2005; Feng, Foskey, Chen, & Shen, 2010; Boujelben, Chaabani, Tmar, & Abid,

2009). To my knowledge, two papers from the University of Nottingham used a case based reasoning approach for radiotherapy planning. Song, Petrovic, and Sundar (2007) used the features of tumour staging, Gleason score, PSA and DVH of the rectum to find the similarity for the dose planning. In addition, Jagannathan, Petrovic, McKenna, and Newton (2010) utilised the features of tumour volume, distance between tumour and OAR, and angle between tumour and OAR to search the similarity for brain treatment planning.

The direction cosine was used for prostate IMRT/VMAT plans similarity search in this study. First, a set of previous prostate IMRT/VMAT plans were collected and transformed into the vectors to establish a database reference. To reduce requirements for medical images storage and time of matching of medical images, the features of medical images were extracted and encoded as a vector. Since CT images and structure contours are in DICOM format, the features were extracted using MATLAB (The MathWorks, Inc., version 7.10.0.499, 2010). Features extracted from CT images for the vector model included tumour dimensions, tumour volume, Hounsfield unit (HU) in CT images and target volume overlapped with OARs.

Then, the similarity between a present case and previous prostate IMRT/VMAT plans was calculated using the direction cosine (Equation 5) because of the simpler CPU demands. As some of the previous prostate IMRT/VMAT plans might not have good plan quality, the quality of similar plans was compared and the most suitable previous prostate IMRT/VMAT plan was selected for reference. Planning parameters could be retrieved from the selected reference plan and applied to the present case to reduce the time spent gradually adjusting planning parameters. The planning optimization was then calculated with a routine dose calculation

algorithm and needed only few adjustments to meet clinical constraints for the individual case.

3.2.1 Feature Extraction

Feature extraction requires invariance to scaling, rotation and translation (Keyes & Winstanley, 2001) so that the MATLAB program can compare features from data sets with different tumour locations, tumour sizes and tumour rotations. To retrieve the initial planning parameters of similar prostate IMRT/VMAT cases, structural and physiological features were compared in a similarity search. The structural features for prostate cancer IMRT/VMAT planning included the PTV volume, bladder volume, rectum volume, dimension of the tumour, overlap volume between PTV and OARs, compactness (Rangayyan, 2005), irregularity (Nixon & Aguado, 2012), alternative irregularity (Nixon & Aguado, 2012), and moments of distance to centre for PTV (Rangayyan, 2005).

The physiological feature for prostate cancer IMRT/VMAT planning was the rectal gas that could be extracted as Hu's moment invariants (Hu, 1962). An image moment investigates the distribution of the image pixel's intensities so the distribution of HU in CT images was compared between cases. The PTV was drawn on soft tissue on non-contrast CT images, but the density of PTV has low contrast across the PTV. On the other hand, the rectal gas could be quantified by the HU number because the difference in HU between the rectal gas and the soft tissue is significant (the HU of rectal gas is approximately -1000 HU and soft tissue is around 0 HU). The rectal gas may affect the rectal shape as well as the PTV's shape.

Since the left femoral neck, the right femoral neck, and the body structure is not influential in the prostate IMRT/VMAT plan, features from these three structures were not considered. From CT images, structure contour DICOM files, the tumour characteristics, OAR characteristics and their overlap volume can be quantified as the following features:

Table 3.1. Structural features

Volumes	PTV, rectum, bladder, overlap volume between PTV and rectum, overlap volume between PTV and bladder
Dimensions of PTV	Height, width and length
PTV contour	Compactness, irregularity, alternative irregularity, moments of distance to centroid
Physiological feature of the rectal gas	Hu's moment invariants

3.2.1.1 Volumes

Accurate localization and contouring of the tumour as well as normal healthy tissues are extremely important issues in IMRT/VMAT planning. Although some automatic segmentation methods have been proposed, manual correction remains necessary. The oncologist draws the tumour contour as a planning target volume (PTV) as well as the organs at risk (OAR) on the CT images. The volume of the PTV and OARs were derived from the DICOM data exported from the TPS as follows:

- The DICOM coordinates of PTV and OARs were retrieved from the structure contours' DICOM files (see Figures 2.25 to 2.27).
- The ROI polygon was converted to a region mask using the MATLAB function poly2mask().
- The MATLAB function regionprops() was used to extract the area of the structure on each CT image slice. PTV area in green color on the CT image is shown in Figure 3.1.

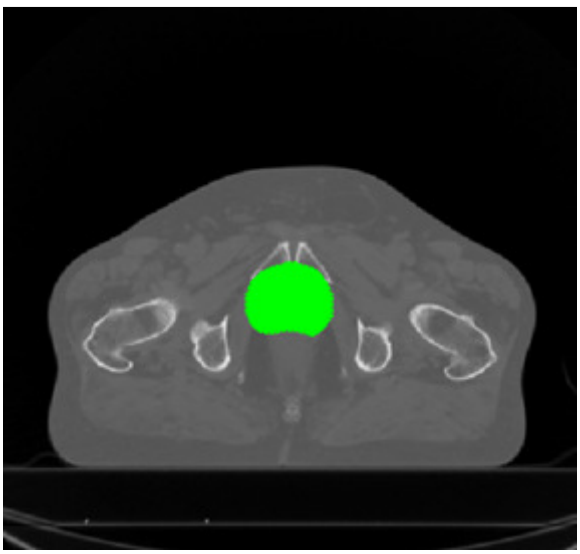

Figure 3.1. PTV area in green on the CT image.

- Each slice volume for the structure was calculated as the product of an area

and a slice thickness. Then, the structure's volume was obtained by summing all the slice volumes, as per Equation 7.

$$\boldsymbol{volume} = \sum_1^n \boldsymbol{area} * \boldsymbol{CT\_slice\ thickness} \qquad \textbf{Equation 7}$$

3.2.1.2 Dimensions of PTV

Dimensions of the PTV used in this study were the height, width and length. The width and length of the PTV were defined as the major axis (using MATLAB function MajorAxisLength) and minor axis (using MATLAB function MinorAxisLength), respectively in the middle of the PTV. The height could be obtained from the number of images multiplied by the slice thickness.

3.2.1.3 Compactness of PTV

Compactness is a shape feature that describes the complexity of the contour (efficiency of a contour to contain a given area). The original value of compactness can take values from 4π to no upper bound, is defined as (Rangayyan, 2005):

$$\boldsymbol{Compactness} = \frac{\boldsymbol{Perimeter^2}}{\boldsymbol{Area}} \qquad \textbf{Equation 8}$$

To easily compare the compactness on each CT image slice, the range was modified to take the values between 0 and 1 (Rangayyan, 2005) as:

$$\boldsymbol{Compactness_{modified}} = 1 - \frac{4\pi A}{\boldsymbol{Perimeter^2}} \qquad \textbf{Equation 9}$$

The $compactness_{modified}$ is equal to zero for a circle and increases with the

shape complexity to one. The feature of compactness was extracted from the PTV contour on each CT image slice.

3.2.1.4 Irregularity and Alternative Irregularity of PTV

Irregularity and alternative irregularity measure the dispersion. They are opposite to the compactness in that irregularity and alternative irregularity increase the value for the complex shape whereas compactness decreases the value for the same complex shape. Nixon and Aguado (2012) define the irregularity of the contour as follow:

$$\boldsymbol{Irregularity} = \frac{\boldsymbol{\pi} \times \mathbf{max}((\boldsymbol{x_i}-\bar{\boldsymbol{x}})^2+(\boldsymbol{y_i}-\bar{\boldsymbol{y}})^2)}{\boldsymbol{area}} \qquad \textbf{Equation 10}$$

where *(x,y)* is the coordinates of the contour and $(\bar{x}, \bar{y})$ represent the center of the contour.

Alternative irregularity of the contour can be defined as the ratio of the maximum to the minimum radius (Nixon & Aguado, 2012). The maximum and the minimum radius could be extracted from PTV contour on each CT image slice. The features of irregularity and alternative irregularity were extracted from the PTV contour on each CT image slice.

3.2.1.5 Moments of Distance to Centroid of the PTV

Moments of distance to centroid are a sequence of distances between the centroid of the contour and all points along the contour (Rangayyan, 2005). The moments of distance to centroid were extracted from PTV contour on each CT image based on shape features (Gupta & Srinath, 1987; Shen, Rangayyan, & Desautels, 1993, 1994; Rangayyan, 2005) as follows:

The p^{th} moment of the distance sequence d (n) is

$$\boldsymbol{m_p = \frac{1}{N}\sum_{n=0}^{N-1}[d(n)]^p} \qquad \textbf{Equation 11}$$

The p^{th} central moment is

$$\boldsymbol{M_p = \frac{1}{N}\sum_{n=0}^{N-1}[d(n) - m_1]^p} \qquad \textbf{Equation 12}$$

Moments of distance to centroid features:

$$\boldsymbol{F_1 = F_1' = \frac{\sqrt[2]{M_2}}{m_1} = \frac{\sqrt[2]{\frac{1}{N}\sum_{n=0}^{N-1}[d(n)-m_1]^2}}{m_1}} \qquad \textbf{Equation 13}$$

$$\boldsymbol{F_2 = \frac{M_3}{(M_2)^{3/2}} = \frac{\frac{1}{N}\sum_{n=0}^{N-1}[d(n)-m_1]^3}{\left\{\frac{1}{N}\sum_{n=0}^{N-1}[d(n)-m_1]^2\right\}^{3/2}}} \qquad \textbf{Equation 14}$$

$$\boldsymbol{F_3 = \frac{M_4}{(M_2)^2} = \frac{\frac{1}{N}\sum_{n=0}^{N-1}[d(n)-m_1]^4}{\left\{\frac{1}{N}\sum_{n=0}^{N-1}[d(n)-m_1]^2\right\}^2}} \qquad \textbf{Equation 15}$$

$$\boldsymbol{F_2' = \frac{M_3^{1/3}}{m_1} = \frac{\left\{\frac{1}{N}\sum_{n=0}^{N-1}[d(n)-m_1]^3\right\}^{1/3}}{m_1}} \qquad \textbf{Equation 16}$$

$$F'_3 = \frac{M_4^{1/4}}{m_1} = \frac{\left\{\frac{1}{N}\sum_{n=0}^{N-1}[d(n)-m_1]^4\right\}^{1/4}}{m_1}$$ **Equation 17**

$$mf = F'_3 - F'_1$$ **Equation 18**

where *m* is the moment of the distance values, *p* is the order of the moment, *N* is number of the distance sequence, *M* is the central moment of the distance values, m_1 is the first order of the moment of the distance values, *F'* is modified equation for centroid feature and *mf* is the modified feature.

All PTV contours were inside the prostate IMRT/VMAT fields but some of the bladder and rectal contours were outside the prostate IMRT/VMAT fields, and thus they were not relevant to the prostate IMRT/VMAT optimization. Therefore, moments of distance to centroid features were extracted from PTV contours only. The PTV contour on each slice had six moments of distance to centroid features. Hence there were hundreds of moments of distance to centroid features for just thirty slices of PTV contours. In order to reduce the dimension of moments of distance features, only a selection of moments of distance to centroid features was used. It has been suggested that F_2' is not better than F_2 for the shape categories (Shen, Rangayyan, & Desautels, 1994) so F_2' was not used in the vector model. In addition, F_3' is better than F_3 because the variation in F_3' is large for different shape complexity (Shen, Rangayyan, & Desautels, 1993, 1994). It has also been suggested that *mf* is a good indicator (Rangayyan, 2005). Hence, finally F_1, F_2, F_3' and *mf* moments of distance to centroid features were used in the vector model.

3.2.1.6 Hu's Moment Invariants of Rectal Gas

Hu's moment invariants (Hu, 1962) had been used in image analysis for the shape description of a probability density function defined as (Rangayyan, 2005; Gonzalez & Woods, 2002):

$$\mu_{pq} = \sum_{m=0}^{M-1} \sum_{n=0}^{N-1} (m - \bar{x})^p (n - \bar{y})^q f(m, n) \quad \textbf{Equation 19}$$

where $\mu_{pq}\ is\ the\ central\ moments\ \ of\ order\ (p+q)$, *f (m, n)* is a M x N pixels digital image, *m, n* is the coordinate of the column and the row, $\bar{x}$ is the mean of the column, and $\bar{y}$ is the mean of the row.

Gonzalez and Woods (2002) defined the following relationships of central moments:

$$\mu_{00} = m_{00} = \mu \quad \textbf{Equation 20}$$

$$\mu_{10} = \mu_{01} = 0 \quad \textbf{Equation 21}$$

$$\mu_{20} = m_{20} - \mu\bar{x}^2 \quad \textbf{Equation 22}$$

$$\mu_{11} = m_{11} - \mu\bar{x}\bar{y} \quad \textbf{Equation 23}$$

$$\mu_{02} = m_{02} - \mu\bar{y}^2 \quad \textbf{Equation 24}$$

$$\mu_{30} = m_{30} - 3m_{20}\bar{x} + 2\mu\bar{x}^3 \quad \textbf{Equation 25}$$

$$\mu_{21} = m_{21} - m_{20}\bar{y} - 2m_{11}\bar{x} + 2\mu\bar{x}^2\bar{y} \quad \textbf{Equation 26}$$

$$\mu_{12} = m_{12} - m_{02}\bar{x} - 2m_{11}\bar{y} + 2\mu\bar{y}^2\bar{x} \quad \textbf{Equation 27}$$

$$\mu_{03} = m_{03} - 3m_{02}\bar{y} + 2\mu\bar{y}^3 \quad \textbf{Equation 28}$$

The normalized moments obtained as (Gonzalez & Woods, 2002):

$$\nu_{pq} = \frac{\mu_{pq}}{\mu_{00}^{(\frac{p+q}{2}+1)}} \quad \textbf{Equation 29}$$

Hu proposed seven moment invariants M_1 through M_7 with functions of the second-order and third-order central moments (Hu, 1962):

$$M_1 = \nu_{20} + \nu_{02} \quad \textbf{Equation 30}$$

$$M_2 = (\nu_{20} - \nu_{02})^2 + 4\nu_{11}^2 \quad \textbf{Equation 31}$$

$$M_3 = (\nu_{30} - 3\nu_{12})^2 + (3\nu_{21} - \nu_{03})^2 \quad \textbf{Equation 32}$$

$$M_4 = (\nu_{30} + \nu_{12})^2 + (\nu_{21} + \nu_{03})^2 \quad \textbf{Equation 33}$$

$$\begin{aligned} M_5 = {} & (\nu_{30} - 3\nu_{12})(\nu_{30} + \nu_{12})[(\nu_{30} + \nu_{12})^2 - 3(\nu_{21} + \nu_{03})^2] \\ & + (3\nu_{21} - \nu_{03})(\nu_{21} + \nu_{03})[3(\nu_{30} + \nu_{12})^2 - (\nu_{21} + \nu_{03})^2] \end{aligned}$$

Equation 34

$$M_6 = (\nu_{20} - \nu_{02})[(\nu_{30} + \nu_{12})^2 - (\nu_{21} + \nu_{03})^2] + 4\nu_{11}(\nu_{30} + \nu_{12})(\nu_{21} + \nu_{03})$$

Equation 35

$$\begin{aligned} M_7 = {} & (3\nu_{21} - \nu_{03})(\nu_{30} + \nu_{12})[(\nu_{30} + \nu_{12})^2 - 3(\nu_{21} + \nu_{03})^2] \\ & - (\nu_{30} - 3\nu_{12})(\nu_{21} + \nu_{03})[3(\nu_{30} + \nu_{12})^2 - (\nu_{21} + \nu_{03})^2] \end{aligned}$$

Equation 36

Using Equations 19 through 36, Hu's moment invariants were extracted from the HU distribution on the CT images using MATLAB scripts. As the PTV and bladder have low contrast HU, the differentiation between Hu's moment invariants is difficult. Conversely, the rectal gas in the rectum structure has high contrast HU, so Hu's moment invariants of the rectum structure have distinct values. Therefore, Hu's moment invariants were used for the rectum structure only. As each slice of the rectum contour has seven moment invariants, hundreds of moments features were

obtained for all slices with the rectum contour. Since the rectal gas was not the main focus in the vector model, only the maximum and minimum of seven moment invariants for the entire structure were put in the vector model.

3.3 Vector Model Implementation

After the contouring of the PTV and OARs, the CT information was retrieved from CT image DICOM files. Features were extracted from both DICOM structure contours files and CT image files. All the features were extracted and some features were eliminated to reduce the dimension of the vector model. After the elimination, 155 features were transformed into the vector model. Every radiotherapy case underwent feature extraction with the features in the normalized vector format but only the reference cases were stored in a database.

3.3.1 Vector Weighing

Every case underwent feature extraction, and the features were stored in the weighted vector format. Different weightings were applied to different features (see Table 3.2). Magome et al. (2013) recommended each institute should decide the appropriate weights of the features based on their planning policy. PTV volume and the overlap volume between PTV and the OARs could be the crucial variables that determine the plan quality, but these features can be overwhelmed by any combination of the other features, such as OAR volumes which are not indicative of the true patient similarity. Therefore, the specific term weighting method described by Chan et al. (2015) was used in the vector model to emphasise the importance of these crucial variables with specific weight assigned. Because feature reweighting may increase classifier robustness, it was performed many times to optimize the vector model with different types of training cases. Feature weighting algorithms may be too computationally demanding to use (De Amorim, 2012). Hence, feature reweighting operations did not use any feature weighting algorithm on the vector model. Many feature reweighting

operations were performed, and the final specific weight of each feature is presented in Table 3.2.

Table 3.2. Weighting factors of different features

Features	Weight
PTV volume	0.025673941
Bladder volume	0.006418485
Rectal volume	0.006418485
Overlap volume of PTV and rectum	0.025673941
Overlap volume of PTV and bladder	0.025673941
PTV height	0.01283697
PTV width	0.01283697
PTV length	0.01283697
PTV contour compactness	0.006418485
PTV contour irregularity	0.006418485
PTV contour alternative irregularity	0.006418485
PTV contour moment	0.006418485
Hu's moment invariants of rectal gas	0.001283697

As creating an IMRT/VMAT prostate plan involves volume optimization, the organ volume is the key factor in IMRT/VMAT prostate optimization. An IMRT/VMAT prostate plan is more difficult to plan with increasing PTV volume or overlap volume between PTV and OARs. This was the reason why the PTV volume and the overlap volume between PTV and OARs were given the highest weightings. PTV dimension was given the second highest weighting, as it is indirectly gives volume information, and affects MLC leaf positions surrounding the PTV. Although

the OAR volumes and the PTV contour had an impact on the IMRT/VMAT prostate optimization, these parameters had lower priority compared with the PTV volume or the overlap volume. For that reason, the weighting of OAR volumes and the PTV contour features was given the third highest weighting. The rectal gas was a physiological feature of less importance in the IMRT/VMAT prostate optimization so its weight was significantly smaller in comparison with the structure features.

3.4 Reference Selection

Generally, MATLAB took a few minutes for features extraction. Then, the similarity between a test case and previous IMRT/VMAT patients was calculated using the direction cosine. The direction cosine between two feature vectors indicated the potential similarity between two cases. Due to the lower computational load, the direction cosine (Equation 5) was used to evaluate the similarity between the feature vectors. For a given testing case, the direction cosine was used to find a number of previous prostate IMRT/VMAT plans in the reference database which were similar to the testing case.

As some of the previous optimized plans might not have the optimal plan quality, the quality of similar plans was compared and the most suitable previous optimized plan was selected for reference. The MATLAB program proposed a list of top three reference cases with highest similarity score allowing the planner to choose the most appropriate one. Since the planning documents of each clinical prostate S&S IMRT/VMAT plan had previously been uploaded to the MOSAIQ Oncology Information System Interface (Elekta Oncology Systems, Crawley, UK) , the plan quality could be assessed from the planning goals document (Figure 3.2) in MOSAIQ.

If the reference case with the highest similarity score resulted in an optimized plan lacking the required quality, the planner could choose the reference case whose anatomical features had the second highest similarity score if it had better plan quality than the rest.

IMRT	CRITICAL TISSUE CONSTRAINTS		Planned Dose		
1	normal case	special case	Minimum	Mean	Maximum
Rectum (whole)	V75<7%		1.5	5.415789	9.1
	V65<17%		9.3	15.05	18.6
	V40<35%	V40<60%	23.2	34.43333	55.5
	Maximum Dose		77.6	80.37579	82.3
	cc > 78 Gy		0	0.822941	2.5
	Post rectal wall ≤ 40 Gy			yes	
Bladder (whole)	V65<25%	V65<30%	2.8	17.23667	36.6
	V40<50%	V40<60%	7.5	33.62333	61
	Maximum dose		79.1	81.19105	82.6
Lt Femoral neck	V50<10%		0	0.248333	7.1
	V35<100%		0	8.267333	45
Rt Femoral neck	V50<10%		0	0.664333	13.7
	V35<100%		0	9.243333	40
Large Bowel		Max Dose <70Gy	18.9	29.6	40.3
		V65<17%	0	0	0
Small Bowel		100cc<45Gy	0	1.1475	4.4
		Max dose<57Gy	2.6	27.475	57.5
Surrounding normal tissue to receive < 110% target dose				yes	
Conformality of 40Gy isodose around PTV acceptable				yes	
AVOID Prostatae/Bladder Interface (PBI) AND APEX				yes	
HOT SPOT >5mm ANT TO ANT RECTAL WALL				yes	
2	TARGET GOALS		Planned Dose (Gy)		
			Minimum	Mean	Maximum
	PTV D2		79.5	81.14	82.4
	PTV D50		74.1	78.85	80
	PTV D98		69.5	75.07	79.4
	D99 CTV to receive ≥78 Gy		75.1	77.7	79.1
	D99 PTV to receive ≥ 74.1 Gy		64.6	73.7	78
	PTV Maximum dose		79.9	81.5	82.5
3	**Plan Maximum dose**		80.8	82.7	84.7

VMAT	CRITICAL TISSUE CONSTRAINTS		Planned Dose		
1	normal case	special case	Minimum	Mean	Maximum
Rectum (whole)	V75<5-8%		1.2	5.787333	10.8
	V65<17%		4.7	13.38333	21.8
	V40<35%		14.5	29.749	39
		PRV < 81 Gy	80.8	81.2	81.7
	Max dose		78.46	80.258	82.1
	2cc<102%		0	0.424375	1.85
Bladder (whole)	Post rectal wall ≤ 40 Gy			yes	
	V65<25%		4.1	13.52833	26.2
	V40<50%		10	28.90667	49.8
	Maximum dose		78.34	79.76233	82.2
Lt Femoral neck	V50<10%		0	0.242667	2.3
	V35<100%		0	18.20724	49.5
	Max Dose		29.83	43.08636	56.7
Rt Femoral neck	V50<10%		0	0.113333	1.7
	V35<100%		0	12.58828	54.2
	Max Dose		26.2	41.67043	54.3
Small Bowel		100cc<45	0	0.19	0.38
		150cc < 52Gy	0	0.124444	1.12
		Dmax < 56Gy	4.5	31.88417	57.96
		PRV < 64 Gy		63.6	
Large Bowel		V40<35%	0	0.102	0.5
		V65<17%	0	0.09625	0.67
		Max<70Gy	4.9	37.715	71
Memb Urethra		<78Gy		77.7	
Apex		<81.9Gy	80.3	81	81.5
Prostatae/Bladder Interface (PBI)		<81Gy		80.4	
Surrounding normal tissue to receive < 110% target dose				yes	
Conformality of 40Gy isodose around PTV acceptable				yes	
Keep hot spot off ant rectal wall, away form apex and PBI				yes	
2	TARGET GOALS		Planned Dose (Gy)		
			Minimum	Mean	Maximum
	PTV D2		79.4	80.8	81.7
	PTV D50		77.6	78.6	79.9
	PTV D98		68.5	74.2	78
	D99 CTV to receive ≥78 Gy		84	97.6	100
	D99 PTV to receive ≥ 74.1 Gy		94.9	98.5	100
	PTV Maximum dose		80.3	80.8	81.7
3	**Plan Maximum dose**		80.4	81.9	83.3

Figure 3.2. Summary of the planning goals for IMRT and VMAT.

Planning parameters were retrieved from the planning document in MOSAIQ. An example of the planning document is in Figure 3.3. Planning parameters were obtained from the selected reference case and applied in the test case to save time on the gradual adjustment of planning parameters.

Plan Summary Sheet

Beam Setup

Beam	Machine	Energy	Modality	Prescription	Isocenter	SSD (cm) Start / Avg	MU Per Fraction
01 ARC 78	PA6_LG	6 MV	Photons	01PELVIS78	ISOCEN...	82.37 / 83.03	**349.1**

Beam	Collimators (cm) (Control Pt 1) X2	X1	Y1	Y2	Gantry Start / Stop	Couch	Coll	Block	Wedge	Bolus	Comp
01 ARC 78	4.9	3.9	4.5	4.5	180 / 181	0	15	MLC	None	No	No

IMRT Summary

Objectives

ROI	Type	Constraint	Target (Gy)	Volume (%)	Variation (%)	Weight (%)	Objective Value	*a*	gEUD (Gy)
CTV	Max Dose	No	81.80	—	—	20.00	0.0000	—	—
CTV	Min Dose	No	79.50	—	—	26.00	0.0007	—	—
CTV	Uniform Dose	No	80.50	—	—	25.00	0.0034	—	—
O PTV	Max Dose	No	78.00	—	—	40.00	0.0010	—	—
O PTV	Min Dose	No	77.50	—	—	35.00	0.0240	—	—
O PTV	Uniform Dose	No	77.50	—	—	35.00	0.0261	—	—
O NTT	Max Dose	No	40.00	—	—	5.00	0.0039	—	—
Ring	Max Dose	No	69.00	—	—	3.00	0.0007	—	—
rectal void	Max Dose	No	40.00	—	—	5.00	0.0270	—	—
bladder	Max EUD	No	32.00	—	—	1.00	0.0016	1.000	34.860
rectum	Max EUD	No	33.00	—	—	1.00	0.0000	1.000	32.286
pbi	Max Dose	No	77.00	—	—	50.00	0.0011	—	—
membranous ureth..	Max Dose	No	77.00	—	—	20.00	0.0001	—	—

Composite objective value: 0.0896077

Optimization

Beam Name	Optimization Type
01 ARC 78	SmartArc

Maximum iterations:	40
Convolution dose iteration:	20
Stopping tolerance:	1.0e−05
Tumor overlap fraction (%):	NA
MLC delivery:	Yes

Figure 3.3. Planning parameters from the planning document. O PTV and O NTT in the objectives are the virtual structures used for optimization. Pbi is the structure of prostate/bladder interface to optimize.

3.5 Study Structures

The optimization of IMRT/VMAT planning comprises of the choice of the number of beams, the beam angles, the collimator angles, the dose constraints and their priorities. During an optimization in current inverse planning systems, it is often unclear how strongly each of the optimization parameters is affecting the resulting plan. However, it is known that optimization is sensitive to the choice of initial parameters because they determine which local minimum will be reached (Cotrutz & Xing, 2002; Xing, Li, Pugachev, Le, & Boyer, 1999).

The direction cosine was used to calculate the similarity score of the testing case. The planning parameters can be obtained from the reference case and applied to the testing case in a new treatment plan. This research provided a template for the initial values of the planning parameters. This initialises the testing case to the reference prostate IMRT/VMAT plan that had been used for a similar tumour location, shape and size on the CT image. Therefore, the prostate S&S IMRT/VMAT plans with the vector-model-based optimization needed only few adjustments to meet clinical constraints for the testing case. Hence, the planning time spent on the conventional manual trial-and-error method at the beginning of optimization could be saved. Fine adjustment was still then required to achieve the original plan criteria based on the oncologist's requirements.

First, two sets of previous 101 prostate S&S IMRT/ VMAT plans were collected and transformed into the vectors that were used to establish database references for prostate S&S IMRT/VMAT. A leave-one-out method was used for the prostate S&S IMRT/VMAT reference database (i.e. the original plan of the test case was left out from the reference database and each test case had 100 reference cases).

This study investigated thirty prostate IMRT testing cases (low risk prostate cancer/intermediate risk prostate cancer/high risk prostate cancer, 5/9/16) to one hundred reference prostate IMRT cases (low risk prostate cancer/intermediate risk prostate cancer/high risk prostate cancer, 11/45/44), and thirty prostate VMAT testing cases (low risk prostate cancer/intermediate risk prostate cancer/high risk prostate cancer, 3/14/13) to one hundred reference prostate VMAT cases (low risk prostate cancer/intermediate risk prostate cancer/high risk prostate cancer, 7/45/48).

To determine the impact of the vector-model-based optimization, the prostate S&S IMRT/VMAT plans with the first optimization and final optimization were also compared with and without the vector model (Figure 3.4).

S&S IMRT

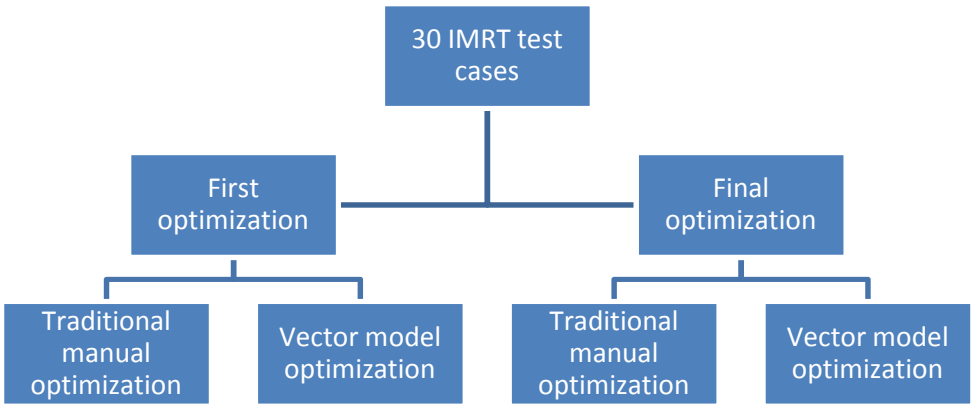

VMAT

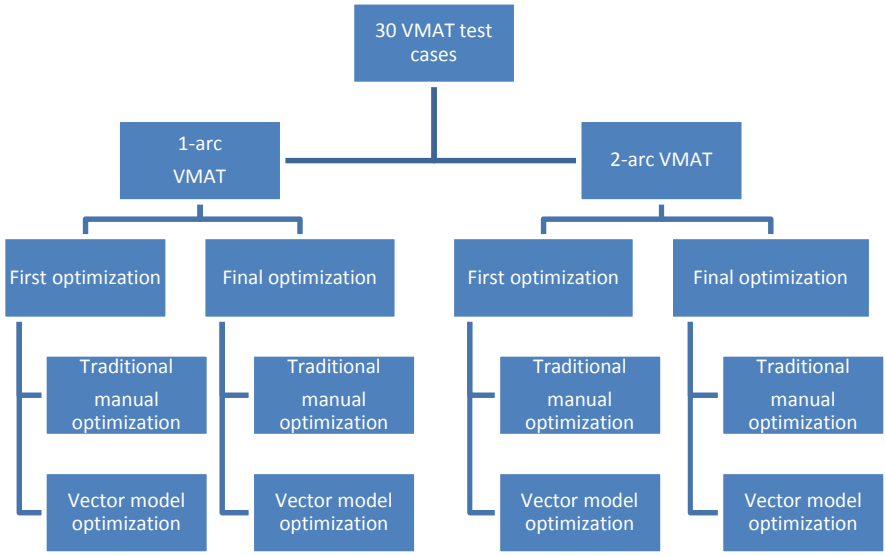

Figure 3.4. Flow Chart of Comparison Studies.

3.6 Comparison between the Vector-Model-Based Optimization and the Conventional Manual Optimization

To determine if the proposed optimizations approach with the vector model was better than the existing conventional optimization approach, the planning time and the plan quality were compared between these two optimization approaches. Planning time comparisons included the vector model processing time, the optimization time, the dose calculation time and the evaluation time.

There are two types of models for the IMRT/VMAT planning: a dose-based model and a radiobiological model. The treatment objective of the radiobiological model is to maximize the tumour control probability (TCP) while maintaining the normal tissue complication probability (NTCP) within acceptable levels.

Unfortunately, the radiobiological model is not well developed yet. Therefore, the dose-based model is used in the conventional IMRT/VMAT planning where a dose-volume histogram (DVH) and the dose distribution are used to evaluate the quality of the IMRT/VMAT plan.

Typical IMRT/VMAT plan evaluation focuses on the tumour coverage, the minimum dose, the maximum dose, the homogeneity and the conformity. A homogeneity requirement demands the uniform dose distribution on the target which is measured by the difference between its maximum and minimum dose. The homogeneity index (*HI*) was defined as ICRU Report 83 (2010):

$$\boldsymbol{HI = \frac{D_2 - D_{98}}{D_{50}}} \qquad \textbf{Equation 37}$$

where D_2 is the dose received by 2% of the target volume, D_{98} is the dose received by 98% of the target volume, and D_{50} is the dose received by 50% of the target volume.

A conformity requirement obligates a planner to keep the prescribed dose as tightly around the target as possible to achieve the target dose coverage while minimizing the damage to normal tissue. The conformity index (*CI*) was calculated using the Paddick's formula (Paddick, 2000):

$$\boldsymbol{CI = \frac{(TV\ in\ PIV)^2}{(TV \times PIV)}} \qquad \textbf{Equation 38}$$

where *TV* is tumour volume, *PIV* is planned isodose volume, and *TV in PIV* is tumour volume covered in planned isodose volume.

To study if the proposed optimizations approach with the vector model was better than the conventional manual optimization approach, the planning time and the plan quality were compared for these two optimization approaches. To compare the planning time for each optimization approach, thirty prostate S&S IMRT cases, thirty prostate 1-arc VMAT and thirty 2-arc VMAT cases were randomized and replanned using both the conventional manual optimization approach and the vector-model-based optimization approach. All dose prescriptions and tolerances were based on the dose constraints prescribed by the oncologist for the original clinical treatments and planned by the same certified medical dosimetrist. Planning time was defined as the sum of the vector model processing time for the test case, the optimization time, the dose calculation time and the evaluation time.

All S&S IMRT cases were replanned using 40 pairs of 1 cm wide MLCs on a Synergy machine (Elekta Oncology Systems, Crawley, UK) using Eclipse treatment planning system (TPS) version 10. All VMAT cases were replanned with 80 pairs of 5 mm wide MLCs on an Infinity machine (Elekta Oncology Systems, Crawley, UK) using Pinnacle TPS version 9.4 and 9.8. As this research focused on prostate IMRT/VMAT, seven static coplanar beams were enough for prostate S&S IMRT plans, and one full coplanar arc and two full coplanar arcs (clockwise and anticlockwise) were for prostate VMAT plans. All the beams and arc were coplanar. Therefore, the number of beams was the same for both the vector-model-based optimization and the conventional manual optimization. The planning dose was then calculated with an analytical anisotropic algorithm (AAA) for S&S IMRT plans, and collapsed cone convolution superposition (CCCS) for VMAT plans.

The vector model was assessed based on the comparison of planning time, number of iterations, number of monitor units (MUs), number of control points and the dosimetric indices criteria (Table 3.3).

Table 3.3. Dosimetric indices for various target volumes and OARs of the prostate cancer.

ROI	Dosimetric indices
PTV	D_{99}, D_{98}, D_{50}, D_2, V_{95}, conformity index (CI) and homogeneity index (HI)
CTV	D_{99}, D_{98}, D_{50}, D_2, V_{95}, HI
Rectum	V_{75}, V_{65}, V_{40} and $V_{79.6\ (cc)}$
Bladder	V_{65}, V_{40}, and D_{max}
Femoral head	V_{35}, V_{50} and D_{max}
Body	D_{max}

3.7 Statistical Analysis

As the concern was the difference between the conventional manual approach and the vector-model-based approach, IMRT/VMAT plans were compared between these two approaches. Therefore, the paired t-test and Wilcoxon signed rank test for dependent samples were used to compare the planning time, number of iterations, and plan quality of IMRT/VMAT plans created by application of the conventional manual approach and the vector-model-based approach. The nonparametric test (e.g. Wilcoxon signed rank test) is generally less powerful than the parametric test (e.g. paired t-test). In other words, the nonparametric test may be less likely to reject a null hypothesis even though the alternative hypothesis is true. Depended on the Shapiro-Wilk normality test results, the parametric paired t-test for dependent samples was chosen if the distribution was normal. Otherwise, the nonparametric test Wilcoxon signed rank test was used for the skew distribution. MATLAB was used to process all statistical analysis.

A total of 360 plans (30 cases of S&S IMRT, 30 cases of 1-arc VMAT, and 30 cases of 2-arc VMAT plans including first optimization and final optimization with/without the vector-model-based optimization) were compared using the two-sided t-test and paired Wilcoxon signed rank test with a significance level of 0.05.

Multiple statistical tests with a significance of 0.05 were used for comparison of the planning time, the number of iterations, the number of MUs, the targets dose coverage, and OARs dose constraints including V_{65}, V_{40}, V_{35} and the maximum dose. Since multiple statistical tests were performed with a standard *p*-value cut-off of 0.05, some results may be "significant" by chance. The False Discovery Rate (FDR) was introduced to control the proportion of false positives among the rejected hypotheses

in the multiple testing (Benjamini & Hochberg, 1995). In this study the statistical significance was maintained for a Benjamini–Hochberg false discovery rate (BHFDR) of less than 0.05. The *p*-value was adjusted by the MATLAB function, mafdr (P, 'BHFDR', true).

For a sample size of 90 testing cases (30 cases of S&S IMRT, 30 cases of 1-arc VMAT, and 30 cases of 2-arc VMAT), an effect size of 0.5 and an alpha value of 0.05, the power of 0.9968 for two-tailed t-test and 0.9956 for paired Wilcoxon signed rank test were calculated using G*Power software (Heinrich Heine University, version 3.1.9.2, 2014) for this study.

Chapter 4 Results

4.1 Feature Extraction

Different structure contours data were retrieved from the structure contour DICOM-RT file and different structure volumes were calculated according to those contours. The following figure in three-dimensions represents different structure contours extracted from DICOM-RT file:

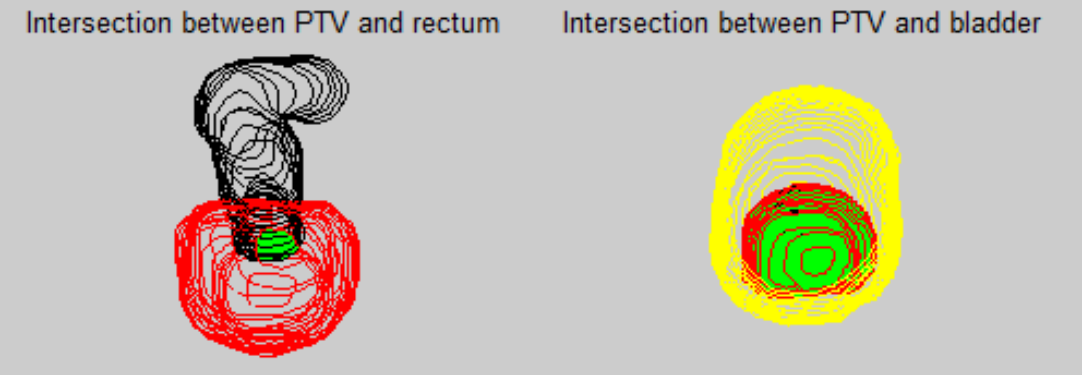

Figure 4.1. Overlap regions between PTV and OARs are shown in green; rectum in black; bladder in yellow; PTV in red.

From the Table 4.1, it can be seen that the MATLAB script reads the structures contours from DICOM files without error, as all the volumes and tumour dimensions calculated by MATLAB software agreed with the volumes calculated by the commercial planning system software shown in Figure 4.2. The deviation between TPS and the MATLAB extracted data were all under 2%. Since the commercial TPS software could not calculate the contour features and moments features, these features could not be verified with TPS. This program took approximately few minutes to calculate 155 features for each prostate IMRT/VMAT case. Some extracted data from the prostate S&S IMRT reference database and the prostate VMAT reference database are displayed in Appendix 1 and Appendix 2, respectively.

Table 4.1. Difference between MATLAB extraction and TPS

Features	MATLAB extracted data	Measurement from TPS	Difference in %
PTV_volume (cc)	105.22	105.6	-0.4%
Bladder_volume (cc)	411.70	412.6	-0.2%
Rectum_volume (cc)	55.85	56.7	-1.5%
Overlap_PTV_bladder volume (cc)	11.83	11.8	0.3%
Overlap_PTV_rectum volume (cc)	2.95	2.9	1.7%
PTV height (mm)	56.00	55.9	0.2%
PTV width (mm)	61.62	62.5	-1.4%
PTV length (mm)	51.30	51.3	0.0%

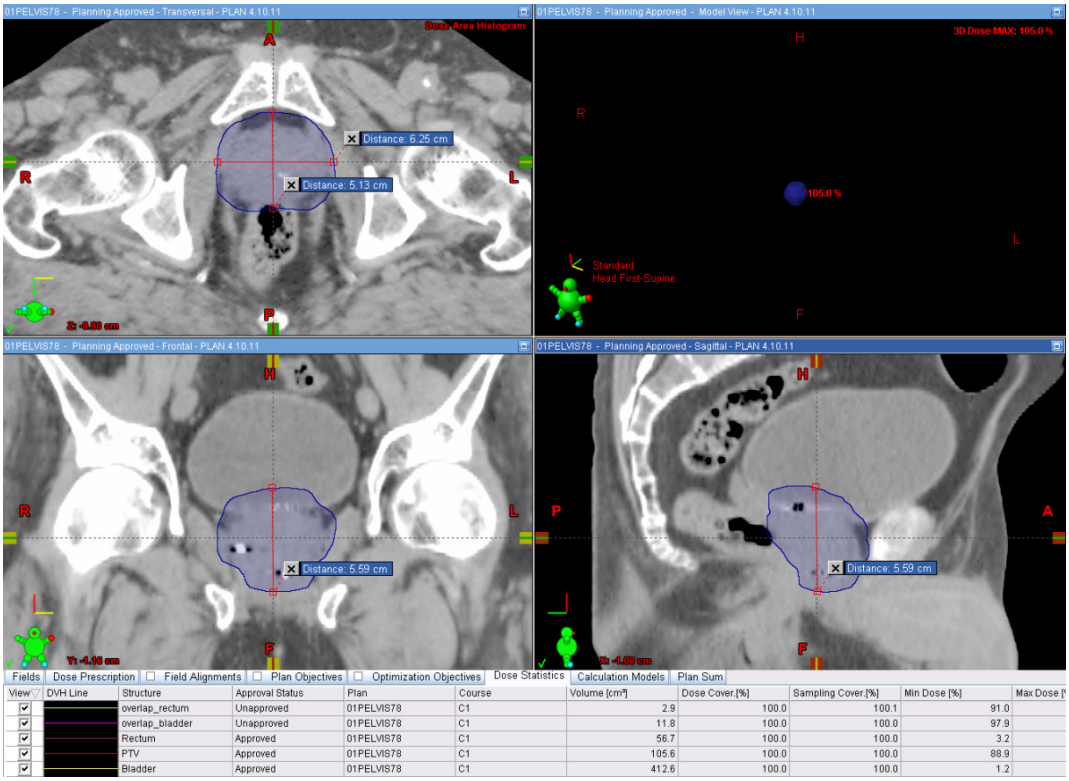

Figure 4.2. PTV volume and dimension verification from Eclipse TPS.

4.2 Reference Selection

Reference cases with 155 features each were formulated into a matrix in which features were put into columns and each reference case was put into separate row. Each new testing case with same number of features was put as an additional row. The relationship between PTV and OARs was emphasized in the model so that the reference with the most similar relationship between PTV and OARs was identified. Figure 4.3 shows different prostate shapes, bladder shapes and rectum shapes among ten cases. The similarity between the testing case (Figure 4.4) and all reference cases was calculated using the direction cosine (Equation 5). The first three highest scoring reference cases shown in Figure 4.5 were obtained automatically from the program. The user could choose any of the three highest scoring reference cases if the user opined that the first highest scoring reference case lacked the quality sought after by the planner, or was not the best match to the testing case.

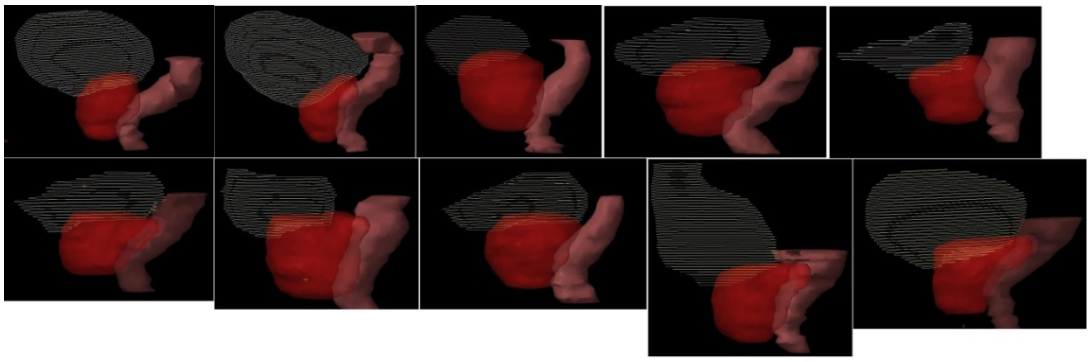

Figure 4.3. Example of different prostate shapes, bladder shapes and rectum shapes.

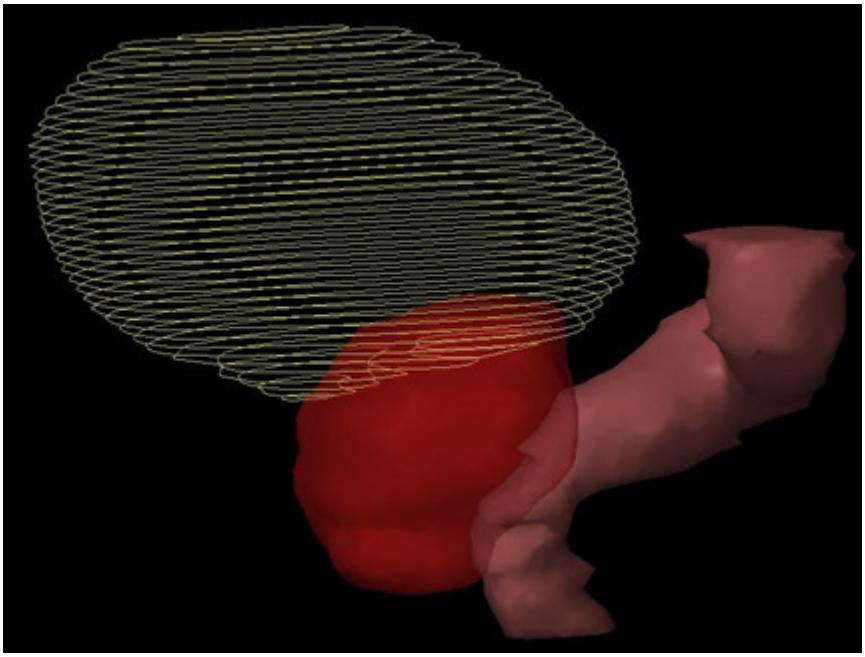

Figure 4.4. Example of the testing case.

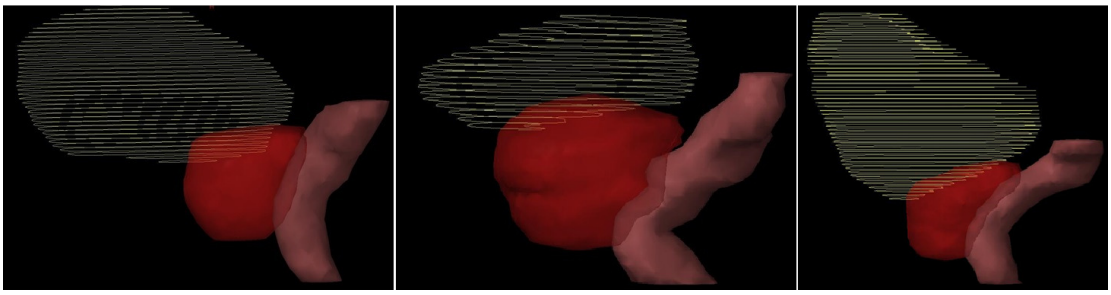

Figure 4.5. Top three reference cases of the testing case (the highest similarity score was on the left, the second similarity score was in the middle and the third similarity score was on the right).

4.3 Vector-Model-Based Optimization Comparison

4.3.1 Statistical Tests

Three hundred and sixty prostate IMRT/VMAT plans were compared between the conventional manual optimization approach and the vector-model-based optimization approach. Shapiro-Wilk normality test was used to check for the normal distribution. For pairs of normally distributed data, means were compared using the parametric t-test. Otherwise the Wilcoxon signed rank test was performed with the median comparison.

4.3.2 False Positive Filtration

There was a list of one hundred and seventy-six dosimetric indices in Appendix 3. Forty-eight of one hundred and seventy-six indices were significantly different between the conventional optimization approach and the vector-model-based optimization approach according to the raw *p*-value being less than the 0.05 threshold. However, seventeen of these were identified false positives according to their FDR values. Hence, there was a significant difference in planning time and number of iterations for all prostate S&S IMRT and all prostate VMAT cases. In addition, there was a significant difference in the plan quality.

4.3.3 Planning Time Comparison

There was a significant difference in the planning time between the plan created using the conventional manual optimization approach and the new plan obtained with the support of the vector model. As shown in Table 4.2, the planning time of the vector model optimization approach was almost 50% reduction compared to the conventional manual optimization approach. A reduction in planning time was observed from 5.16 to 3.16 hours ($p = 3.4\text{x}10^{-6}$) for S&S IMRT prostate plans, from 7.3 to 1.86 hours ($p = 4.6\text{x}10^{-7}$) for 1-arc VMAT prostate plans, and from 4.6 to 1.83 hours ($p = 1.7\text{x}10^{-6}$) for 2-arc VMAT prostate plans. The plan with the vector model had significantly shorter planning times in comparison with the conventional planning approach.

Table 4.2. Planning time comparison between the conventional manual optimization and the vector-model-based optimization for all testing cases: mean value (range).

Comparison	Indices	Conventional optimization	Vector-model-based optimization	Raw *p*-value	BHFDR-adjusted *p*-value
Planning time (hours)	S&S IMRT	5.16 (0.72 - 9.82)	3.16 (0.47 - 9.77)	$3.4\text{x}10^{-6}$	$1.2\text{x}10^{-4}$
	1-arc VMAT	7.30 (1.95 - 23.28)	1.86 (0.6 - 5.03)	$4.6\text{x}10^{-7}$	$8.1\text{x}10^{-5}$
	2-arc VMAT	4.60* (2.23 - 18.67)	1.83* (0.65 - 5.23)	$1.7\text{x}10^{-6}$	$1.1\text{x}10^{-4}$

* median value instead of mean value

Both prostate S&S IMRT and VMAT planning times were significantly reduced (Figure 4.6 through Figure 4.8). The reduction in planning time was greater for prostate VMAT treatments where the planning time was reduced for all cases.

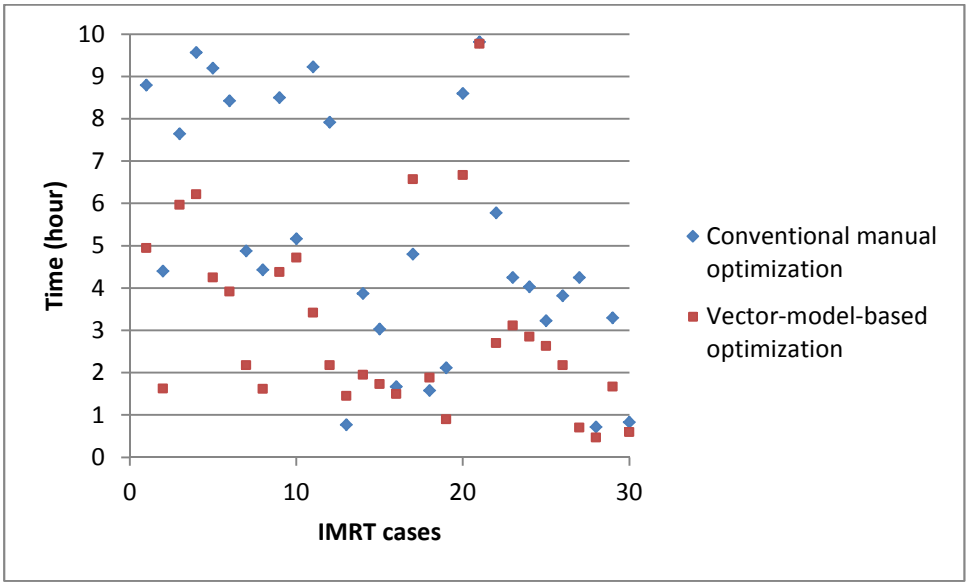

Figure 4.6. Planning time with both optimization approaches for thirty S&S IMRT prostate cases.

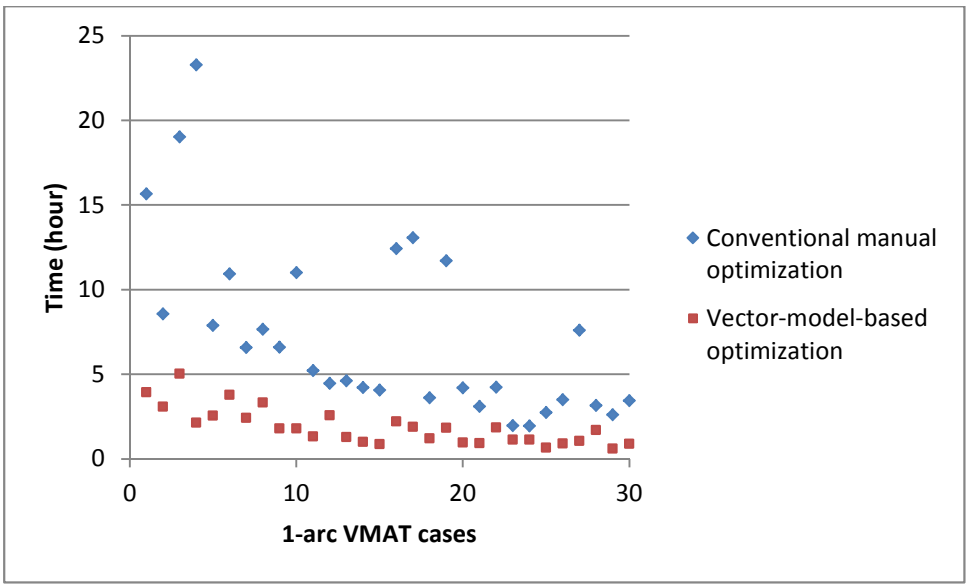

Figure 4.7. Planning time with both optimization approaches for thirty 1-arc VMAT prostate cases.

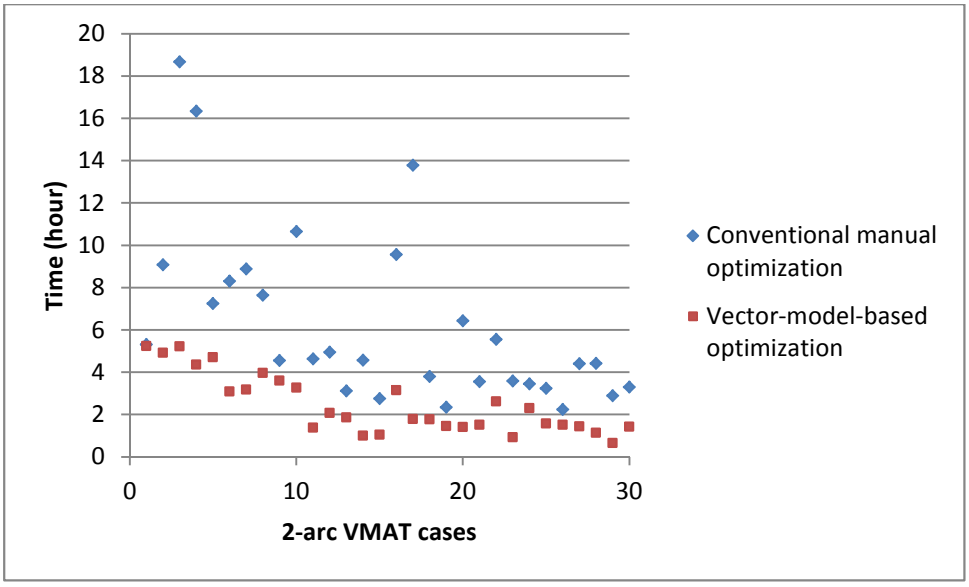

Figure 4.8. Planning time with both optimization approaches for thirty 2-arc VMAT prostate cases.

4.3.4 Number of Iterations Comparison

There was a significant difference in the number of iterations between the conventional manual optimization approach and the vector-model-based optimization approach (see Table 4.3). The vector–model-based optimization plans had less iterations than the conventional manual optimization plans in every case. The median number of iterations was reduced from 10 to 6 iterations ($p = 1.2\text{x}10^{-5}$) for S&S IMRT prostate plans, from 13 to 4.5 iterations ($p = 1.9\text{x}10^{-6}$) for 1-arc VMAT prostate plans. The mean number of iterations was decreased from 8.3 to 3.67 iterations ($p = 3.5\text{x}10^{-6}$) for 2-arc VMAT prostate plans.

Table 4.3. Number of iterations comparison between the conventional manual optimization and the vector-model-based optimization for all testing cases: mean value (range).

Comparison	Indices	Conventional optimization	Vector-model-based optimization	Raw *p*-value	BHFDR-adjusted *p*-value
Number of iterations	S&S IMRT	10* (2 - 27)	6* (2 -21)	$1.2\text{x}10^{-5}$	$3.0\text{x}10^{-4}$
	1-arc VMAT	13* (7 - 34)	4.5* (2 - 11)	$1.9\text{x}10^{-6}$	$1.1\text{x}10^{-4}$
	2-arc VMAT	8.3 (3 - 18)	3.67 (2 - 8)	$3.5\text{x}10^{-6}$	$1.4\text{x}10^{-3}$

* median value instead of mean value

From Figure 4.9 through Figure 4.11, number of iterations for plans with the vector-model-based optimization was generally lower than with the conventional manual optimization.

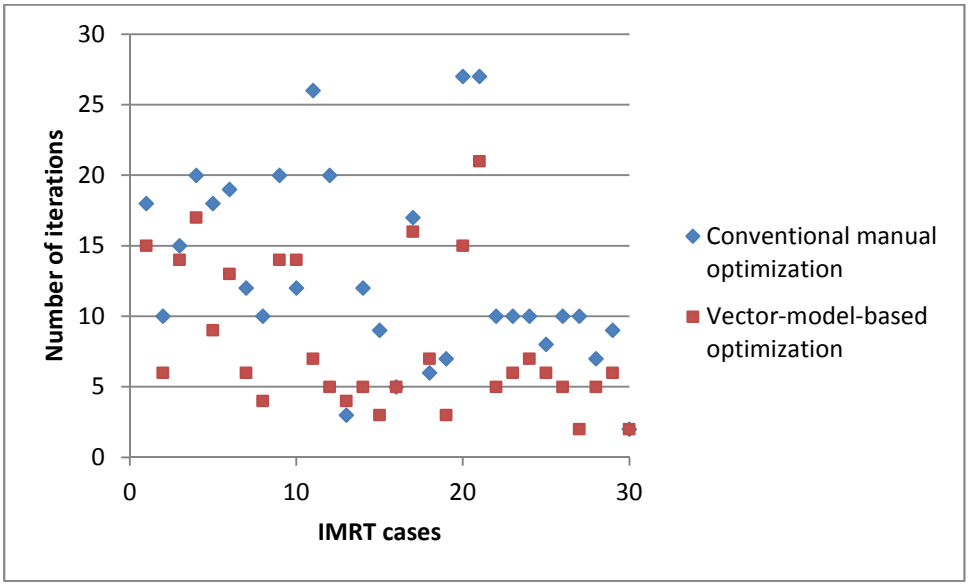

Figure 4.9. Number of iterations with both optimization approaches for thirty S&S IMRT prostate cases.

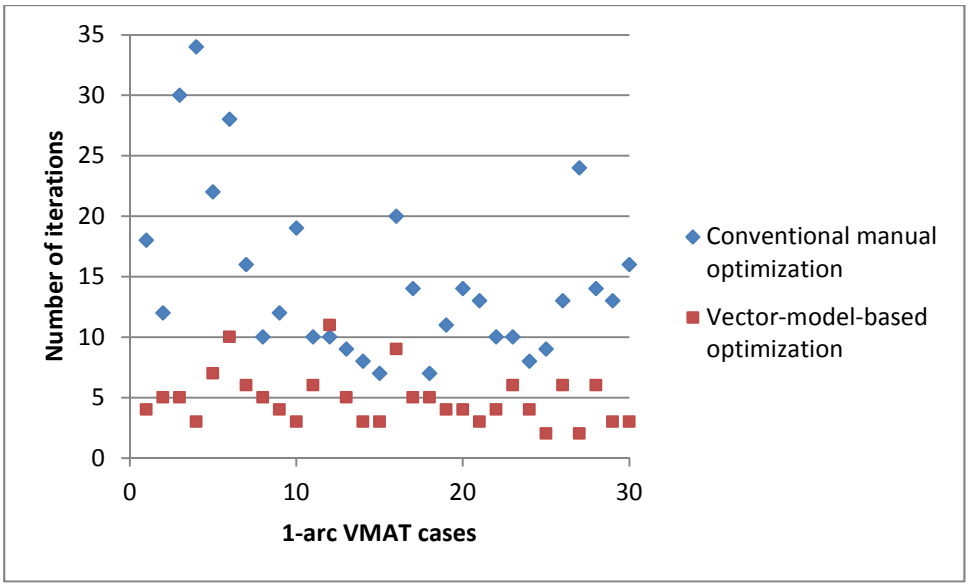

Figure 4.10. Number of iterations with both optimization approaches for thirty 1-arc VMAT prostate cases.

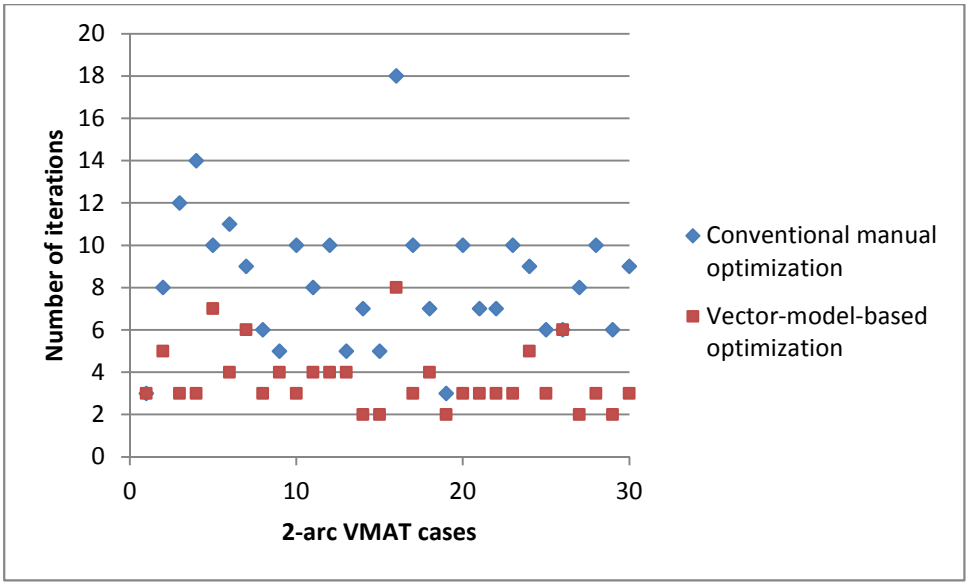

Figure 4.11. Number of iterations with both optimization approaches for thirty 2-arc VMAT prostate cases.

4.3.5 Number of MUs and Number of Control Points Comparison

There was no significant difference in the number of MUs and number of control points obtained using the conventional manual optimization or the vector-model-based optimization planning.

4.3.6 Plan Quality Comparison

The plan quality of final optimization was comparable even though the planning time was shorter with the vector-model-based optimization. Example of comparable DVH comparison was displayed in Figure 4.12, Figure 4.13 and Figure 4.14 for S&S IMRT prostate plans, 1-arc VMAT prostate plans and 2-arc VMAT prostate plans, respectively.

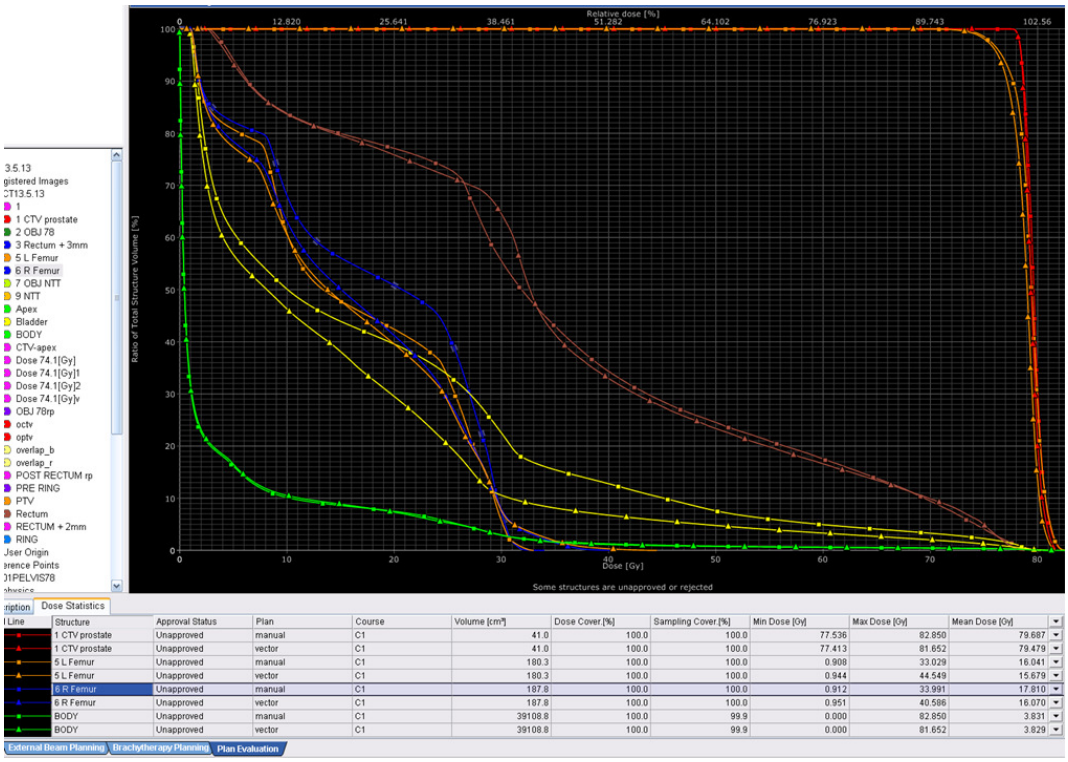

Structure	Approval Status	Plan	Course	Volume [cm³]	Dose Cover.[%]	Sampling Cover.[%]	Min Dose [Gy]	Max Dose [Gy]	Mean Dose [Gy]
1 CTV prostate	Unapproved	manual	C1	41.0	100.0	100.0	77.536	82.850	79.687
1 CTV prostate	Unapproved	vector	C1	41.0	100.0	100.0	77.413	81.652	79.479
5 L Femur	Unapproved	manual	C1	180.3	100.0	100.0	0.908	33.029	16.041
5 L Femur	Unapproved	vector	C1	180.3	100.0	100.0	0.944	44.549	15.679
6 R Femur	Unapproved	manual	C1	187.8	100.0	100.0	0.912	33.991	17.810
6 R Femur	Unapproved	vector	C1	187.8	100.0	100.0	0.951	40.586	16.070
BODY	Unapproved	manual	C1	39108.8	100.0	99.9	0.000	82.850	3.831
BODY	Unapproved	vector	C1	39108.8	100.0	99.9	0.000	81.652	3.829

Figure 4.12. DVH comparison between the conventional manual optimization (square) and the vector-model-based optimization (triangle) for S&S IMRT prostate plans.

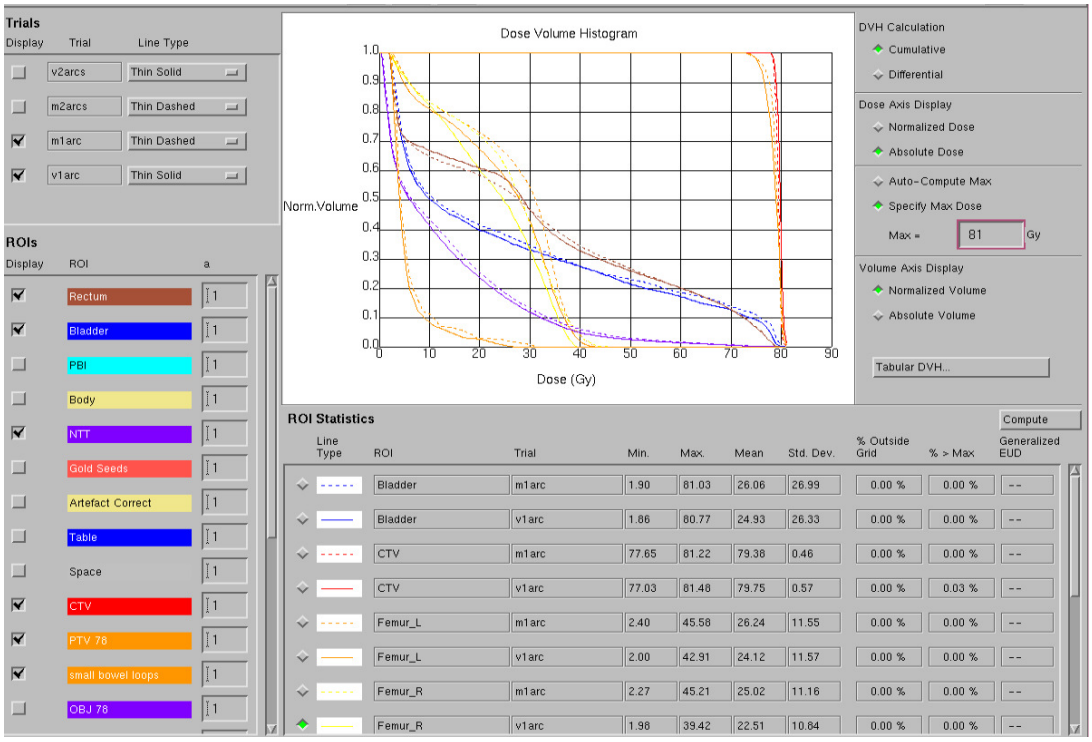

Figure 4.13. DVH comparison between the conventional manual optimization (thin dashed line) and the vector-model-based optimization (thin solid line) for 1-arc VMAT prostate plans.

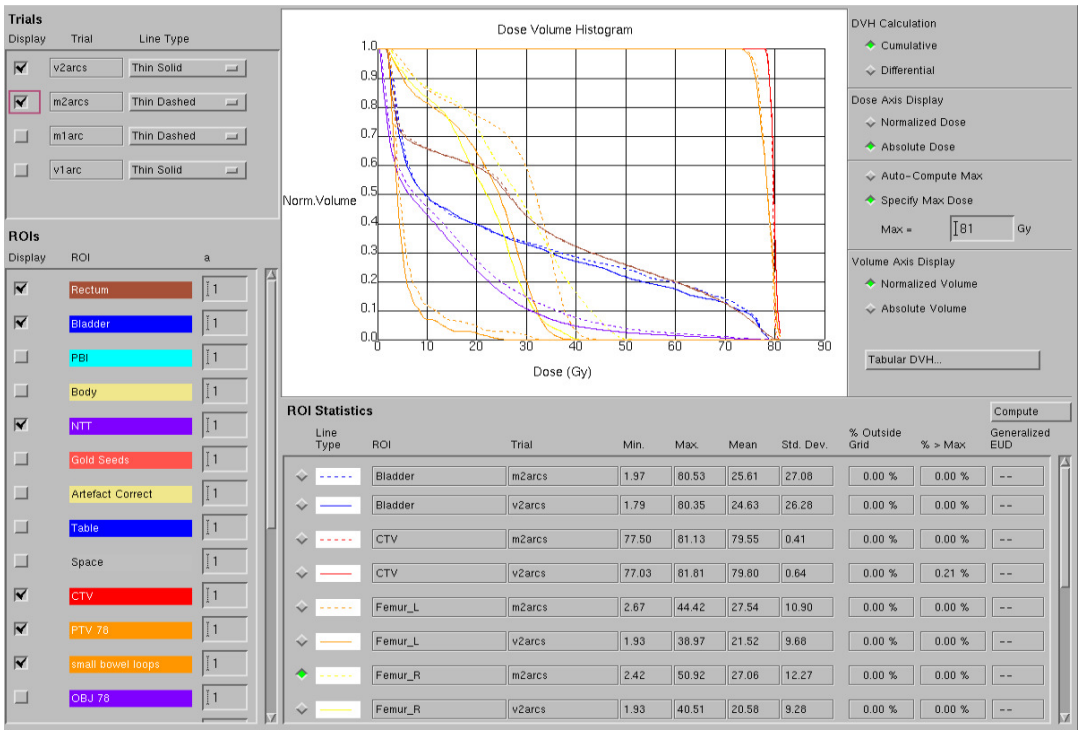

Figure 4.14. DVH comparison between the conventional manual optimization (thin dashed line) and the vector-model-based optimization (thin solid line) for 2-arc VMAT prostate plans.

4.3.6.1 CTV

There was no significant difference in the coverage of CTV for the final optimization between the conventional manual optimization approach and the vector-model-based optimization approach. However, there was a significant difference in the first optimization that the vector-model-based optimization approach was 0.7 Gy higher dose in D_{98} and D_{99} than the conventional manual optimization approach for S&S IMRT prostate plans and 1-arc VMAT prostate plans shown in Table 4.4.

Table 4.4. CTV dose distribution comparison between the conventional manual optimization and the vector-model-based optimization for all testing cases: mean value (range).

Comparison	Indices	Conventional optimization	Vector-model-based optimization	Raw *p*-value	BHFDR-adjusted *p*-value
CTV 1st optimization	D_2 1-arc VMAT	78.59 (76.0 - 82.5)	79.39 (76.98 - 83.15)	3.5×10^{-3}	2.8×10^{-2}
	D_2 S&S IMRT	80.95 (78.41- 82.61)	81.97 (80.33 - 84.02)	2.5×10^{-5}	4.6×10^{-4}
	D_{50} 1-arc VMAT	76.65 (75.0 - 78.8)	77.29 (75.17 - 79.01)	5.5×10^{-3}	3.8×10^{-2}
	D_{50} S&S IMRT	79.12 (77.24 - 80.64)	80.1 (78.88 - 81.77)	4.2×10^{-6}	1.2×10^{-4}

	D_{98} S&S IMRT	77.51* (73.34 - 78.93)	78.36* (76.8 - 80.02)	$2.6x10^{-5}$	$4.6x10^{-4}$
	D_{99} 1-arc VMAT	74.16 (71.38 - 76.7)	74.89 (72.91-77.14)	$8.5x10^{-3}$	$4.8x10^{-2}$
	D_{99} S&S IMRT	77.34* (72.13 - 78.58)	78.10* (76.5 - 79.66)	$2.1x10^{-5}$	$4.5x10^{-4}$

* median value instead of mean value

4.3.6.2 PTV

From Table 4.5, there was significant difference for the first optimization in that the vector-model-based optimization approach had higher D_{50} and D_2 dose than the conventional manual optimization for S&S IMRT prostate plans and 1-arc VMAT prostate plans. While the vector-model-based approach was more conformal to the PTV than the conventional manual approach in 2-arc VMAT prostate plans, the vector-model-based approach was less conformal to the PTV than the conventional manual approach in S&S IMRT prostate plans at the first optimization. However, 1-arc VMAT prostate plans with the vector-model-based approach showed better conformity than the plans created with the conventional approach at the final optimization. Conversely, S&S IMRT prostate plans planned with the vector-model-based approach had slightly poorer homogeneity than the plan created with the conventional approach for the final optimization.

Table 4.5. PTV dose distribution comparison between the conventional manual optimization and the vector-model-based optimization for all testing cases: mean value (range).

Comparison	Indices	Conventional optimization	Vector-model-based optimization	Raw *p*-value	BHFDR-adjusted *p*-value
PTV 1st optimization	CI 2-arc VMAT	0.73 (0.58-0.83)	0.78 (0.65-0.90)	$6.9x10^{-3}$	$4.4x10^{-2}$
	CI S&S IMRT	0.79 (0.48 - 0.92)	0.73 (0.47- 0.90)	$9.8x10^{-4}$	$1.1x10^{-2}$

	D_2 1-arc VMAT	78.56 (76.0 - 81.9)	79.25 (76.81 - 2.77)	$7.3x10^{-3}$	$4.4x10^{-2}$
	D_2 S&S IMRT	80.95 (78.27 - 83.7)	81.9 (80.08 - 84.1)	$3.1x10^{-5}$	$5.0x10^{-4}$
	D_{50} 1-arc VMAT	75.76 (73.24 - 78.2)	76.55 (74.92 - 78.84)	$1.5x10^{-3}$	$1.4x10^{-2}$
	D_{50} S&S IMRT	78.84* (76.2 - 80.1)	79.46* (78.1-81.08)	$4.6x10^{-5}$	$6.8x10^{-4}$
PTV final optimization	CI 1-arc VMAT	0.78 (0.66 - 0.91)	0.81 (0.73 - 0.97)	$6.5x10^{-3}$	$4.4x10^{-2}$
	HI S&S IMRT	0.081* (0.051 - 0.19)	0.085* (0.055 - 0.19)	$9.6x10^{-4}$	$1.1x10^{-2}$

* median value instead of mean value

4.3.6.3 Rectum

For the final optimization, the vector-model-based approach had slightly higher V_{75} than the conventional manual approach for 2-arc VMAT prostate plans in Table 4.6. However, S&S IMRT prostate plans with the vector-model-based approach showed less volume in $V_{79.6}$ than the conventional manual approach for S&S IMRT prostate plans.

Table 4.6. Rectal dose distribution comparison between the conventional manual optimization and the vector-model-based optimization for all testing cases: mean value (range).

Comparison	Indices	Conventional optimization	Vector-model-based optimization	Raw *p*-value	BHFDR-adjusted *p*-value
Rectum final optimization	V_{75} 2-arc VMAT	5.43 (2.91- 9.46)	5.99 (2.35 - 10.49)	$1.2x10^{-3}$	$1.2x10^{-2}$
	$V_{79.6\ (cc)}$ S&S IMRT	0.145* (0.0 - 1.0)	0.085* (0.0 - 0.55)	$4.7x10^{-4}$	$6.3x10^{-3}$

* median value instead of mean value

4.3.6.4 Bladder

There was a significant difference in V_{65} for the S&S IMRT prostate plans first optimization between the vector-model-based approach and the conventional manual approach in Table 4.7. The vector-model-based optimization initially had higher volume in V_{65} compared to the conventional manual approach.

Table 4.7. Bladder dose distribution comparison between the conventional manual optimization and the vector-model-based optimization for all testing cases: mean value (range).

Comparison	Indices	Conventional optimization	Vector-model-based optimization	Raw *p*-value	BHFDR-adjusted *p*-value
Bladder 1st optimization	V_{65} S&S IMRT	13.85* (3.16 - 43.4)	15.52* (1.51 - 45.3)	3.6×10^{-3}	2.8×10^{-2}

* median value instead of mean value

4.3.6.5 Femur

The femoral head dose of the vector-model-based optimization was generally lower than that of the conventional manual optimization for 2-arc VMAT prostate plans. The volume receiving 35 Gy in the femoral head for 2-arc VMAT prostate plans was reduced by almost 10% with the vector-model-based optimization compared to the conventional manual optimization approach in Table 4.8. The maximum dose was roughly 3 Gy less with the vector-model-based optimization.

Table 4.8. Femoral dose distribution comparison between the conventional manual optimization and the vector-model-based optimization for all testing cases: mean value (range).

Comparisons	Indices	Conventional optimization	Vector-model-based optimization	Raw *p*-value	BHFDR-adjusted *p*-value
Right femur 1st optimization / Final optimization	V_{35} 2-arc VMAT	13.74* (0.0-59.91)/ 32.91 (1.29-62.93)	5.19* (0.0 - 57.15)/ 22.89 (0.16-61.04)	0.0071 / $4.4x10^{-3}$	0.044 / $3.2x10^{-2}$
	D_{max} 2 arc VMAT	46.3 (30.67 - 64.04)/ 49.75 (38.04-65.71)	43.87 (27.37 - 57.85)/ 46.07 (36.34-58.08)	0.0081 / $6.1x10^{-4}$	0.048 / $7.7x10^{-3}$
Left femur	V_{35}	5.38*	2.01*	0.0014	0.014

1st optimization / final optimization	2-arc VMAT	(0.0 - 45.19)/ 24.67 (0.0 - 73.67)	(0.0 - 31.27)/ 14.27 (0.0 -51.63)	/ $3.1x10^{-3}$	/ $2.6x10^{-2}$

* median value instead of mean value

4.3.6.6 Body Maximum Dose

There was a significant difference in the body maximum dose between the conventional and the vector-model-based plans for the S&S IMRT prostate plans at the first optimization. The plans created with the vector model had higher hotspot dose in comparison with the conventional plans for the first optimization in Table 4.9.

Table 4.9. Body maximum dose comparison between the conventional manual optimization and the vector-model-based optimization for all testing cases: mean value (range).

Comparison	Indices	Conventional optimization	Vector-model-based optimization	Raw *p*-value	BHFDR-adjusted *p*-value
Body D_{max} 1st optimization	D_{max} S&S IMRT	82.72 (78.92 – 89.08)	83.74 (81.27 – 88.37)	2.1×10^{-3}	1.8×10^{-2}

4.4 1-Arc VMAT and 2-Arc VMAT Prostate Plans Comparison

From Figure 4.15, 2-arc VMAT prostate plans achieved higher target coverage than 1-arc VMAT prostate plans at the first optimization. Table 4.10 summarizes the dosimetric differences between 1-arc VMAT prostate plans and 2-arc VMAT prostate plans. That was, the D_{99} and D_{98} in CTV and PTV, conformity, and homogeneity of 2-arc VMAT prostate plans were better while the femur doses were lower than that in the 1-arc VMAT prostate plan. For the final optimization, the dose in femur and bladder were lower for 2-arc VMAT prostate plans than 1-arc VMAT prostate plans. Although the number of control points of 2-arc VMAT prostate plans was double than that of 1-arc VMAT prostate plans, 2-arc VMAT prostate plans was roughly just 10 to 20 MUs higher than that of 1-arc VMAT prostate plans.

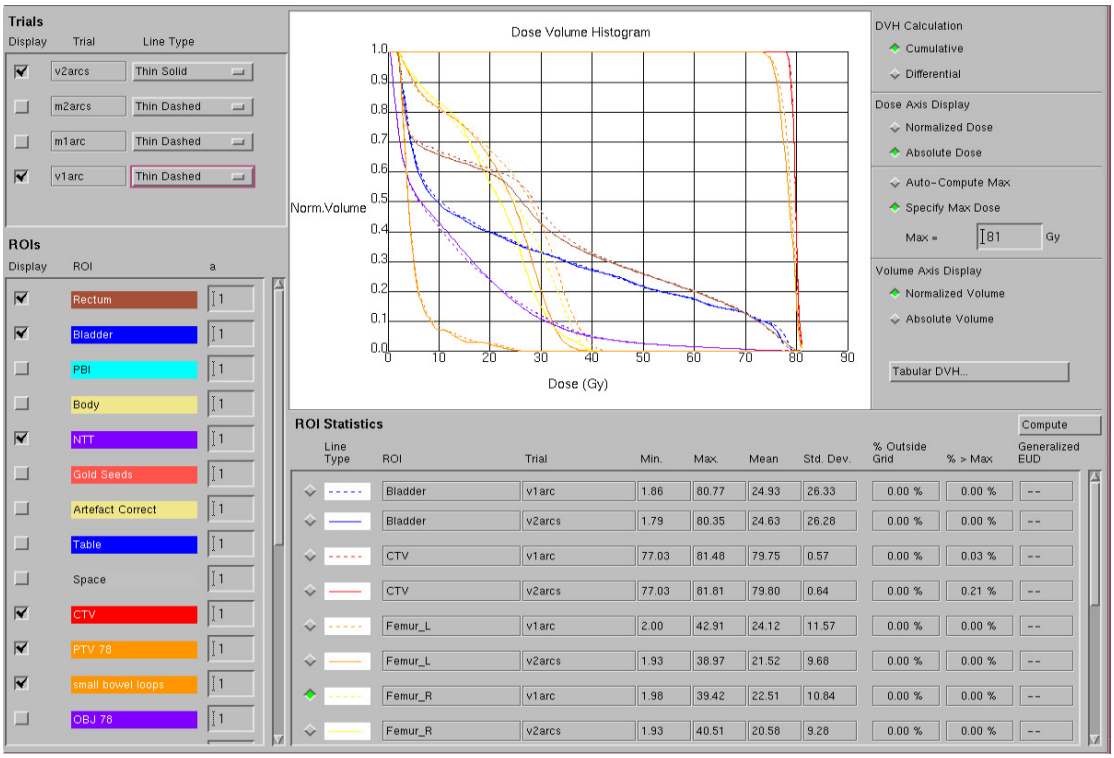

Figure 4.15. DVH comparison between 1-arc VMAT plan (thin dashed line) and the 2-arc VMAT prostate plan (thin solid line).

Table 4.10. Significant dosimetric difference, with false positive filtration, between 1-arc VMAT prostate plans and 2-arc VMAT prostate plans with the vector-based optimization approach: mean value (range).

Comparisons		1-arc VMAT	2-arc VMAT	Raw *p*-value	BHFDR-adjusted *p*-value
MUs 1st optimization/ final optimization		336.3 (271.4 - 418)/ 365.6* (283.3 - 473.2)	353.9 (285.5 - 444.5)/ 376.5* (303.9 - 460.9)	$2x10^{-11}$/ $1.4x10^{-4}$	$1.2x10^{-9}$/ $7.7x10^{-4}$
CTV 1st optimization	HI	0.055 (0.023 - 0.11)	0.050 (0.019 - 0.095)	$8.60x10^{-3}$	$2.20x10^{-2}$
	D_{50} (Gy)	77.2* (75.2 - 79.0)	77.7* (75.6 - 80.0)	$1.90x10^{-3}$	$6.00x10^{-3}$
	D_{98} (Gy)	75.1 (71.8 - 77.3)	75.8 (72.6 - 77.7)	$3.10x10^{-6}$	$8.70x10^{-5}$
	D_{99} (Gy)	74. 9 (72.9 - 77.1)	75.6 (73.7 - 77.5)	$2.00x10^{-5}$	$2.30x10^{-4}$
PTV 1st optimization	CI	0.75* (0.58 - 0.88)	0.77* (0.65 - 0.90)	$4.40x10^{-3}$	$1.30x10^{-2}$

	D_2 (Gy)	79.3 (76.8 - 82.8)	79.7 (77.2 - 82.6)	$2.00x10^{-2}$	$4.50x10^{-2}$
	D_{50} (Gy)	76.5 (74.9 - 78.8)	77.1 (75.4 - 79.2)	$4.30x10^{-4}$	$1.50x10^{-3}$
	V_{95} (%)	98.1* (90.5 - 100)	98.4* (92.2 - 100)	$1.40x10^{-3}$	$4.70x10^{-3}$
	D_{98} (Gy)	70.0 (63.6 - 75.0)	70.7 (64.9 - 75.0)	$8.20x10^{-6}$	$1.60x10^{-4}$
	D_{99} (Gy)	68.8 (60.9 - 74.6)	69.4 (62.4 - 74.5)	$1.50x10^{-5}$	$2.20x10^{-4}$
Bladder 1st optimization	V_{40} (%)	28.0 (7.9 - 48.7)	29.2 (8.7 - 53.2)	$4.40x10^{-5}$	$3.10x10^{-4}$
	V_{65} (%)	13.6 (3.6 - 26.3)	13.8 (3.9 - 26.6)	$6.70x10^{-3}$	$1.90x10^{-2}$
Rectum 1st optimization	V_{75} (%)	0.5* (0 - 6.3)	1.7* (0 - 6.4)	$9.50x10^{-5}$	$6.00x10^{-4}$
Left femur 1st optimization/ final optimization	V_{35} (%)	12.0 (0 - 35.4)/ 16.7* (0 - 50.9)	6.5 (0 - 31.3)/ 7.9*(0 - 51.6)	$3.2x10^{-4}$/ $1.7x10^{-2}$	$1.3x10^{-3}$/ $3.9x10^{-2}$
	D_{max} (Gy)	44.7 (28.3 - 58.8)/	42.1 (28.8 - 55.0)/	$2.8x10^{-5}$/ $1.7 x10^{-4}$	$2.6x10^{-4}$/ $8.7x10^{-4}$

		47.6 (33.6 - 64.5)	44.9 (35.1 - 61.3)		
Right femur 1st optimization	D_{max} (Gy)	45.9*(29.3 - 60.3)	44.5*(27.4 - 57.9)	$3.40x10^{-5}$	$2.80x10^{-4}$
	V_{35} (%)	15.0 (0.0 - 56.2)	11.6 (0.0 - 57.2)	$2.20x10^{-2}$	$4.80x10^{-2}$
	V_{50} (%)	0.5 (0.0 - 7.2)	0.3 (0.0 – 5.4)	$7.8x10^{-3}$	$2.1x10^{-2}$
Right femur final optimization	D_{max} (Gy)	48.7 (39.3 - 61.2)	46.1 (36.3 - 58.1)	$2.60x10^{-4}$	$1.30x10^{-3}$
Bladder final optimization	D_{max} (Gy)	79.9 (77.4 - 81.8)	79.6 (78.1 - 81.4)	$1.42x10^{-2}$	$3.50x10^{-2}$

*** median value instead of mean value**

Chapter 5 Discussion

5.1 Application of the Vector-Model-Based Optimization

A similarity reference database is a database of previous radiotherapy treatment cases. Princess Alexandra Hospital does not have such commercial patient database for S&S IMRT /VMAT prostate planning. Every S&S IMRT/ VMAT prostate plan is based on an individual oncologist's preferences of prescription dose and an individual planner's experience. Without a similarity reference database, it is impossible to manually identify, retrieve and assess all similar S&S IMRT/ VMAT prostate cases from thousands of patient records. This forces a planner to use the conventional trial-and-error manual approach to search for optimization parameters, which normally takes a lot of time. With a similarity reference database, a vector model could retrieve previously successful radiotherapy cases that share various anatomical/physiological features with the current case. Using the optimization parameters from those references as a template for the current case can then reduce optimization time or improve the optimization results. The proposed optimization approach can improve the workflow of every radiotherapy department.

Different methods were used to find the similarity. To calculate the similarity score, Schreibmann and Fox (2014) used the mean distance on the surfaces of the prostate, bladder and rectum whereas Chanyavanich, Das, Lee, and Lo (2011) used the average of the seven mutual information values from the beam's eye view projections of the structure contour. However, this study took different volumes, PTV dimension, PTV contour and physiological features into account to calculate the similarity. Besides, many authors evaluated the commercial knowledge-based

planning (Tol, Delaney, Dahele, Slotman, & Verbakel, 2015; Nwankwo, Mekdash, Sihono, Wenz, & Glatting, 2015; Krayenbuehl, Norton, Studer, & Guckenberger, 2015; Hussein et al., 2016) e.g. knowledge-based radiotherapy planning in the Eclipse TPS and auto-planning software in the Pinnacle TPS. However, the relatively high price of such commercial reference model software prohibits having such commercial reference model software option at our clinical department. Therefore, an in-house MATLAB scripts were implemented to extract the similarity features and to take into account the relationship between the PTV and the OARs. Since all the data were transformed into the vectors, the hard disk storage was minimal. Our similarity search method does not demand computing so much and yields results within half a minute. In addition, the vector model is a standalone application so it can support any TPS.

Vector-model-based optimization could be applied to many clinical sites. Vector-model-based optimization resulted in planning time reduction while maintaining plan quality in VMAT stereotactic radiotherapy planning for brain metastasis at the Princess Alexandra Hospital. Due to the requirement of case availability and consistent dose prescription, the prostate site was chosen to investigate the vector-model-based approach in this study.

5.2 Planning Time

Using the conventional S&S IMRT/VMAT prostate optimization approach, it may take a few days to complete the S&S IMRT/VMAT prostate planning process. Although the total optimization time including the dose calculation and the evaluation time was only approximately 30 minutes for each iteration, many iterations with different optimization settings were required in order to find the one that would achieve the oncologist's goals. From the results (Table 4.2), the longest mean planning time with the conventional optimization approach was 9.8 hours, 23.3 hours and 18.7 hours for S&S IMRT prostate plans, 1-arc VMAT, and 2-arc VMAT prostate plans, respectively with the conventional manual optimization approach. Radiation therapists normally work 8 hours per day, and they work on several patients' plans at the same time. Therefore, radiation therapists cannot put all their working hours on one day for one patient only. In addition, an adaptive plan may be required due to a change in the patient's anatomy. The quality of the adaptive plan may be compromised because of the planning time limitations arising from the planner's workload and the fast turnaround required for an adaptive plan.

There are multiple factors that lead to an increase in planning time. One important factor is the degree of overlap between the PTV and the OARs. The optimization algorithm had to make a compromise between the PTV coverage and the OAR dose tolerance. The more overlap between the PTV and the OARs, the more difficult it was to optimize, leading to longer planning time. The longest planning time for the conventional manual S&S IMRT prostate plan was case 25 where there was 15% of PTV volume overlap with bladder and 5.9% of PTV volume overlap with rectum. It was also concluded that high PTV volume was a factor that increased the

planning time. The planning time more than 16 hours for two conventional manual VMAT prostate plans were case 3 and case 4 and was due to high PTV volume (more than 175 cc) with 8% of PTV volume overlap with bladder.

The planning time was significantly reduced with the vector-model-based approach. The planning time of conventional manual optimization approach was 1.6 times higher for S&S IMRT prostate plans than that of the vector-model-based optimization approach. The average VMAT prostate planning time with the use of the conventional manual optimization alone was almost four times higher for 1-arc VMAT prostate plans and 2.5 times higher for 2-arc VMAT prostate plans than the average planning time with the vector-model-based approach and manual fine tune adjustment. No matter the treatment techniques, the vector-model-based approach can reduce the manual optimization planning time.

Since a prostate VMAT plan applied a full arc rotation around the patient, the planner did not have to spend time finding the optimal number of beams and gantry angles, and could focus on the optimization of the priorities and constraints. Hence, the planner could save additional time in VMAT optimization with the vector-model-based approach.

5.3 Number of Iterations

The reason for the high number of iterations in S&S IMRT was because it attempted to reduce the dose hot spot caused by the limited number of fields. Many virtual structures with appropriate dose constraints were created on the hot spot in order to lower the maximum dose in S&S IMRT prostate plans. There was a compromise between the target coverage and the hot spot dose which took many iterations to achieve. Conversely, the hot spot was not an issue in the VMAT prostate plans because the dose was spread across the full arc angle.

The number of iterations affected not only the planning time but also the plan quality. The more iterations the planner attempted, the lower the planner's confidence in achieving a plan of better quality. In such situations, under the pressure of time, with a queue of other patients lining up for planning, a planner often abandons the plan even if there is room for improvement. With the vector-model-based approach, the number of iterations was significantly reduced in comparison with the conventional manual approach. The vector model could retrieve the most similar reference case and hence better optimization parameters could be obtained from the reference case. Therefore, the plan with the vector-model-based approach requires less iterations to achieve a plan quality similar to the conventional trial-and-error optimization method.

5.4 Plan Quality

The plan quality was analyzed by examining the target dose distribution and the OARs dose distribution. There were several plan quality parameters with significant difference in the first optimization between the conventional manual optimization approach and the vector-model-based approach. The vector-model-based optimization provided the reference optimization parameters so it could push the limit to the targets and OARs at the first optimization. In other words, the vector-model-based saved the optimization time by bypassing the gradual adjustment of planning parameters.

There was little significant difference in the final optimization for the target dose distribution and the OARs dose distribution between the plan created using the conventional method and the new plan obtained with the support of the vector model. The final optimization must meet the planning goals criteria and both the conventional manual and the vector-model-based optimization approaches achieved the same planning goals at the final optimization. Hence, the vector-model-based approach offers much improved planning time and iteration number, but also guarantees the plan quality.

5.4.1 Target Dose Distribution

There was higher CTV target coverage (D_{98} and D_{99}) in the first optimization with the vector-model-based approach than with the conventional manual approach. Among the final optimization plans, the PTV conformity in the vector-model-based 1-arc VMAT prostate plans was slightly better than that of the conventional manual

approach. A ring pseudo-structure was required so that the dose distribution conforms to the target.

Conformity and homogeneity of the PTVs in the vector-model-based S&S IMRT plans were slightly lower, which was probably due to lower rectal dose, that makes the plan harder to achieve with limited number of beam angles in the reference cases.

5.4.2 OARs Dose Distribution

The vector-model-based optimization had higher bladder V_{65} and body maximum dose in the S&S IMRT plans at the first optimization than the conventional manual optimization approach. This was because the vector-model-based optimization had higher CTV coverage (D_{98} and D_{99}) than the conventional manual optimization approach at the first optimization for the S&S IMRT plans.

The vector-model-based optimization provided the reference optimization parameters so it could push the OARs dose lower than the oncologist's criteria. For example, the femoral head dose (V_{35} and D_{max}) and the rectal $V_{79.6}$ were lower in the final optimization with the vector-model-based optimization approach than with the conventional manual optimization approach. On the other hand, the rectal V_{75} was slightly higher with the vector-model-based optimization for 2-arc VMAT prostate plans than with the conventional manual optimization because results of each optimization plan approach were blind to another approach and the optimization was only driven only to meet the oncologist's criteria.

5.5 1-arc VMAT and 2-arc VMAT Prostate Plans Comparison

Although the number of MLC control points of 2-arc VMAT prostate plans (180 control points) was double than that of 1-arc VMAT prostate plans (90 control points), 2-arc VMAT prostate plans was roughly just 10 to 20 MUs higher than that of 1-arc VMAT plans. Therefore, the integral dose of 2-arc VMAT plans was only 3 to 6% higher than that of 1-arc VMAT prostate plans, not double the integral dose.

Although the same optimization parameters were applied in the first optimization for both the 1-arc and the 2-arc vector-model-based VMAT plans, 2-arc VMAT prostate plans showed higher targets coverage (V_{95}, D_{98} and D_{99}), was more conform to CTV and more homogeneous dose to PTV than 1-arc VMAT prostate plans in the first optimization. The bladder dose (V_{40} and V_{65}) and rectal dose of V_{75} of 2-arc VMAT plans were slightly higher than 1-arc VMAT prostate plan in the first optimization because 2-arc VMAT prostate plans had higher targets dose than 1-arc VMAT prostate plans. 2-arc VMAT prostate plans significantly reduced both left and right femoral head dose (V_{35} and D_{max}) than 1-arc VMAT prostate plans in the first optimization. 2-arc VMAT prostate plans provided double MLC control points than 1-arc VMAT prostate plans so the intensity modulation of 2-arc VMAT prostate plans was higher than 1-arc VMAT prostate plans. Hence, 2-arc VMAT prostate plans achieved higher targets coverage and lower femoral dose than 1-arc VMAT prostate plans.

For the final optimization, there was no difference in target coverage between 1-arc and 2-arc VMAT prostate plans. However, 2-arc VMAT prostate plans had lower femoral dose (V_{35} and D_{max}) and bladder dose (D_{max}) than 1-arc VMAT prostate plans in the final optimization.

2-arc VMAT prostate plans required double dose calculation time of 1-arc VMAT prostate plans because the dose calculation time was based on the number of control points and 2-arc VMAT prostate plans had twice control points of 1-arc VMAT prostate plans. However, the total planning time of 1-arc VMAT prostate plans and 2-arc VMAT prostate plans was comparable even though the dose calculation time was double for 2-arc VMAT plans. This was because 2-arc VMAT prostate plans had high intensity modulation than 1-arc VMAT prostate plans and required less iterations to achieve the similar plan quality as 1-arc VMAT prostate plan. For complex prostate cases, the planner should choose 2-arc VMAT rather than 1-arc VMAT because 2-arc VMAT can provide higher intensity modulation than 1-arc VMAT for complex prostate situation and save the total planning time to achieve the tight dose criteria.

The long dose calculation time discouraged planners from pursuing a better plan quality for 2-arc VMAT prostate plans. Therefore, planners did not attempt too many iterations to improve the plan quality further for 2-arc VMAT prostate plans. However, 2-arc VMAT prostate plan with the vector-model-based approach could guarantee plan quality. Hence, the planner could save additional time in 2-arc VMAT prostate planning with the vector-model-based approach.

5.6 Feedback System

Because the vector-based model offers significant time saving to reach similar plan quality levels, the planner could spend additional time to get a better optimized plan. And by using a feedback system, which implied putting these plans with better plan quality into a new reference database and eventually removing plans with poor quality, plans of truly high quality could be created at a faster rate than this study.

5.7 Limitations of the Study

To eliminate the impact of various levels of planning experience on this study, all 78 Gy prostate IMRT/VMAT plans were replanned by the same dosimetrist at the same hospital. Once the collaboration with the other oncology department or TPS vendors is established, the vector-model-based optimization approach can be validated there with different planners, different sites, and different prescriptions.

The program proposed a list of top three reference cases with highest similarity score allowing the planner to choose the most appropriate one. If the reference case with the highest similarity score in the S&S IMRT/VMAT prostate plan was lacking the quality sought after by the planner, the planner could choose the reference case whose anatomical features had the second highest similarity score but met all the IMRT/VMAT plan quality criteria. The MATLAB scripts developed in this study is not fully automatic and requires human intervention to choose the most suitable reference case from the top three highest similarity score. Also, it requires the planner to fine tune the optimization to achieve better plan quality.

Artificial intelligence (AI) can improve the vector model better by machine learning of choosing the reference case and perform optimization. For example, IBM's Watson Oncology is an AI system that provides cancer treatment options by analysing the patient database, research and clinical trials (IBM Watson Oncology, 2015). Also, Google's DeepMind also uses AI for head and neck auto segmentation based on the head and neck patient database from multiple hospitals (DeepMind Technologies Limited, 2016).

Chapter 6 Conclusion

Conventional manual trial-and-error IMRT/VMAT planning optimization requires a long planning process. The aim of this study was to apply the vector-model-based approach of former cases to investigate expedition and improvement of the optimization in IMRT and VMAT planning. The vector-model-based optimization could find the reference case most anatomically similar to a test case, from which the optimization parameters in the reference case could then be taken and applied to the new case as an initial optimization parameters template.

The scope of this research involved literature review, data collection, MATLAB script development for features extraction, the vector model implementation, similarity score calculation, reference retrieval, IMRT/VMAT replanning and statistical analysis between the vector-model-based optimization and the conventional manual optimization in terms of planning time and quality of the IMRT/VMAT prostate plan.

The proposed vector-model-based approach was shown to have a positive influence on the planning time and the quality of final plans. A total of 360 plans (30 cases of IMRT, 30 cases of 1-arc VMAT, and 30 cases of 2-arc VMAT prostate plans including first optimization and final optimization with/without the vector-model-based optimization) were replanned and compared. The vector-model based approach increased effectiveness of IMRT/VMAT optimization in that the planning time and the number of iterations were reduced by almost fifty percent.

Since prostate VMAT applied full arc rotation around the patient, the planner did not have to spend time attempting to find the optimal number of beams and gantry angles, but just had to focus on the optimization of the priorities and constraints.

Hence, the planner could save additional time in VMAT optimization with the vector-model-based approach. Since 2-arc VMAT provided higher intensity modulation than 1-arc VMAT, 2-arc VMAT prostate plan with the vector-model-based approach could reduce the planning time while guarantee plan quality for complex prostate cases.

Dosimetric indices for PTV and OAR were compared with both the conventional manual optimization approach and the vector-model-based optimization approach. Comparisons of the conformity and homogeneity for the PTV were also performed in this study. From the first optimization plans comparison, CTV D_{99} of IMRT and 1-arc VMAT prostate plans with the vector-model-based optimization was 0.7 Gy higher than that of the conventional manual optimization. For the final optimization, 1-arc VMAT plans with the vector-model-based optimization approach showed better conformity than with the conventional manual optimization approach. The volume receiving 35 Gy in the femoral head for 2-arc VMAT prostate plans was reduced by 10% with the vector-model-based optimization compared to the conventional manual optimization approach in the final optimization. Otherwise, the quality of plans from both approaches was comparable. Hence, the vector model achieved the aim of this study.

This proposed approach extracts data from all department planning records and indirectly draws from the experience of people who created IMRT/VMAT prostate plans. An inexperienced planner can learn from the vector-model-based optimization to create a good treatment plan. The time saving benefit of the proposed approach can also improve the quality of plans for experienced planners who are under pressure of a tight time deadline. Much better plans can be achievable if time is available. The proposed optimization approach can improve the workflow of every radiotherapy department. From the results, providing the initial planning parameters

for IMRT/VMAT prostate optimization can significantly reduce the amount of time required to create the treatment plan with this approach. Shortening the time consumed by planning can effectively increase the efficiency of the whole department, reduce waiting time, and improve the treatment outcome.

Vector-model-based optimization not only saves S&S IMRT/VMAT planning time but also guarantees the quality of the IMRT/VMAT plans. The IMRT/VMAT quota can be increased because the IMRT/VMAT planning time can be reduced with the vector model. Therefore, more patients will be benefit from IMRT/VMAT planning with the vector-model-based optimization. Not only can the quantity of output can be increased with the vector model, but also the quality of the IMRT/VMAT plan can be improved as well. In addition, the adaptive IMRT/VMAT plan can be finished within a few hours with the vector-model-based optimization. Therefore, the treatment outcome will be better with the adaptive IMRT/VMAT plan that can overcome the change of target/OARs shapes.

Appendices

Appendix 1. Some extracted data of the S&S IMRT prostate reference database.

Case	PTV volume (cc)	Bladder volume (cc)	Rectum volume (cc)	Overlap PTV bladder volume (cc)	Overlap PTV rectum volume (cc)	Height (mm)	Width (mm)	Length (mm)
1	105.22	411.70	55.85	11.83	2.95	56	61.62	51.30
2	130.29	625.64	91.25	14.93	7.26	66	59.37	47.18
3	204.14	109.80	38.90	12.32	1.92	64	74.05	65.08
4	112.34	119.97	37.38	8.10	2.83	48	61.77	56.33
5	79.04	82.20	48.74	7.24	2.00	44	50.06	49.29
6	103.23	123.84	38.80	8.12	5.23	40	63.10	55.55
7	185.46	147.79	71.02	14.22	5.51	58	68.90	58.93
8	141.05	134.18	37.68	12.61	2.19	52	68.77	55.26
9	171.02	381.76	69.06	14.75	4.70	58	66.71	52.76
10	121.97	399.91	52.19	18.29	6.91	50	59.53	46.76
11	57.72	249.80	29.94	8.50	3.86	48	41.52	40.61

12	144.66	216.24	48.31	4.63	4.89	54	66.16	56.10
13	178.59	150.97	57.62	17.08	5.33	60	69.97	56.21
14	186.71	386.00	47.36	11.84	5.22	64	63.75	56.50
15	117.94	364.28	42.67	7.85	3.00	58	57.93	51.89
16	175.89	149.96	44.40	19.28	4.14	66	63.41	55.74
17	144.16	616.22	59.82	8.69	2.46	58	63.07	54.46
18	95.55	157.71	65.77	3.54	4.93	46	57.65	46.63
19	106.34	349.33	45.63	2.58	2.09	64	55.26	48.05
20	110.86	406.31	51.39	13.63	3.73	52	59.41	50.23
21	120.23	46.90	67.54	7.89	3.68	58	57.27	49.14
22	67.76	140.21	46.35	8.42	2.91	44	49.78	43.83
23	101.77	261.45	44.28	4.96	3.61	54	54.40	45.23
24	132.12	253.83	47.46	8.37	4.61	50	68.17	53.14
25	129.00	101.78	53.63	19.75	7.55	62	54.69	48.81
26	201.23	290.16	70.30	21.07	7.93	62	65.76	58.29
27	96.96	178.59	50.59	5.55	4.70	54	54.54	43.40
28	101.53	379.71	69.66	11.35	5.75	50	60.46	46.70
29	215.75	102.62	45.83	10.21	4.67	66	70.48	62.55

30	176.82	211.40	57.46	3.10	3.10	80	57.60	55.73
31	166.16	147.49	82.39	10.20	4.67	74	58.50	56.92
32	103.96	368.36	65.61	12.56	7.89	56	52.70	46.36
33	63.83	203.70	49.43	5.64	4.54	44	47.76	40.49
34	143.06	125.00	41.81	14.94	5.73	62	64.39	49.28
35	187.38	379.59	55.36	11.94	6.30	70	74.01	54.89
36	125.09	80.32	82.65	6.50	2.92	58	64.06	52.74
37	164.43	179.93	47.57	10.84	2.67	60	67.82	59.28
38	99.37	201.67	70.39	9.10	5.64	54	52.32	42.26
39	89.23	103.00	76.70	9.25	4.95	46	58.80	44.15
40	117.29	118.37	65.75	8.59	3.40	74	51.46	42.88
41	186.32	375.34	46.99	16.48	6.71	58	73.00	58.60
42	157.33	141.40	60.57	11.25	2.54	68	60.89	54.29
43	117.79	201.51	65.21	5.66	3.57	60	62.26	48.15
44	137.99	198.72	91.56	2.95	1.24	68	58.38	48.81
45	164.11	442.67	88.94	21.79	6.16	60	69.43	53.65
46	79.25	252.73	68.75	7.08	2.20	48	50.99	43.87
47	104.60	154.02	92.67	6.56	4.77	50	56.58	48.63

48	80.17	220.54	60.85	1.43	6.01	50	50.10	43.14
49	126.91	143.12	33.30	6.49	1.27	64	58.45	46.67
50	88.56	190.38	53.65	12.52	5.81	42	57.28	50.75
51	100.61	149.81	54.62	9.17	4.89	48	60.03	46.61
52	120.47	104.54	79.36	7.71	4.26	54	58.21	51.43
53	99.83	521.19	34.21	7.64	1.06	50	53.03	50.73
54	96.98	94.97	37.45	3.57	5.57	44	55.30	46.07
55	115.56	130.09	81.19	8.62	8.01	54	57.88	46.62
56	125.60	186.01	68.24	4.14	6.18	60	62.86	52.13
57	94.92	498.25	53.45	14.29	4.46	50	52.26	45.30
58	101.60	628.37	47.84	13.30	4.61	52	60.65	45.77
59	132.37	155.36	43.38	14.67	3.00	52	65.47	54.15
60	85.70	230.13	80.65	8.38	3.77	50	52.95	45.69
61	119.40	149.75	53.11	7.79	2.94	62	57.08	47.82
62	185.13	589.92	54.45	14.27	4.53	58	71.75	61.55
63	133.65	374.51	55.90	6.96	2.03	52	64.84	54.52
64	159.63	220.60	66.35	19.74	4.65	62	64.06	50.83
65	101.37	92.08	80.90	9.13	5.18	46	50.20	43.06

66	91.96	100.92	40.52	7.59	1.65	48	59.55	46.54
67	101.91	140.89	76.27	5.52	5.25	62	52.32	43.80
68	62.12	357.44	33.75	3.79	0.87	50	46.72	36.76
69	66.46	96.43	46.57	2.61	0.71	44	51.18	45.35
70	117.40	65.43	49.42	5.09	2.97	54	60.42	48.75
71	178.68	409.03	51.33	14.39	6.25	62	72.48	60.61
72	114.59	65.12	61.29	7.87	5.05	60	58.28	48.80
73	88.76	89.95	73.15	6.80	5.99	50	53.11	42.16
74	122.21	271.85	55.17	7.19	3.75	56	60.04	49.92
75	133.37	218.87	58.31	15.46	4.68	44	75.64	66.92
76	114.52	157.73	72.90	10.70	5.26	60	60.60	45.97
77	144.84	128.78	68.91	8.96	4.58	62	64.56	53.53
78	97.06	215.67	42.76	9.86	5.02	52	56.84	45.72
79	87.53	438.07	111.05	7.20	6.96	48	59.13	45.17
80	93.05	659.79	52.76	8.02	7.29	44	60.54	46.71
81	84.20	169.04	47.84	7.44	6.18	56	52.03	36.61
82	111.74	260.02	31.57	7.90	3.72	52	60.03	51.38
83	166.69	370.81	61.00	12.91	4.48	58	65.64	57.26

84	102.16	166.78	96.70	9.67	5.33	54	56.65	47.69
85	61.24	292.17	71.09	5.55	3.53	42	51.15	40.00
86	157.70	85.30	64.91	9.18	3.68	62	68.71	55.36
87	162.73	114.84	71.99	13.80	5.01	64	70.67	49.97
88	175.67	191.56	64.05	8.11	4.52	66	70.42	55.75
89	110.10	138.91	78.75	15.20	7.24	54	57.01	49.63
90	159.88	155.66	40.90	18.59	4.60	64	67.42	53.02
91	113.80	155.73	52.54	9.90	3.00	46	61.68	47.23
92	117.00	93.14	69.71	9.29	4.62	52	63.44	46.52
93	123.50	328.78	73.49	8.38	6.58	54	60.15	52.02
94	126.02	71.02	52.26	3.80	4.43	64	50.06	49.46
95	144.11	170.98	64.96	9.71	4.83	62	57.93	51.55
96	117.83	113.89	52.71	6.95	3.08	62	59.76	46.91
97	150.09	283.85	60.79	10.37	5.73	62	63.11	51.85
98	154.73	194.07	62.69	19.80	5.24	60	69.00	53.26
99	232.63	184.87	129.85	8.59	3.46	68	77.14	69.08
100	130.92	251.67	118.05	13.55	5.63	44	69.20	66.16
101	156.90	242.06	117.44	6.33	6.71	60	70.38	55.63

Appendix 2. Some extracted data of the VMAT prostate reference database.

Case	PTV volume (cc)	Bladder volume (cc)	Rectum volume (cc)	Overlap PTV bladder volume (cc)	Overlap PTV rectum volume (cc)	Height (mm)	Width (mm)	Length (mm)
1	118.34	121.66	64.23	6.63	2.21	46	62.27	50.06
2	85.19	125.74	76.57	7.11	4.85	58	53.37	37.74
3	175.36	131.85	48.87	13.67	2.48	64	67.65	59.78
4	189.43	174.54	61.76	14.28	14.28	64	79.45	70.54
5	165.28	275.01	106.97	20.54	9.10	58	71.13	52.83
6	85.91	463.24	27.33	7.93	2.87	54	52.47	46.24
7	93.37	257.61	48.34	14.11	3.59	50	51.03	45.66
8	167.38	226.38	45.47	15.52	6.95	66	61.79	56.12
9	142.47	115.67	57.12	8.53	3.45	62	65.24	52.85
10	77.54	80.77	47.92	1.94	2.18	44	54.55	44.97
11	123.58	307.34	53.78	2.46	4.42	52	58.31	56.56
12	84.78	76.31	66.43	7.13	4.93	56	51.00	39.41

13	118.33	141.78	40.74	13.20	2.02	54	60.05	48.70
14	94.52	117.91	55.24	4.18	4.58	48	59.78	45.30
15	101.51	309.34	35.35	7.03	1.96	54	54.44	47.20
16	130.23	260.82	49.24	11.29	4.71	60	62.11	53.52
17	232.30	138.40	66.82	19.82	6.54	74	64.74	59.40
18	115.62	190.99	48.25	12.46	3.30	60	50.94	45.94
19	122.02	337.36	72.12	7.86	3.92	66	50.79	44.89
20	96.91	217.72	72.25	7.16	4.32	54	54.35	45.54
21	126.25	365.73	86.02	15.26	4.87	60	56.88	50.72
22	119.95	106.99	41.47	1.29	1.65	64	56.80	49.46
23	116.82	225.16	57.08	14.23	5.73	56	56.94	49.57
24	106.07	142.58	54.11	2.64	3.76	60	60.36	50.33
25	190.15	207.70	61.39	13.53	7.45	58	69.41	63.69
26	102.45	126.49	68.24	6.44	4.75	54	58.22	46.34
27	117.78	242.01	47.56	20.47	2.40	52	62.07	52.91
28	130.12	97.22	51.31	14.55	2.38	70	59.26	52.99
29	174.13	580.14	56.55	19.86	9.30	52	68.05	61.46
30	106.45	485.30	89.80	9.50	5.05	48	59.45	48.73

31	147.96	82.23	60.80	10.11	2.66	68	60.44	47.42
32	92.48	412.95	34.31	6.90	1.39	58	48.04	42.76
33	179.79	92.55	64.87	4.37	4.72	48	69.69	56.67
34	155.25	162.38	73.54	10.03	3.87	62	61.11	58.63
35	73.04	455.07	40.22	4.26	1.54	40	53.42	44.20
36	104.84	501.19	100.11	8.90	3.61	56	59.55	46.75
37	95.88	360.48	45.97	6.99	3.34	48	59.91	47.94
38	76.75	443.85	59.43	7.49	2.53	52	54.81	41.89
39	117.12	59.79	42.59	7.57	1.73	56	55.85	45.92
40	140.89	386.53	62.95	11.05	2.95	60	59.23	54.07
41	148.66	387.37	52.94	12.79	3.10	66	65.63	51.68
42	143.79	276.02	67.11	7.68	5.56	54	64.95	54.51
43	102.64	505.52	56.58	6.88	2.11	42	62.22	58.71
44	153.44	316.07	49.69	13.99	4.18	72	62.00	52.83
45	166.34	529.71	76.73	12.33	5.38	64	67.51	55.23
46	128.95	67.66	40.83	7.17	2.58	56	59.17	51.93
47	152.40	130.28	44.06	2.30	2.94	68	64.49	56.66
48	85.78	388.85	62.79	0.15	2.63	40	57.58	43.63

49	81.38	214.73	37.50	10.08	3.83	48	54.82	45.41
50	141.27	194.57	94.40	14.35	4.72	64	61.94	54.67
51	172.64	90.85	38.91	10.70	1.52	66	63.99	62.70
52	105.83	160.67	66.37	7.43	2.46	46	63.19	54.48
53	54.25	146.82	87.97	2.05	3.79	40	48.39	37.82
54	94.87	472.07	80.40	4.71	2.18	50	58.64	44.95
55	160.01	299.50	80.43	20.20	5.42	66	61.01	52.04
56	217.87	380.36	58.71	2.66	4.63	64	73.60	65.64
57	124.09	284.74	76.15	5.73	2.26	60	57.61	49.53
58	107.20	189.29	41.60	5.66	3.04	54	53.94	45.63
59	90.11	104.39	54.93	8.44	2.80	44	58.94	51.91
60	148.21	170.49	53.67	11.83	6.27	58	65.21	51.92
61	126.91	283.77	76.12	9.46	8.29	66	57.11	50.77
62	108.20	349.54	52.54	14.36	1.62	50	60.67	53.71
63	173.60	390.15	50.30	18.37	2.58	64	68.15	62.31
64	129.16	435.39	69.90	11.94	1.59	62	56.15	52.14
65	85.21	123.93	37.74	4.58	2.18	52	53.44	43.81
66	94.30	297.39	82.27	4.79	1.98	52	58.75	44.79

67	91.34	203.13	79.83	10.82	5.40	52	59.38	45.24
68	80.58	465.56	31.36	14.07	3.42	50	51.54	41.03
69	134.27	106.63	68.28	4.77	3.34	78	54.87	42.06
70	99.78	234.13	102.33	16.23	4.51	54	50.93	41.51
71	123.99	226.69	50.48	16.90	6.11	52	58.93	52.50
72	97.79	56.46	57.66	2.85	0.92	56	54.80	44.35
73	85.88	603.64	48.81	9.63	3.56	50	54.73	48.54
74	99.78	234.13	102.33	16.23	4.51	54	50.93	41.51
75	145.32	174.92	55.70	12.47	4.32	56	66.16	54.89
76	87.86	154.81	54.36	0.02	2.29	44	54.81	49.94
77	101.04	427.37	78.98	9.71	3.47	56	52.56	47.69
78	145.91	202.37	69.70	14.90	3.31	78	53.37	51.41
79	100.24	80.86	60.46	3.70	2.02	58	51.29	43.61
80	146.14	90.98	39.78	13.89	2.56	66	60.35	57.57
81	102.14	216.82	51.89	7.88	4.09	64	55.82	40.88
82	127.31	315.68	68.04	12.89	2.54	64	50.15	48.28
83	111.92	96.89	40.30	11.16	3.81	62	54.71	44.09
84	56.45	149.50	40.29	3.12	0.43	42	46.50	38.25

85	81.55	54.08	53.06	1.94	0.06	50	47.39	38.68
86	125.18	275.87	75.33	8.34	5.26	60	57.47	46.57
87	158.09	150.52	49.94	4.91	4.26	64	66.92	53.29
88	126.06	132.70	70.51	7.53	5.85	64	57.05	49.11
89	91.13	471.98	105.11	6.16	2.40	42	58.56	49.19
90	104.40	224.94	65.55	6.98	2.53	50	61.54	46.38
91	137.41	269.63	46.76	6.77	4.65	62	58.50	52.76
92	70.98	181.54	46.81	5.04	2.60	46	46.98	44.11
93	112.02	455.37	55.25	9.01	2.53	60	56.01	49.76
94	143.82	126.43	63.28	9.89	2.42	76	56.30	50.17
95	85.34	63.41	29.40	6.40	3.00	52	47.80	43.70
96	112.53	324.58	67.14	10.76	2.53	50	62.25	49.31
97	102.62	403.36	60.49	11.71	2.85	58	58.99	46.68
98	106.20	272.95	53.12	8.86	2.35	52	63.55	50.78
99	139.80	210.75	50.20	9.38	4.42	52	67.18	60.47
100	94.63	503.04	68.22	12.45	3.54	56	54.41	45.23
101	57.04	149.92	37.76	0.02	0.95	46	55.33	41.51

Appendix 3. Comparison between the conventional manual optimization approach and the vector-model-based optimization approach with the raw *p*-value and the BHFDR-adjusted *p*-value.

Number of comparison	Comparison item	Raw *p*-value	BHFDR-adjusted *p*-value
1	Planning Time 1-arc VMAT	4.609×10^{-7}	8.11×10^{-5}
2	Planning Time 2- arc VMAT	1.7344×10^{-6}	0.00011
3	Iteration 1-arc VMAT	1.8711×10^{-6}	0.00011
4	Planning Time IMRT	3.4307×10^{-6}	0.000122
5	Iteration 2-arc VMAT	3.48×10^{-6}	0.000122
6	$CTVD_{50}$ IMRT 1st optimization	4.2383×10^{-6}	0.000124
7	Iteration IMRT	1.18×10^{-5}	0.000297
8	CTV D_{99} IMRT 1st optimization	0.00002059	0.000453
9	$CTVD_2$ IMRT 1st optimization	0.000025381	0.000456
10	$CTVD_{98}$ IMRT 1st optimization	0.000025903	0.000456
11	$PTVD_2$ IMRT 1st optimization	0.000031285	0.000501
12	$PTVD_{50}$ IMRT 1st optimization	4.60×10^{-5}	0.000675
13	Rectal max IMRT final optimization	0.00046892	0.006348
14	R femur max 2-arc VMAT final optimization	0.00061491	0.00773
15	PTV HI IMRT final optimization	0.00096266	0.0108
16	PTV CI IMRT 1st optimization	0.00098186	0.0108
17	Rectal V_{75} 2-arc VMAT final optimization	0.0012	0.012424
18	L femur V_{35} 2-arc VMAT 1st optimization	0.0014	0.013689
19	$PTVD_{50}$ 1-arc VMAT1st optimization	0.0015	0.013895

20	Body D_{max} IMRT 1st optimization	0.0021	0.01848
21	L femur V_{35} 2-arc VMAT final optimization	0.0031	0.025981
22	$CTVD_2$ 1-arc VMAT 1st optimization	0.0035	0.027548
23	Bladder V_{65} IMRT 1st optimization	0.0036	0.027548
24	R femur V_{35} 2-arc VMAT final optimization	0.0044	0.032267
25	$CTVD_{50}$ 1-arc VMAT1st optimization	0.0055	0.03872
26	PTV CI 1-arc VMAT final optimization	0.0065	0.044
27	PTV CI 2-arc VMAT 1st optimization	0.0069	0.044303
28	R femur V_{35} 2-arc VMAT 1st optimization	0.0071	0.044303
29	$PTVD_2$ 1-arc VMAT 1st optimization	0.0073	0.044303
30	R femur max 2-arc VMAT 1st optimization	0.0081	0.04752
31	$CTVD_{99}$ 1-arc VMAT 1st optimization	0.0085	0.048258
32	PTV CI 1-arc VMAT 1st optimization	0.0097	0.05335
33	L femur max 2-arc VMAT final optimization	0.0108	0.0576
34	CTV V_{95} 1-arc VMAT 1st optimization	0.0149	0.077129
35	Bladder max IMRT 1st optimization	0.0157	0.078949
36	Rectal V_{75} IMRT 1st optimization	0.0171	0.082292
37	Rectal max 2-arc VMAT final optimization	0.0173	0.082292
38	L femur max 2-arc VMAT 1st optimization	0.0185	0.085684
39	Rectal V_{65} IMRT 1st optimization	0.019	0.085744
40	CTV D_{98} 1-arc VMAT 1st optimization	0.0249	0.10956

41	PTV V_{95} 1-arc VMAT final optimization	0.0311	0.12934
42	PTV D_2 IMRT final optimization	0.0314	0.12934
43	Bladder V_{40} 2-arc VMAT 1st optimization	0.0316	0.12934
44	Rectal V_{75} 1-arc VMAT final optimization	0.0423	0.1692
45	CTV D_{50} IMRT final optimization	0.0437	0.170916
46	CTV D_2 IMRT final optimization	0.0471	0.176749
47	MU 1-arc VMAT final optimization	0.0472	0.176749
48	R femur V_{50} 2-arc VMAT final optimization	0.0494	0.179168
49	Bladder max 1-arc VMAT 1st optimization	0.0505	0.179168
50	PTV D_{99} IMRT final optimization	0.0509	0.179168
51	Rectal max IMRT 1st optimization	0.0529	0.182557
52	PTV D_{98} IMRT 1st optimization	0.0584	0.197662
53	Rectal V_{65} 1-arc VMAT final optimization	0.0671	0.222823
54	Bladder V_{40} 1-arc VMAT 1st optimization	0.0752	0.245096
55	L femur D_{50} 2-arc VMAT 1st optimization	0.0781	0.24992
56	Bladder V_{40} IMRT 1st optimization	0.0822	0.256542
57	R femur D_{50} 1-arc VMAT final optimization	0.084	0.256542
58	Rectal V_{75} 2-arc VMAT 1st optimization	0.0856	0.256542
59	Rectal V_{75} IMRT final optimization	0.086	0.256542
60	CTV D_{99} 2-arc VMAT final optimization	0.0929	0.267406
61	Bladder V_{65} 2-arc VMAT 1st optimization	0.0937	0.267406
62	PTV D_{99} 1-arc VMAT final optimization	0.0942	0.267406

63	PTV D_{50} 2-arc VMAT final optimization	0.0964	0.268603
64	PTV V_{95} IMRT final optimization	0.0977	0.268603
65	CTV HI IMRT final optimization	0.0992	0.268603
66	R femur max 1-arc VMAT final optimization	0.1019	0.271733
67	Bladder V_{40} 1-arc VMAT final optimization	0.1156	0.303666
68	CTV D_{98} 2-arc VMAT final optimization	0.1235	0.319647
69	PTV D_{98} IMRT final optimization	0.129	0.323741
70	L femur D_{50} IMRT 1st optimization	0.1298	0.323741
71	PTV V_{95} 1-arc VMAT 1st optimization	0.1306	0.323741
72	Bladder V_{65} 1-arc VMAT 1st optimization	0.147	0.351762
73	Rectal max 1-arc VMAT final optimization	0.147	0.351762
74	L femur max 1-arc VMAT final optimization	0.1479	0.351762
75	PTV D_{98} 1-arc VMAT final optimization	0.1558	0.365611
76	PTV D_{98} 1-arc VMAT 1st optimization	0.1711	0.391771
77	PTV CI 2-arc VMAT final optimization	0.1714	0.391771
78	PTV D_{99} 1-arc VMAT 1st optimization	0.1758	0.394775
79	PTV HI 1-arc VMAT final optimization	0.1772	0.394775
80	L femur V_{35} IMRT 1st optimization	0.1836	0.401975
81	PTV D_{98} 2-arc VMAT 1st optimization	0.185	0.401975
82	Bladder V_{40} 2-arc VMAT final optimization	0.1934	0.412222

83	PTV D_{99} 2-arc VMAT 1st optimization	0.1944	0.412222
84	L femur max IMRT 1st optimization	0.1978	0.414438
85	PTV D_{99} IMRT 1st optimization	0.2124	0.439793
86	PTV HI 2-arc VMAT 1st optimization	0.2191	0.448391
87	R femur max IMRT 1st optimization	0.2279	0.461039
88	Body D_{max} 1-arc VMAT 1st optimization	0.2336	0.4672
89	CTV D_{99} 1-arc VMAT final optimization	0.2466	0.487658
90	R femur max IMRT final optimization	0.2511	0.49104
91	CTV D_{98} 1-arc VMAT final optimization	0.261	0.504791
92	L femur V_{35} 1-arc VMAT 1st optimization	0.2687	0.513049
93	PTV D_{50} 2-arc VMAT1st optimization	0.2711	0.513049
94	$PTVV_{95}$ 2-arc VMAT 1st optimization	0.2788	0.521145
95	CTV D_{50} 2-arc VMAT final optimization	0.2813	0.521145
96	Rectal V_{75} 1-arc VMAT 1st optimization	0.2893	0.523072
97	Bladder max 2-arc VMAT final optimization	0.2942	0.523072
98	R femur D_{50} IMRT 1st optimization	0.2958	0.523072
99	R femur V_{35} 1-arc VMAT final optimization	0.2962	0.523072
100	CTV D_2 2-arc VMAT final optimization	0.2972	0.523072
101	R femur max 1-arc VMAT 1st optimization	0.3067	0.534448
102	R femur V_{35} IMRT 1st optimization	0.3389	0.58473
103	CP IMRT 1st optimization	0.3422	0.58473
104	L femur V_{35} 1-arc VMAT final	0.3482	0.586164

	optimization		
105	Bladder max IMRT final optimization	0.3497	0.586164
106	L femur max 1-arc VMAT 1st optimization	0.367	0.609358
107	PTV D_{99} 2-arc VMAT final optimization	0.376	0.618467
108	R femur V_{35} 1-arc VMAT 1st optimization	0.3901	0.6347
109	L femur max IMRT final optimization	0.3954	0.6347
110	L femur V_{35} IMRT final optimization	0.399	0.6347
111	Bladder max 1-arc VMAT final optimization	0.4019	0.6347
112	Body 1-arc VMAT final optimization	0.4039	0.6347
113	PTV V_{95} 2-arc VMAT final optimization	0.4319	0.672694
114	Rectal V_{40} IMRT 1st optimization	0.4405	0.676299
115	Bladder V_{65} 2-arc VMAT final optimization	0.4419	0.676299
116	Rectal V_{65} 2-arc VMAT final optimization	0.45	0.682759
117	CTV D_{99} 2-arc VMAT 1st optimization	0.4619	0.694007
118	Rectal V_{40} 2-arc VMAT 1st optimization	0.4653	0.694007
119	MU IMRT 1st optimization	0.4711	0.696753
120	CTV D_{50} 1-arc VMAT final optimization	0.4754	0.697253
121	PTV D_{98} 2-arc VMAT final optimization	0.4938	0.712598
122	Rectal max 1-arc VMAT 1st optimization	0.5	0.712598
123	Rectal V_{65} 1-arc VMAT 1st optimization	0.5038	0.712598
124	R femur D_{50} IMRT final optimization	0.5083	0.712598
125	PTV HI IMRT 1st optimization	0.5163	0.712598

126	R femur D_{50} 1-arc VMAT 1st optimization	0.5195	0.712598
127	Rectal V_{40} IMRT final optimization	0.5224	0.712598
128	CTV HI 2-arc VMAT 1st optimization	0.528	0.712598
129	Bladder max 2-arc VMAT 1st optimization	0.529	0.712598
130	L femur D_{50} IMRT final optimization	0.5303	0.712598
131	CTV D_2 2-arc VMAT 1st optimization	0.5304	0.712598
132	CTV V_{95} 2-arc VMAT 1st optimization	0.5595	0.746
133	CTV D_2 1-arc VMAT final optimization	0.5741	0.759711
134	PTV CI IMRT final optimization	0.5987	0.782353
135	L femur D_{50} 2-arc VMAT final optimization	0.6001	0.782353
136	CTV D_{98} 2-arc VMAT 1st optimization	0.6191	0.801188
137	PTV D_2 2-arc VMAT 1st optimization	0.6435	0.826686
138	CTV HI 1-arc VMAT 1st optimization	0.6566	0.833531
139	PTV HI 2-arc VMAT final optimization	0.6583	0.833531
140	PTV D_2 2-arc VMAT final optimization	0.6807	0.855737
141	CTV D_{98} IMRT final optimization	0.7066	0.881997
142	CTV HI 2-arc VMAT final optimization	0.7149	0.8833
143	R femur V_{35} IMRT final optimization	0.7213	0.8833
144	PTV V_{95} IMRT 1st optimization	0.7227	0.8833
145	R femur D_{50} 2-arc VMAT 1st optimization	0.7422	0.89422
146	PTV D_{50} IMRT final optimization	0.7493	0.89422
147	Bladder V_{65} IMRT final optimization	0.7549	0.89422
148	Rectal V_{65} 2-arc VMAT 1st optimization	0.7577	0.89422

149	Body D_{max} IMRT final optimization	0.7619	0.89422
150	CTV D_{50} 2-arc VMAT 1st optimization	0.7655	0.89422
151	MU 2-arc VMAT final optimization	0.7672	0.89422
152	MU 2-arc VMAT 1st optimization	0.7892	0.908413
153	PTV HI 1-arc VMAT 1st optimization	0.7897	0.908413
154	Rectal V_{40} 1-arc VMAT final optimization	0.805	0.912154
155	Rectal V_{65} IMRT final optimization	0.8074	0.912154
156	PTV D_2 1-arc VMAT final optimization	0.8085	0.912154
157	PTV D_{50} 1-arc VMAT final optimization	0.8192	0.915089
158	Bladder V_{40} IMRT final optimization	0.8215	0.915089
159	Bladder V_{65} 1-arc VMAT final optimization	0.8327	0.921731
160	L femur D_{50} 1-arc VMAT 1st optimization	0.8501	0.93511
161	Rectal V_{40} 2-arc VMAT final optimization	0.8652	0.945809
162	CTV D_{99} IMRT final optimization	0.9076	0.982469
163	Body D_{max} 2-arc VMAT 1st optimization	0.9099	0.982469
164	CTV HI IMRT 1st optimization	0.9167	0.983776
165	Rectal V_{40} 1-arc VMAT 1st optimization	0.9344	0.996627
166	CTV HI 1-arc VMAT final optimization	0.94	0.996627
167	CP IMRT final optimization	0.9662	1
168	MU IMRT final optimization	0.968	1
169	Body D_{max} 2-arc VMAT final optimization	0.9733	1
170	L femur D_{50} 1-arc VMAT final optimization	0.9811	1

171	MU 1-arc VMAT 1st optimization	0.9918	1
172	Rectal max 2-arc VMAT 1st optimization	1	1
173	CTVv95 IMRT 1st optimization	1	1
174	CTVv95 IMRT final optimization	1	1
175	CTVv95 1-arc VMAT final optimization	1	1
176	CTVv95 2-arc VMAT final optimization	1	1

References

Allampalli-Nagaraj, G., & Bichindaritz, I. (2009). Automatic semantic indexing of medical images using a web ontology language for case-based image retrieval. *Engineering Applications of Artificial Intelligence, 22*(1), 18-25. doi:10.1016/j.engappai.2008.04.018

American Association of Physicists in Medicine (AAPM). (2012). *AAPM Report No.166: The use and QA of biologically related for treatment planning* [PDF file]. Retrieved from http://www.aapm.org/pubs/reports/RPT_166.pdf

American Joint Committee on Cancer. (2009). *7th Edition Staging Posters* [PDF file]. Retrieved from https://cancerstaging.org/references-tools/quickreferences/Documents/ProstateSmall.pdf

Australian Institute of Health and Welfare & Australasian Association of Cancer Registries. (2012). *Cancer in Australia: an overview 2012* [PDF file]. Retrieved from http://www.aihw.gov.au/WorkArea/DownloadAsset.aspx?id=60129542353

Australian Institute of Health and Welfare. (2012). *Australian Cancer Incidence and Mortality (ACIM) books* [Data file]. Retrieved from http://www.aihw.gov.au/acim-books/

Benjamini, Y., & Hochberg, Y. (1995). Controlling the false discovery rate: A practical and powerful approach to multiple testing. *Journal of the Royal Statistical Society. Series B (Methodological), 57*(1), 289-300.

Bortfeld, T. (2006). IMRT: a reivew and preview. *Physics in Medicine and Biology, 51*(13), R363-R379. doi:10.1088/0031-9155/51/13/R21

Boujelben, A., Chaabani, A. C., Tmar, H., & Abid, M. (2009, December). *Feature extraction from contours shape for tumor analyzing in mammographic images*. Paper presented at the 2009 Digital Image Computing: Techniques and Applications Conference, Melbourne, Australia. Retrieved from http://ieeexplore.ieee.org/document/5384934/

Breedveld, S., Storchi, P., Keijzer, M., Heemink, A. W., & Heijmen, B. (2007). A novel approach to multi-criteria inverse planning for IMRT. *Physics in Medicine and Biology, 52*(20), 6339-6353. doi:10.1088/0031-9155/52/20/016

Cancer Council Australia. (2009). *Advanced prostate cancer guide: a guide for men and their families* [PDF file]. Retrieved from www.cancer.org.au/content/pdf/HealthProfessionals/ClinicalGuidelines/Advanced_Prostate_Cancer_Guide_2009_BOOKMARKS.pdf

Cancer Council Australia. (2010). *Localised prostate cancer: a guide for men and their families* [PDF file]. Retrieved from http://www.cancer.org.au/content/pdf/HealthProfessionals/ClinicalGuidelines/Localised_Prostate_Cancer_book_Web_2010.pdf

Cancer Council Australia. (2016a). *Understanding Prostate Cancer. Cancer Council Australia* [PDF file]. Retrieved from https://www.cancercouncil.com.au/wp-content/uploads/2014/05/Prostate-2016-Web-Lo-Res.pdf

Cancer Council Australia. (2016b). *Understanding Radiotherapy* [PDF file]. Retrieved from

http://www.cancervic.org.au/downloads/booklets/Understanding-Radiotherapy.pdf

Canzeri, R. (2010). Elekta Synergy [Photograph]. Retrieved from http://blog.elekta.com/blog/2010/10/fortis-hospitals-launches-comprehensive-cancer-care-under-one-roof/elekta-synergy-oncology-linac_jpg-med/

Chan, L. W. C., Chan, T., Cheng, L. F., & Mak, W. S. (2010, December). *Machine Learning of Patient Similarity: A Case Study on Predicting Survival in Cancer Patient after Locoregional Chemotherapy*. Paper present at the 2010 IEEE International Conference on Bioinformatics and Biomedicine Workshops (BIBMW), Hong Kong, China. Retrieved from http://ieeexplore.ieee.org/document/5703846/

Chan, L. W. C., Liu, Y., Chan, T., Law, H. K., Wong, S. C. C., Yeung, A. P. H., ... Shyu, C. R. (2015). PubMed-supported clinical term weighting approach for improving inter-patient similarity measure in diagnosis prediction. *BMC Medical Informatics and Decision Making, 15*(1), 43. doi:10.1186/s12911-015-0166-2

Chan, L. W. C., Liu, Y., Shyu, C. R., & Benzie, I. F.F. (2011). A SNOMED supported ontological vector model for subclinical disorder detection using EHR similarity. *Engineering Applications of Artificial Intelligence, 24*(8), 1398-1409. doi:10.1016/j.engappai.2011.05.013

Chanyavanich, V., Das, S., Lee, W., & Lo, J. (2011). Knowledge-based IMRT treatment planning for prostate cancer. *Medical Physics, 38*(5), 2515-2522. doi:10.1118/1.3574874

Chou, R., Croswell, J. M., Dana, T., Bougatsos, C., Blazina, I., Fu, R., ... Lin, K. (2011). Screening for prostate cancer: a review of the evidence for the U.S. Preventive Services Task Force. *Annals of Internal Medicine, 155*(11), 762-771. doi:10.7326/0003-4819-155-11-201112060-00375

Chu, M., Zinchenko, Y., Henderson, S. G., & Sharpe, M. B. (2005). Robust optimization for intensity modulated radiation therapy treatment planning under uncertainty. *Physics in Medicine and Biology, 50*(23), 5463-5477. doi:10.1088/0031-9155/50/23/003

Cotrutz, C., & Xing, L. (2002). Using voxel-dependent importance factors for interactive DVH-based dose optimization. *Physics in Medicine and Biology, 47*(10), 1659-1669. doi: 10.1088/0031-9155/47/10/304

Croswell, J. M., Kramer, B. S., & Crawford, E. D. (2011). Screening for prostate cancer with PSA testing: current status and future directions. *Oncology (Williston Park), 25*(6), 452-460. Retrieved from http://www.cancernetwork.com/oncology-journal/screening-prostate-cancer-psa-testing-current-status-and-future-directions

De Amorim, R. C. (2012). *Feature weighting for clustering: Using K-Means and the Minkowski metric.* Saarbrücken: Lap Lambert Academic Publishing.

DeepMind Technologies Limited. (2016). *Applying machine learning to radiotherapy planning for head & neck cancer.* Retrieved from https://deepmind.com/blog/applying-machine-learning-radiotherapy-planning-head-neck-cancer/

Dewhurst, J., Lucas, J., & Hardy, M. J. (2015, April). *EP-1548: A comparative audit of IMRT and VMAT for prostate cancer*. Paper presented at the 3rd ESTRO Forum, Barcelona, Spain. doi:10.1016/S0167-8140(15)41540-3

Ezzell, G. A., Galvin, J. M., Low, D., Palta, J. R., Rosen, I., Sharpe, M. B., ... Yu, C. X. (2003). AAPM Report No. 82: Guidance document on delivery, treatment planning, and clinical implementation of IMRT: Report of the IMRT subcommittee of the AAPM radiation therapy committee. *Medical Physics, 30*(8), 2089-2115. Retrieved from https://www.aapm.org/pubs/reports/rpt_82.pdf

Felipe, J. C., Olioti, J. B., Traina, A. J. M., Ribeiro, M. X., Sousa, E. P. M., & Traina, C. (2005, December). *A low-cost approach for effective shape-based retrieval and classification of medical images.* Paper presented at the 7th IEEE International Symposium on Multimedia, Irvine, United States. Retrieved from http://ieeexplore.ieee.org/document/1565883/

Feng, Q., Foskey, M., Chen, W., & Shen, D. (2010). Segmenting CT prostate images using population and patient specific statistics for radiotherapy. *Medical Physics, 37*(8), 4121-4132. doi:10.1118/1.3464799

Frey, B. J., & Dueck, D. (2007). Clustering by passing messages between data points. *Science, 315*(5814), 972-976. doi:10.1126/science.1136800

Gletsos, M., Mougiakakou, S. G., Matsopoulos, G. K., Nikita, K. S., Nikita, A. S., & Kelekis, D. (2003). A computer-aided diagnostic system to characterize CT focal liver lesions: Design and optimization of a neural network classifier.

IEEE Transactions on Information Technology in Biomedicine, 7(3), 153-162. doi: 10.1109/TITB.2003.813793

Gonzalez, R. C., & Woods, R. E. (2002). *Digital Image Processing* (2nd ed.). New Jersey: Prentice Hall.

Gupta, L., & Srinath, M. D. (1987). Contour sequence moments for the classification of closed planar shapes. *Pattern Recognition, 20*(3), 267-272. doi:10.1016/0031-3203(87)90001-X

Hoofring, A. (2007). Digital rectal examination (Male) [Image]. Retrieved from https://visualsonline.cancer.gov/details.cfm?imageid=4351

Hu, M. K. (1962). Visual pattern recognition by moment invariants. *IEEE Transactions on Information Theory, 8*(2), 179-187. doi:10.1109/TIT.1962.1057692

Huang, Y. L., Chen, J. H., & Shen, W. C. (2006). Diagnosis of hepatic tumors with texture analysis in non-enhanced computed tomography images. *Academic Radiology, 13*(6), 713-720. doi:10.1016/j.acra.2005.07.014

Hussein, M., South, C. P., Barry, M. A., Adams, E. J., Jordan, T. J., Stewart, A. J., & Nisbet, A. (2016). Clinical validation and benchmarking of knowledge-based IMRT and VMAT treatment planning in pelvic anatomy. *Radiotherapy Oncology, 120*(3), 473-479. doi:10.1016/j.radonc.2016.06.022

IBM Watson Oncology. (2015). *IBM Watson Oncology*. Retrieved from http://www.ibm.com/watson/health/oncology/

International Agency for Research on Cancer (IARC). (2012). *Cancer fact sheets: prostate cancer* [Fact sheet]. Retrieved from Cancer today: http://gco.iarc.fr/today/fact-sheets-cancers?cancer=19&type=0&sex=1

International Commission on Radiation Units & Measurements (ICRU). (1993). *ICRU Report 50: Prescribing, recording, and reporting photon beam therapy.* Bethesda: ICRU.

International Commission on Radiation Units & Measurements (ICRU). (1999). *ICRU Report 62: Prescribing, recording and reporting photon beam therapy (supplement to ICRU Report 50).* Bethesda: ICRU.

International Commission on Radiation Units & Measurements (ICRU). (2010). ICRU Report 83: Prescribing, recording, and reporting photon-beam intensity-modulated radiation therapy (IMRT). *Journal of the ICRU, 10*(1). doi:10.1093/jicru/ndq002

Jagannathan, R., Petrovic, S., McKenna, A., & Newton, L. (2010, October). *A fuzzy non-linear similarity measure for case-based reasoning systems for radiotherapy treatment planning*. Paper presented at the 6th IFIP International Conference on Artificial Intelligence Applications and Innovations, Larnaca, Cyprus. doi:10.1007/978-3-642-16239-8_17

Keyes, L., & Winstanley, A. (2001). Using moment invariants for classifying shapes on large-scale maps. *Computers, Environment and Urban Systems, 25*(1), 119-130. doi:10.1016/S0198-9715(00)00041-7

Kopp, R. W., Duff, M., Catalfamo, F., Shah, D., Rajecki, M., & Ahmad, K. (2011). VVMAT vs. 7-field-IMRT: assessing the dosimetric parameters of prostate

cancer treatment with a 292-patient sample. *Medical Dosimetry, 36*(4), 365-372. doi:10.1016/j.meddos.2010.09.004

Krayenbuehl, J., Norton, I., Studer, G., & Guckenberger, M. (2015). Evaluation of an automated knowledge based treatment planning system for head and neck. *Radiatian Oncology, 10*(226). doi:10.1186/s13014-015-0533-2

Lee, C. C., Chen, S. H., & Chiang, Y. C. (2007). Classification of liver disease from CT Images ssing a support vector machine. *Journal of Advanced Computational Intelligence and Intelligent Informatics*, *11*(4), 396-402. doi:10.20965/jaciii.2007.p0396

Liu, L., Tian, Z., Zhang, Z., & Fei, B. (2016). Computer-aided detection of prostate cancer with MRI: Technology and applications. *Academic Radiology, 23*(8), 1024-1046. doi: 10.1016/j.acra.2016.03.010

Lu, R. (2007). *Simplifying the optimization process in intensity modulated radiotherapy* (Doctoral dissertation, The Rensselaer Polytechnic Institute). Retrieved from http://search.proquest.com.ezproxy.lb.polyu.edu.hk/docview/304839549

Magome, T., Arimura, H., Shioyama, Y., Nakamura, K., Honda, H., & Hirata, H. (2013). Similar-case-based optimization of beam arrangements in stereotactic body radiotherapy for assisting treatment planners. *BioMed Research International, 2013*, 10. doi:10.1155/2013/309534

Megalooikonomou, V., Barnathan, M., Kontos, D., Bakic, P. R., & Maidment, A. D. A. (2009). A representation and classification scheme for tree-like structures in medical images: analyzing the branching pattern of ductal trees in X-ray

galactograms. *IEEE Transactions on Medical Imaging, 28*(4), 487-493. doi:10.1109/TMI.2008.929102

Mohler, J., Bahnson, R. R., Boston, B., Busby, J. E., D'Amico, A., Eastham, J. A., ... Walsh, P. C. (2010). NCCN clinical practice guidelines in oncology: prostate cancer. *Journal of the Natlonal Comprehensive Canccer Network, 8*(2), 162-200. Retrieved from http://www.jnccn.org/content/8/2/162.long

Moreno, J., Caicedo, J., & Gonzalez, F. (2010). A kernel-based multi-feature image representation for histopathology image classification. *Acta Biológica Colombiana, 15*(3), *251-260.*

National Cancer Institute. (2012a). *Prostate-Specific Antigen (PSA) Test* [Fact sheet]. Retrieved from https://www.cancer.gov/types/prostate/psa-fact-sheet

National Cancer Institute. (2012b). *What You Need to Know About Prostate Cancer* [PDF file]. Retrieved from https://www.cancer.gov/publications/patient-education/prostate.pdf

National Electrical Manufacturers Association (NEMA). (1997). *Digital Imaging and Communications in Medicine (DICOM) supplement 11 radiotherapy objects* [PDF file]. Retrieved from ftp://medical.nema.org/medical/dicom/final/sup11_ft.pdf

Niemierko, A. (1997). Reporting and analyzing dose distributions: a concept of equivalent uniform dose. *Medical Physics, 24*(1), 103-10. doi:10.1118/1.598063

Nixon, M., & Aguado, A. (2012). *Feature Extraction & Image Processing for Computer Vision* (3rd ed.). London: Academic Press.

Nwankwo, O., Mekdash, H., Sihono, D. S., Wenz, F., & Glatting, G. (2015). Knowledge-based radiation therapy (KBRT) treatment planning versus planning by experts: validation of a KBRT algorithm for prostate cancer treatment planning. *Radiation Oncology (London England), 10*, 111. doi:10.1186/s13014-015-0416-6

Paddick, I. (2000). A simple scoring ratio to index the conformity of radiosurgical treatment plans. Technical note. *Journal of neurosurgery, 93*(suppl 3), 219-22.

Pancewicz-Janczuk, B., Topczewska-Bruns, J., & Filipowski, T. (2013, March). *EP-1201: A planning comparison study of VMAT and IMRT for prostate cancer*. Paper presented at the 2nd ESTRO Forum, Geneva, Switzerland. doi:10.1016/S0167-8140(15)33507-6

Philips Medical Systems. (2008). *Pinnacle3 Radiation Therapy planning system smartarc 510(k) Notification* [PDF file]. Retrieved from https://www.accessdata.fda.gov/cdrh_docs/pdf9/K090808.pdf

Philips Medical Systems. (2010). *Classic Pinnacle Planning Instruction for use.* United States of America: Philips Medical Systems.

Quan, E. M., Li, X., Li, Y., Wang, X., Kudchadker, R. J., Johnson, J. L., ... Zhang, X. (2012). A comprehensive comparison of IMRT and VMAT plan quality for prostate cancer treatment. *International Journal of Radiation Oncology, Biology and Physics, 83*(4), 1169-1178. doi:10.1016/J.IJROBP.2011.09.015

Rangayyan, R. M. (2005). *Biomedical image analysis.* London: CRC Press.

Rodrigues, G., Warde, P., Pickles, T., Crook, J., Brundage, M., Souhami, L., & Lukka, H. (2012). Pre-treatment risk stratification of prostate cancer patients:

A critical review. *Canadian Urological Association Journal, 6*(2), 121-7. doi:10.5489/cuaj.11085

Sachdeva, J., Kumar, V., Gupta, I., Khandelwal, N., & Ahuja, C. K. (2013). Segmentation, feature extraction, and multiclass brain tumor classification. *Journal of Digital Imaging, 26*(6), 1141-1150. doi:10.1007/s10278-013-9600-0

Saldana, R., Gan, G., Mandapat, J. M., Fernandez, F., Bengson, M., & Bernal, S. (2010). *An application of the latent semantic indexing method to computer aided retrieval of knee meniscus magnetic resonance images.* Retrieved from http://citeseerx.ist.psu.edu/viewdoc/download?doi=10.1.1.100.9507&rep=rep1&type=pdf

Salton, G. (1991). Developments in automatic text retrieval. *Science, 253*(5023), 974-980. doi:10.1126/science.253.5023.974

Salton, G., & Buckley, C. (1991). Global text matching for information retrieval. *Science, 253*(5023), 1012-1015. doi:10.1126/science.253.5023.1012

Schreibmann, E., & Fox, T. (2014). Prior-knowledge treatment planning for volumetric arc therapy using feature-based database mining. *Journal of Applied Clinical Medical Physics, 15*(2), 19-27. doi:10.1120/jacmp.v15i2.4596

Shapiro, L. G., Atmosukarto, I., Cho, H., Lin, H. J., Ruiz-Correa, S., & Yuen, J. (2008). Similarity-based retrieval for biomedical applications. In P. Perner (Ed.), *Case-Based Reasoning on Images and Signals. Studies in*

Computational Intelligence (Vol. 73, pp. 355-387). Berlin: Springer Berlin Heidelberg. doi: 10.1007/978-3-540-73180-1_12

Shen, L., Rangayyan, R. M., & Desautels, J. E. L.(1993). Detection and classification of mammographic calcifications. *International Journal of Pattern Recognition and Artificial Intelligence, 7*(6), 1403-1416. doi:10.1142/S0218001493000686

Shen, L., Rangayyan, R. M., & Desautels, J. E. L.(1994). Application of shape analysis to mammographic calcifications. *IEEE Transactions on Medical Imaging, 13*(2), 263-274. doi:10.1109/42.293919

Shiraishi, K., Yamamoto, K., Haga, A., Sakumi, A., & Nakagawa, K. (2014, September). *Volumetric Modulated Arc Therapy (VMAT) in the Treatment of Localized Prostate Cancer: Initial Experience in 200 Patients.* Paper presented at the Proceedings of the American Society for Radiation Oncology 56th Annual Meeting, San Francisco, United States. doi:10.1016/j.ijrobp.2014.05.1372

Song, X., Petrovic, S., & Sundar, S. (2007, August). *A Case-Based Reasoning Approach to Dose Planning in Radiotherapy*. Paper presented at the Seventh International Conference on Case-Based Reasoning, Belfast, Northern Ireland. Retrieved from http://citeseerx.ist.psu.edu/viewdoc/download?doi=10.1.1.180.6158&rep=rep1&type=pdf

Spratt, D., Pei, X., Yamada, J., Kollmeier, M. A., Cox, B., Zhang, Z., & Zelefsky, M. J. (2012, November). *Long-term Survival and Toxicity of Patients Treated With Ultra-high-dose IMRT for Localized Prostate Cancer*. Paper presented at

the Proceedings of the American Society for Radiation Oncology 54th Annual Meeting, Boston, United States. doi:10.1016/j.ijrobp.2012.07.041

Thompson, I., Thrasher, J. B., Aus, G., Burnett, A. L., Canby-Hagino, E. D., Cookson, M. S., & ...Tangen, C. M. (2007). Guideline for the management of clinically localized prostate cancer: 2007 update. *The Journal of Urology, 177*(6), 2106-31. doi:10.1016/j.juro.2007.03.003

Tol, J. P., Delaney, A. R., Dahele, M., Slotman, B. J., & Verbakel, W. F. (2015). Evaluation of a knowledge-based planning solution for head and neck cancer. *International Journal of Radiation Oncology, Biology, Physics, 91*(3), 612-20. doi:10.1016/j.ijrobp.2014.11.014

Tourassi, G. D., Harrawood, B., Singh, S., Lo, J. Y., & Floyd, C. E. (2007). Evaluation of information-theoretic similarity measures for content-based retrieval and detection of masses in mammograms. *Medical Physics, 34*(1), 140-150. doi:10.1118/1.2401667

Union for International Cancer Control (UICC). (2010). *TNM Classification of Malignant Tumours* (7th ed.). Oxford, United Kindom: Wiley-Blackwell.

Varian Medical Systems. (2010). *Eclipse manual.* Finland: Varian Medical Systems.

Wang, H., Guo, X. H., Jia, Z., Li, H. K., Liang, Z. G., Li, K. C., & He, Q. (2010). Multilevel binomial logistic prediction model for malignant pulmonary nodules based on texture features of CT image. *European Journal of Radiology, 74*(1), 124-129. doi:10.1016/j.ejrad.2009.01.024

Webb, S. (2003). The physical basis of IMRT and inverse planning. *The British Journal of Radiology, 76*(910), 678-689. doi:10.1259/bjr/65676879

Webb, S. (2005). Intensity-modulated radiation therapy (IMRT): a clinical reality for cancer treatment, "any fool can understand this". The 2004 Silvanus Thompson Memorial Lecture. *The British Journal of Radiology, 78*(Spec No 2), S64-72. doi:10.1259/bjr/26711644

Wu, Q., & Mohan, R. (2002). Multiple local minima in IMRT optimization based on dose-volume criteria. *Medical Physics, 29*(7), 1514-1527. doi:10.1118/1.1485059

Xing, L., Li, J. G., Pugachev, A., Le, Q. T., & Boyer, A. L. (1999). Estimation theory and model parameter selection for therapeutic treatment plan optimization. *Medical Physics, 26*(11), 2348-2358. doi:10.1118/1.598749

Xing, L., Li, J. G., Donaldson, S., Le, Q. T., & Boyer, A. L. (1999). Optimization of importance factors in inverse planning. *Physics in Medicine and Biology, 44*(10), 2525-2536. doi:10.1088/0031-9155/44/10/311

Zhang, H. H., Meyer, R. R., Wu, J., Naqvi, S. A., Shi, L., & D'Souza, W. D. (2010). A two-stage sequential linear programming approach to IMRT dose optimization. *Physics in Medicine and Biology, 55*(3), 883-902. Retrieved from 10.1088/0031-9155/55/3/022

Zhou, L., Liao, S., Li, W., & Shen, D. (2011, March). *Learning-based prostate localization for image guided radiation therapy*. Paper presented at the 2011 8th IEEE International Symposium on Biomedical Imaging: From Nano to Macro, Chicago, United States. doi:10.1109/ISBI.2011.5872827